Graduate School of Frontier Sciences, The University of Tokyo
Department of Socio-Cultural Environmental Studies

2020
Master's Thesis

Assessment of natural recovery of mangrove from anthropogenic disturbance using neural network-based classification of satellite images

ニューラルネットワークに基づく衛星画像分類による人為的に攪乱されたマングローブの自然回復に関する評価

Submitted on July 10, 2020
Advisor: Professor Jun SASAKI

Win Sithu Maung
ウェン　シトゥ　マン
47-186848

ABSTRACT

Since mangrove forests around the world are declining due to human disturbances such as shrimp farming, agricultural expansion, urbanization, and over-harvesting for fuelwood, rehabilitation programs should be accelerated for mangrove conservation urgently. Many studies pointed out that the current popular artificial planting approach yielded an unsatisfactory surviving rate for extensive plantations due to the lack of a site-species match. Limited studies focused on natural recovery of mangrove that is an opportunity for mangrove rehabilitation. Hence, the present study examined natural recovery mangrove from different abandoned shrimp ponds through spatial and species analysis. Before any restoration programs, knowing the actual distribution of regional mangrove extent is of great importance for implementation of mangrove rehabilitation and formulation of necessary regulations. Due to the inaccessibility of mangrove nature, remote sensing classification is a time and cost-effective approach to obtain reliable information of extensive mangrove forests. Although a number of studies have applied different classification methods combining with various remotely sensed data for mangrove distribution, there is lack of information about the performance of artificial neural network (ANN) using Sentinel-2 imagery for mangrove classification. In this dissertation, artificial neural network was therefore employed with the combination of Sentinel-2 satellite images in order to propose a promising classification approach for a large extent of mangrove areas. This study firstly conducted two main experiments of input features and hyper-parameter tuning since input features play a key role to improve resultant accuracy in remote sensing classification as has a selection of method deployed. A basic ANN model was applied to the experiments of input feature selection. The most appropriate input combination for mangrove classification was obtained with an overall accuracy of 95.85 %. Hyper-parameter tuning was then explored in order to select a suitable number of hidden layers and neurons for the input features. The optimum design of ANN model was selected as two hidden layers with (544:320) neurons. Through these two main experiments, mangrove distribution of the study area, Wunbaik Mangrove Forest (WMF) in 2020 could be classified with overall accuracy of 95.98% and kappa coefficient of 0.92. Transfer learning

improved the performance of the model in classifying a new dataset in 2015 and the resultant overall accuracy and kappa coefficient were 97.20% and 0.94. Secondly, the study fulfilled information about mangrove changes in WMF from 2015 and 2020 through post-classification change detection. The result of change detection showed that mangrove areas in WMF slightly declined between 2015 and 2020 because of shrimp pond expansion for local livelihoods. Lastly, natural recovering mangrove areas from shrimp farming activities were delineated in terms of spatial and species analysis integrating field survey data. As a result, the study found that mangrove forests can naturally recover around 50 % of a shrimp pond without any restoration effort during a short period of abandonment. Furthermore, recovering mangrove species are diversely distributed at different abandoned ponds depending on their environmental preference. *Avicennia officinalis* and *Avicennia marina* are dominant species with high adaptability to different salinity and elevation range in the early mangrove community recovering at abandoned shrimp ponds. According to research findings, this study reveals that artificial neural network classification using Sentinel-2 image produces a promising accuracy for mangrove distribution and integration of digital terrain and canopy height models can improve resultant accuracy in mangrove classification. Protection measures for existing mangrove should be more enhanced to prevent conversion to other land uses while natural recovery of mangrove is supporting mangrove rehabilitation effectively.

ACKNOWLEDGEMENT

Two years ago, I was just interested in mangrove forests and did not know how to focus on it in a research way. I got an irreplaceable opportunity that I received an acceptance from Professor Jun SASAKI as a master student under his supervision. I would like to express my heartfelt gratitude to my respected supervisor not only for his guidance on my study but also for giving invaluable ideas on how important research is and how to approach it.

I would like to thank my co-supervisor, Professor Hiroyasu SATOH for his kind guidance and very productive suggestions during my thesis preparation. Without his advice, I could not make my study to meet a research presentation of a master student. I really appreciate sharing his valuable time with me whenever I need for my study.

My gratitude goes to U Ohn Winn, Union Minister of Natural Resources and Environmental Conservation, Dr. Nyi Nyi Kyaw, Director General of Forest Department, and other colleagues for allowing and assisting me to be able to study in Japan. I would like to acknowledge Dr. Toe Aung and Dr. Aung Myat San, Assistant Directors, Forest Department who encouraged me to pursue a master degree and provided precious ideas and suggestions about mangrove. I cannot thank enough my juniors; Yan Aung and Phay Kyi Thar, and my colleagues of Forest Department, Yambye Township, for collaborating on the field survey.

I would like to thank Zhiling Guo, a doctoral student of the Department of Sociocultural Environmental Studies, for motivating to study machine learning and suggesting how to figure out the problems I met during this study period. I am deeply indebted to all members of SASAKI Laboratory for their help during two years in Japan.

It would be impossible for me to study at The University of Tokyo although it was my dream in my life. My dream came true by the aid of Asian Development Bank (ADB). I would like to express my gratitude to ADB and Ms. Mari Matsuoka, representative officer for ADB scholarship, International Liaison Office, GSFS for supporting me a lot during my study period.

Last but not least, I would like to convey my special thanks to my family and friends for your warm encouragement in my difficult situations.

Table of Contents

List of Figures

List of Tables

Chapter 1 INTRODUCTION

1.1. Study Background

Mangroves are a salt-tolerant forest community which occurs especially in tropical and subtropical intertidal portions of the world[1]. The global mangrove area was 137,760 km^2 in 2000 [2] and less than 1% of tropical forest worldwide and 0.4% of the global forest estate. They however provide magnificent ecosystem services that are not only tangible goods such as wood and non-wood products but also intangible services such as protecting coastal regions from storm and wave, and acquisition of massive amounts of carbon dioxide[3].

Despite such invaluable ecosystem services, mangrove forests around the world were being depleted with an alarming rate year by year due to human pressures such as the development of aquaculture, agricultural expansion, oil plantations, and urbanization[4]. According to a study of FAO (2007) [5], world mangrove areas decreased from 18.8 million hectares in 1980 to 15.2 million hectares in 2005 as -0.66% of annual changes. In order to compensate for mangrove loss, restoration projects have been implemented primarily by means of artificial plantations. Many studies pointed out that plantation projects may lead to unsatisfied results with low survival rates when a replanted mono-species is not appropriate for a selected site. One of the opportunities is that mangrove possesses a high capacity of self-recovery in which mangrove species can naturally reenter a deforested area if environmental parameters such as natural hydrology, salinity, and elevation of a site meet the preferences of seeds or propagules dispersed along with tidal flow. However, little attention has been paid to the natural recovery of mangrove in considering rehabilitation programs. Therefore, information about natural recovery of mangrove should be more provided for implementing successful reforestation programs.

The study area of this research, Wunbaik Mangrove Forest (WMF), plays a vital role in providing ecological, environmental, and socio-economic goods and services to the local community. However, due to aquaculture and agricultural expansions, WMF and its surrounding mangrove forest have been highly degraded since the 1990s.

According to FAO inventory in 2011 [6], WMF possesses a high capacity of recovery due to abundant seed productivity and high germination rate of mangrove species. Therefore, this region is suitable to explore natural recovery of mangrove from human disturbances. Despite such a large remnant mangrove extent, there is a prominent gap of information about mangrove distribution and changes after 2014. For sustainable mangrove management, updated and accurate information is necessary before implementing any restoration efforts.

Being that mangroves are not only under natural and anthropogenic threats but also growing in remote areas, accessibility of reliable and accurate information is difficult for a large extent of mangrove[7]. With the development of technology in the remote sensing field, advanced approaches were improved to satellite image classification in various disciplines. Remote sensing plays an important role in monitoring mangrove distribution and identifying species, and other attributes such as estimating tree height and biomass. Developing space technology and agencies, satellite data for mangrove areas around the world are accessible and helpful to overcome management barriers in the mangrove field. Still, the interpretation of the remotely sensed data into usable information is challenging due to the complexity of the targeted field. Therefore, features acquired by the earth sensors are needed to perform a further analysis in order to translate into more reliable and understandable information.

Classification is one of the important approaches, which can offer promising information of earth objects by analyzing remotely sensed data from satellite sensors. However, classification accuracy varies depending on not only usage of remotely sensed data but also choice of appropriate classifier[8]. For mangrove distribution, several classification approaches have been developed and explored by using different classifiers and satellite imageries. In recent advanced classification methodologies, machine learning is a new emerging field and classifiers such as artificial neural network (ANN), random forest (RF) and support vector machine (SVM). Among these different methods, ANN has become more popular and widely used in many fields by combining remotely sensed satellite images because of producing a promising result and robustness of the model [9–12].

Launching Sentinel-2 satellite by European Space Agency in 2015 was a great opportunity for the remote sensing community to develop classification approaches for a different variety of fields[13]. With the advantages of spectral, temporal, and spatial resolutions of freely accessible multispectral bands, Sentinel-2 imagery outperformed Landsat 8 by yielding more precise results in remote sensing classification[14–16]. Also, in mapping of mangrove extent and species, Wang et al [17] described that Sentinel-2 sensor bested Landsat 8 by offering more accurate information in their research.

Applying such benefits of ANN method and Sentinel-2 imagery, some studies could improve the results in their targeted fields [18–22]. Although there are limited studies of mangrove using ANN classification with different satellite images, due to the outperformance of recently launched Sentinel-2 imagery, it is worth investigating potential performance of artificial neural network classification in collaboration with Sentinel-2 imagery for mangrove distribution. Through this proposed approach, a promising result for mangrove classification would be achieved in order to provide the lack of information about mangrove changes in the WMF and assess natural recovery of mangrove after human disturbances.

1.2. Study Objectives

Basically, the study has three folds; (a) artificial neural network classification, (b) change detection, and (c) natural recovery process of mangrove after human disturbances. The main objectives are mentioned as follows;

i. To explore artificial neural network classification in collaboration with Sentinel-2 imagery for mangrove distribution,
ii. To fulfill information gap of mangrove changes in the WMF between 2015 and 2020 through post classification change detection, and
iii. To assess natural recovery process of mangrove after human disturbances by comparing different abandoned shrimp ponds in terms of spatial and species analysis

1.3. Literature Review

1.3.1. Artificial neural network for mangrove classification

To management of mangrove forest, remote sensing contributes an essential role by providing reliable information for different research topics such as mangrove extent mapping, species classification, and estimation for above ground biomass [23,24]. However, the resultant accuracy varies depending on the method and the input features in use. Despite the cutting-edge approach in remote sensing classification, ANN was rarely used for mangrove classification but a few studies described the performance of ANN using different remotely sensed imageries.

Xiang Yu et al [25] applied Landsat TM5 image providing 30 m resolution in ANN classification to analyze land use types of mangrove region in Beihai City, Guangxi, P. R. China. In their study, ANN model was designed by a combination of input layer with band 3; red, band 4; near infrared and band 5; short wave near infrared, 5 hidden layers, and output layers with 5 different classes. Compared to other classification methods, ANN produced the highest accuracy of 86.86% in their research while maximum likelihood and spectrum angle approaches yielded 50.79% and 75.39% accuracy, respectively.

For mangrove mapping in Penang island, Ben Bo Chun et al [25] used ANN by combining Thailand Earth Observing System (THEOS) satellite image, which has 15 m resolution of multispectral bands (red, green, blue and near infrared). The four bands of THEOS image in an input layer, one hidden layer with 5 neurons and an output layer with 5 classes were structured to create an ANN model in their analysis. Being achieving overall accuracy of 93.5% and kappa coefficient of 0.900, they revealed that ANN classification is a reliable approach for mangrove mapping. In another analysis [27], they weighed the ANN method with the maximum likelihood classifier by selecting training polygons based on field observation. Their finding showed that higher accuracy of 93.5% could be obtained by applying the ANN classifier whereas maximum likelihood provided 91.5% accuracy for mangrove mapping.

With the aims of distinguishing terrestrial species other than mangrove, Edwin Raczko and Bogdan Zagajewski compared famous three non-parametric algorithms; ANN, RF and SVM by using Airborne Prism Experiment (APEX) hyperspectral data, which contain 288 spectral bands ranging from 413 to 2447 nm with 3.35m spatial resolution. Training and evaluating with the hyperspectral dataset generated from field data collection, they showed that ANN with the highest accuracy of 77 % outperformed the rest classifiers of SVM 68% and RF with 62% for discriminating five different terrestrial species. They finally recommended the ANN with careful selection of optimal spectral bands rather than using massive numbers of bands to improve the resultant accuracy.

1.3.2. Mangrove forest changes

In Asia which covers 38% of global mangrove area representing the highest percentage of mangrove area worldwide, the downing rate is -1.01% of mangrove extent from 7.8 million hectares in 1980 to 5.9 million hectares in 2005. During 2000 to 2012, the percentage of mangrove forest loss was 2.12% in Southeast Asia. In Myanmar, there are three main regions; Rakhine, Ayeyarwaddy, and Tanintharyi where mangroves are primarily thriving along 2832 kilometers of coastline area. FAO stated that mangrove areas in Myanmar have declined from 555,500 hectares in 1980 to 507,000 hectares in 2005 with annual loss rate of -0.4 %. Between 2000-2012, Myanmar was also the number one of top ten countries having the highest average annual mangrove deforestation rate and aquaculture and agricultural conversions are regarded as the main drivers for mangrove area loss.

Being that the study area, WMF is one of the largest remnant mangroves in Myanmar, there were substantial changes of mangrove area since the late 1990s. WMF plays a significant role in the livelihoods of the local community by providing ecological, environmental, and socio-economic goods and services. Main local livelihoods are shrimp farming and agriculture in mangrove forested areas, especially the WMF. Due to the fact that there is insufficient electricity, lack of

job opportunities, and growing population in this region, overexploitation of fuelwood and land encroachment for local livelihoods exacerbated the status of mangrove forest and led to converting other land-uses such as aquaculture and agricultural fields over time [6]. Between 1990 and 2014, 190.98 hectares of mangrove area was decreased to 139.47 hectares dramatically whereas other land-use of shrimp ponds and paddy fields increased significantly from 6.45 to 58.29 (Figure 1.1)[28]. Unfortunately, there is no updated information for this massive remaining mangrove area after 2014.

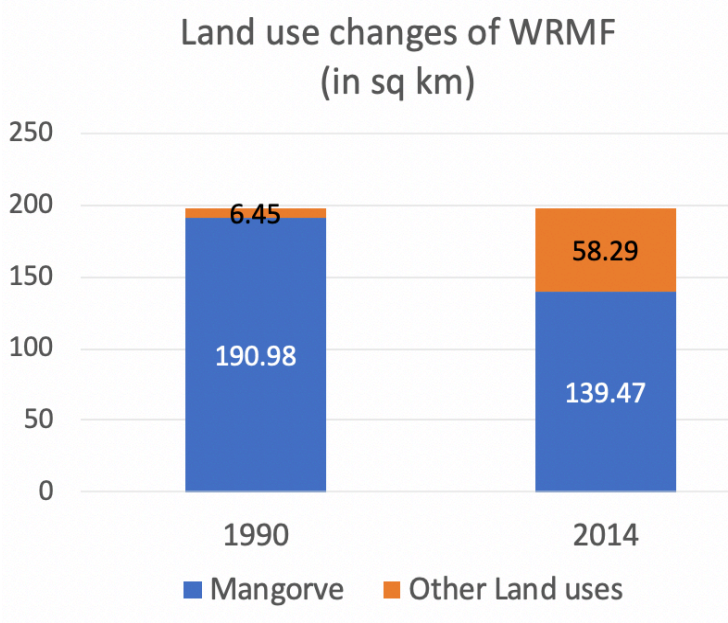

Figure 1.1 Land-use and land cover changes of Wunbaik Reserved Forest between 1990 and 2014

1.3.3. Mangrove restoration programs and natural recovery process

The 2004 Indian Ocean tsunami and the 2008 Nargis Cyclone hitting Myanmar alarmed international organizations to accelerate mangrove rehabilitation. To compensate for mangrove loss and to protect from natural disasters, mangrove reduced areas were implemented in rehabilitation programs whereby mangrove seedlings are nursed and planted.

As international non-governmental organizations and private donors paid attention to mangrove rehabilitations, many plantations could be established to regain mangrove reduced. Unfortunately, many large-scale artificial restoration projects could not achieve satisfied results because their replanted mono-species were not suited to selected sites. Due to abundance and accessibility of *Rhizophora* propagules than other mangrove species, direct sowing of propagules was a popular effort in mangrove restoration projects and planting campaigns. To plantation sites, newly formed tidal flats where soil is unstable under wave fluctuation were carelessly chosen with a lack of knowledge about site and species adaptation, and the consequence of such efforts may lead to low survival rates that cannot address the objectives of mangrove rehabilitation.

Turning to the natural recovery of mangrove, Julien Andrieu at el[29] found that 3000 hectares of Senegalese mangrove could naturally recover from drought-induced mortality between 2000 and 2015. They expressed their findings by combining botanical field data with information derived from remote sensing classification using k-mean algorithm and Landsat 8 imagery.

Moreover, A. Ferreira et al [30] compared natural recovery to planted sites in terms of mangrove species richness and crab diversity in Brazil. According to their findings, although the higher crab density was found in plantation sites, natural recovered mangrove area possesses the higher tree species richness. F. Sidik et al [31] also analyzed planted mangrove inside the abandoned shrimp ponds and naturally recruited mangrove outside the pond in Perancak Estuary, Bali. They found that between 2001 and 2004, mangrove expanded from 20 to 65 ha in natural areas but from 20 to 50 ha in planted sites. To species analysis of their study, only *Rhizophora* species were found as planted mangrove while *Sonneratia* and *Avicennia* were dominant in the natural recovered community.

1.4. Study Significance

To my knowledge, the present study was the first effort to show the performance of artificial neural network classification using Sentinel-2 image for mangrove distribution despite limited studies using ANN classification with other satellite imageries. Unlike traditional classification applying feature extraction for training dataset, this

study applied a ground truth image based on field observation to neural network classification. In addition, the study analyzed two main experiments of input features and hyper-parameter tuning with the aims of selecting the most appropriate method for mangrove classification. By introducing transfer learning approach, the proposed method was improved and able to be applied to a new dataset in different image acquisition dates of the study area.

Furthermore, as the updated information matter for natural resource management, the study fulfilled the prominent gap of mangrove distribution and changes in the WMF between 2015 and 2020. Despite a few studies describing comparison of natural recovered and planted mangrove, this study provided pure natural recovery of mangrove at different abandoned shrimp ponds in terms of spatial and species analysis. Consequently, this study contributed not only a promising method in the remote sensing field but also reliable findings for mangrove conservation.

Chapter 2 MATERIALS AND METHODS

2.1. Study Site

The study area is located between 19˙ 07' 0" – 19˙ 23' 30" North and 9˙3 51' 0" – 94˙ 02' 30" East in Yambye township, Kyauk Phyu district, Rakhine State, Myanmar, and locally known as Wunbaik Mangrove Forest (WMF) where main mangrove distributed area has been constituted as a reserved forest by Forest Department (FD) since 1931(Figure 2.1). Wunbaik Mangrove Reserved Forest is one of the largest remaining mangrove communities with the extent of 22674 ha. 34 mangrove species have been identified by Food and Agricultural Organization (FAO) project since 2011[32].

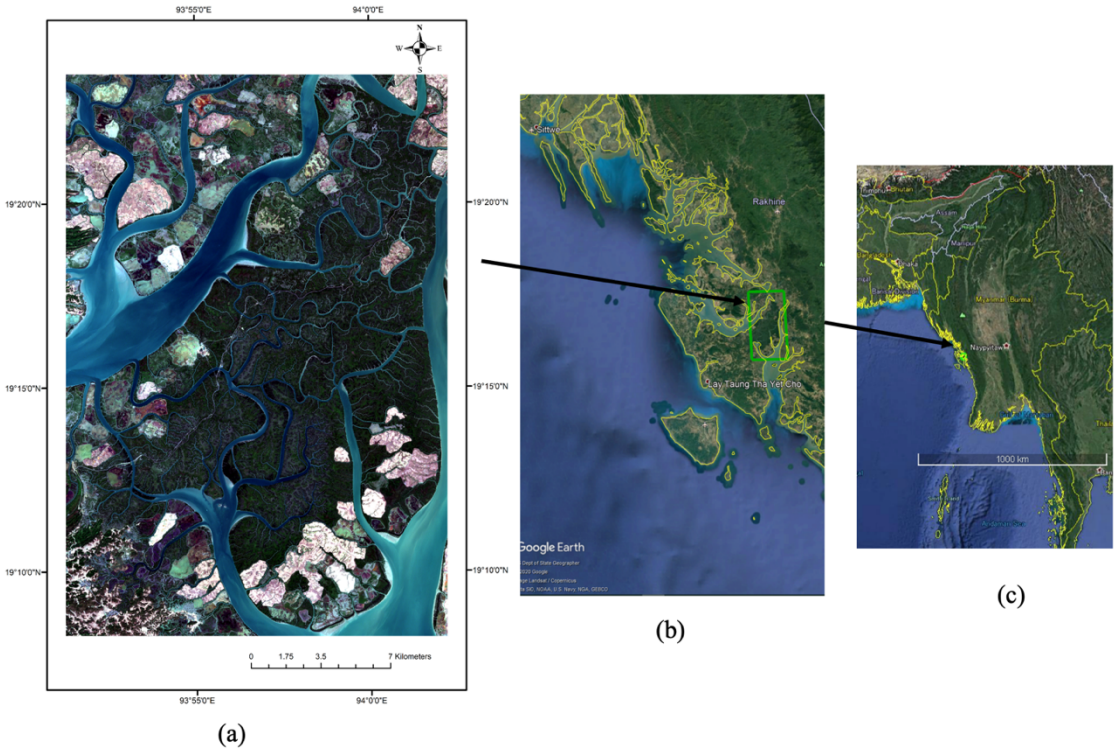

Figure 2.1 Location of the study area, (a) Wunbaik Mangrove Forest (Sentinel-2 true color image), (b) Rakhine coastal region (Google Earth Image), and (c) Myanmar (Google Earth Image)

2.2. Field Survey

2.2.1. Discussion with relevant officials and local community

In order to acquire updated information about the study area, field survey was conducted from September 1, 2019 to October 15, 2019. During the field survey, township staff of FD were interviewed first to know the current status of WMF and mangrove restoration programs. Focus group interview was conducted with the local community of two local villages, Myo Chun and Yan Thit Gyi, in order to understand local livelihood culture and their perspective on mangrove forest.

(a)

(b)

(c)

(d)

Figure 2.2 Interview with (a) Township Officer of FD, (b) local community, (c) and (d) shrimp pond owners

2.2.2. Collecting ground truth data

Being a large extent and various types of land use in the study area, latitudes and longitudes of ground truth points of each land-use types (Table 2.1) were collected using a handheld GPS (GARMIN etrex 10) (Figure 2.7 (a)), which is able to obtain coordinates with a horizontal accuracy of approximately 3m. Locations of the ground truth points are shown by matching photos takn in the field (Figure 2.3) and were used to create a ground truth image in ANN classification. The detailed GPS points were described in Appendix 1.

Table 2.1 Ground location points of different land-uses

Sr	Land-use type	Number of points
1	Water	20
2	Paddy field	6
3	Shrimp pond	13
4	Natural mangrove	30
5	Mangrove plantation	5
6	Other vegetation	6
	Total	80

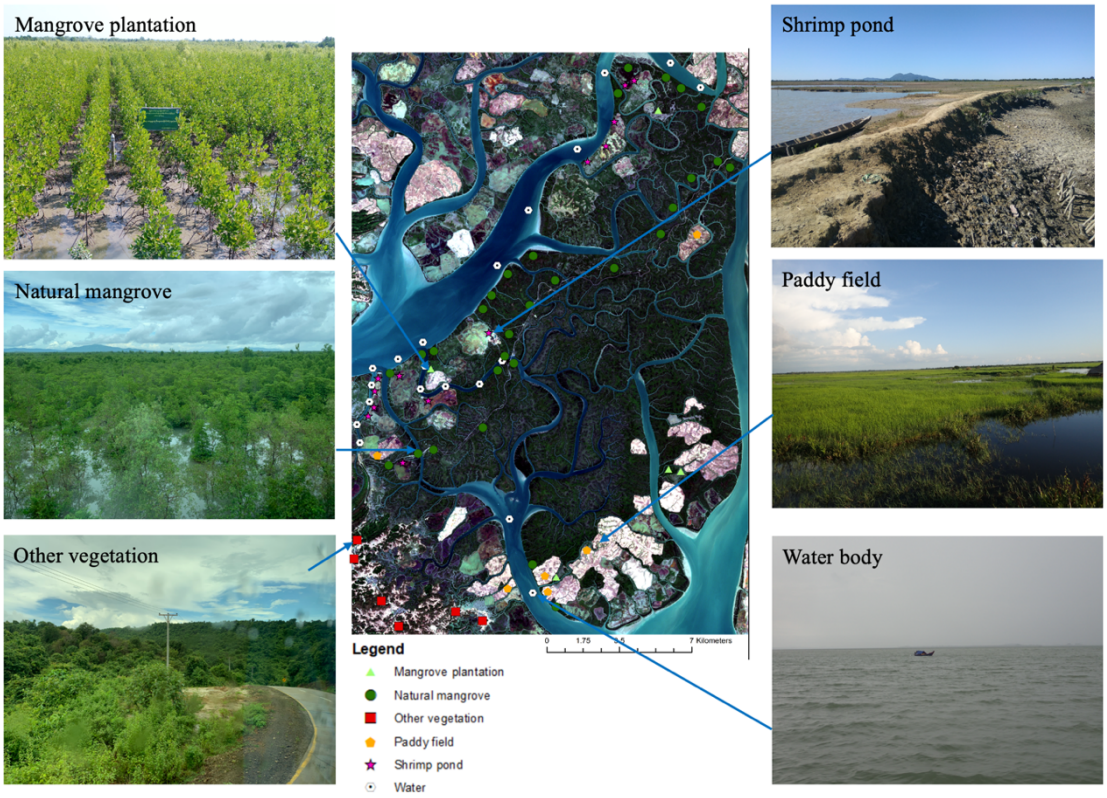

Figure 2.3 Ground location points of different land covers in the study area

2.2.3. Selection for naturally recovering sites

To explore natural recovery of mangrove from anthropogenic disturbances, firstly abandoned sites were selected by setting three criteria below.

(1) The abandoned sites must be under the same abandonment year.
(2) There are no planted mangroves in the abandoned area.
(3) Due to the mangrove area, accessibility to the selected sites was considered.

2.2.4. Surveying mangrove species specifications and environmental parameters

Although mangrove species identification has been attempted by using freely accessible satellite images[33][34], resultant accuracies were not satisfied compared to the performance of commercial satellite images with very high resolution.

Since this study aims to identify early recovered mangrove species at a small extent of abandoned sites, field surveying was more appropriate to delineate species diversity rather than the application of medium resolution satellite images.

To collect mangrove species specification, sample plots were designed into circular shape with 10 m diameters and subplots were established 5 m and 3m diameter (Figure 2.4). To meet the objective of species diversity, before setting up sample plots, the survey team randomly checked where species types are diverse. Within 10 m diameter of each sample plots, every tree, which has a diameter breast height (DBH>3cm) was enumerated by recording species name, DBH (at 1.3 m) and tree heights. Similarly, species having 1-3 cm of DBH were recorded within the 5 m subplot and <1 cm as seedlings in the 3 m subplot. A total of 50 sample plots for three abandoned ponds could be implemented during the field study (Figure 2.5) and their coordinate positions were also recorded as described in Appendix 1.

.

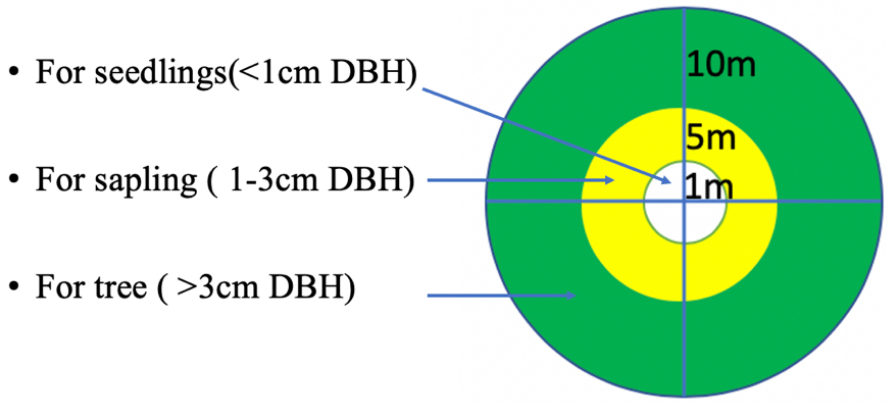

Figure 2.4 Sample plot design used in the field study for surveying mangrove specification

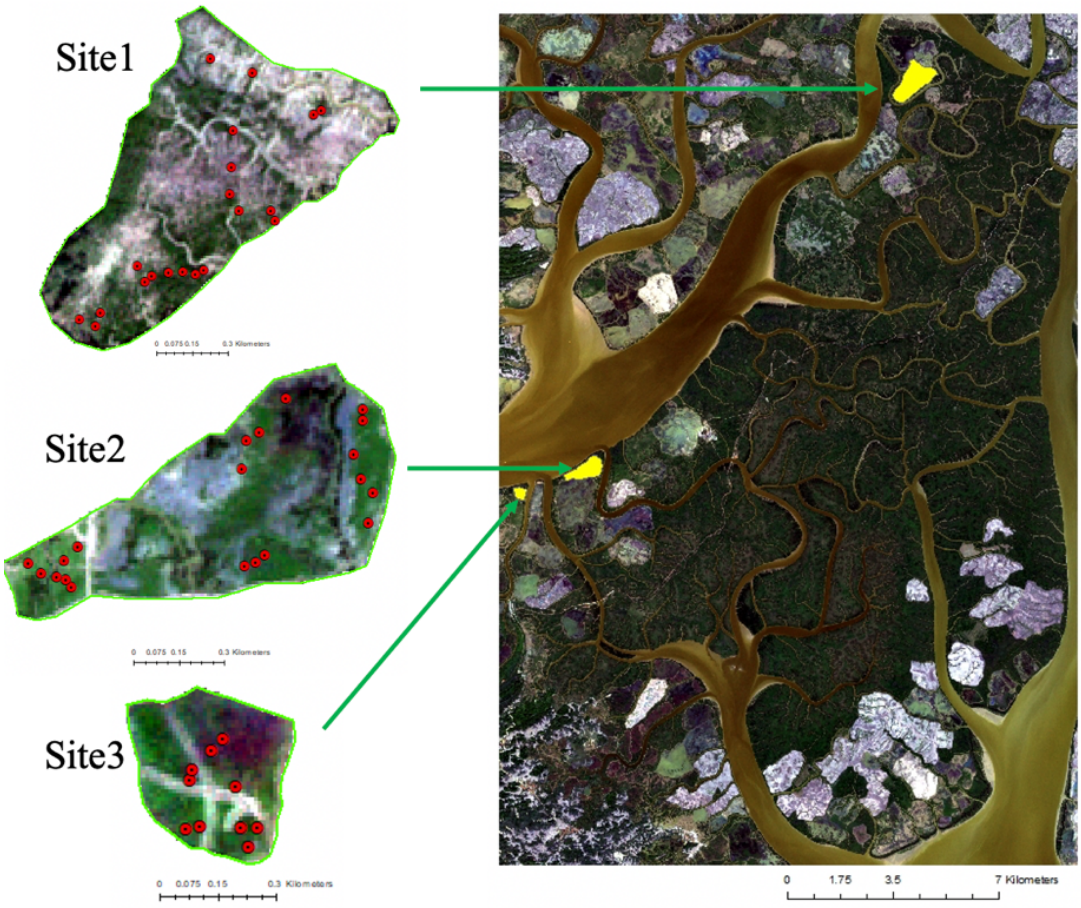

Figure 2.5 Locations of three selected abandoned sites and sample plots (Sentinel-2 true color image)

Figure 2.6 Surveying mangrove species specification in a sample plot

Because each mangrove species has its preferable salinity range, salinity is one of the key parameters, which can affect mangrove species distribution[35]. By knowing the salinity preference of recovered mangrove species, suitable species could be selected if it is necessary to plant in certain areas of abandoned sites for mangrove rehabilitation. Salinity data were collected in each sample plot (Figure 2.8 (b))and surrounding water channels (Figure 2.8(a)) by using AAQ1186-H multi-parameter water quality meter (Figure 2.7 (b)) during high tide period.

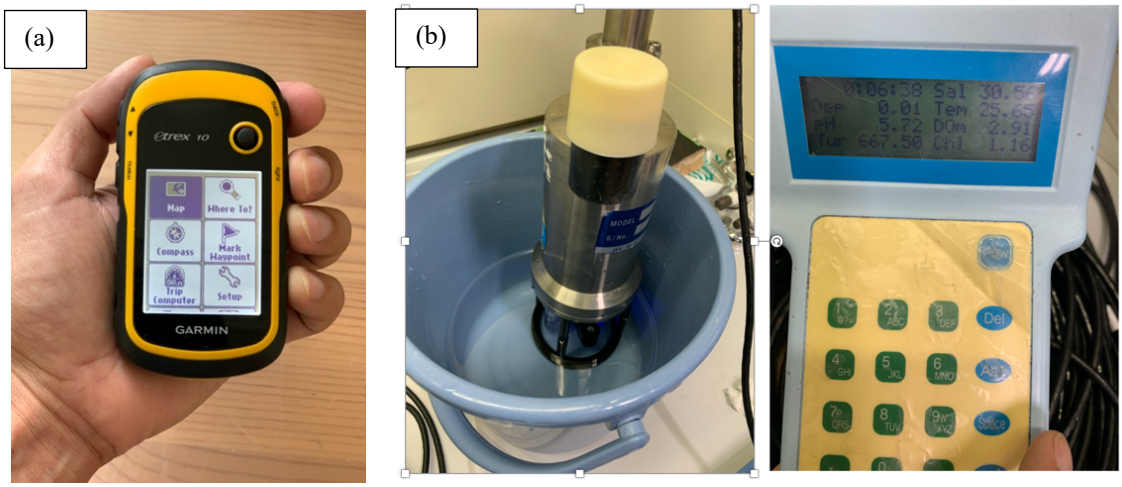

Figure 2.7 (a) Handheld GPS (GARMIN etrex 10) , (b) Water quality meter for salinity data collection

Figure 2.8 (a) Measuring water salinity in a surrounding creek and (b) in a sample plot

Surface elevation plays an important role in the establishment of early stage of different mangrove[36], which is why, in order to compare the occurrence of recovered mangrove species depending on elevation, ground truth of topographical information was acquired in the selected recovering sites by using Post-Processed Kinematic (PPK). In order to obtain elevation of the three selected sites, freely accessible different digital elevation models (DEM) were evaluated by using PPK ground truth elevation.

PPK is an alternative way to Real-Time Kinematic (RTK) and does not require a correction link between base and rover (Figure 2.10). Field measurement from both base and rover was recorded as raw log files separately. Being the fact that PPK is not a real time measurement as RTK, centimeter-level accuracy can only be obtained through RTKLIB software in which starting and ending collection time were provided to conduct post-processing [37]. Since PPK provides ellipsoidal height in default, geoid height calculator software was used to convert to orthometric values by submitting latitude and longitude information, and processed ellipsoidal height values [38].

(a) (b)

Figure 2.9 Application of PPK in the field;(a) Base station and (b) Rover position

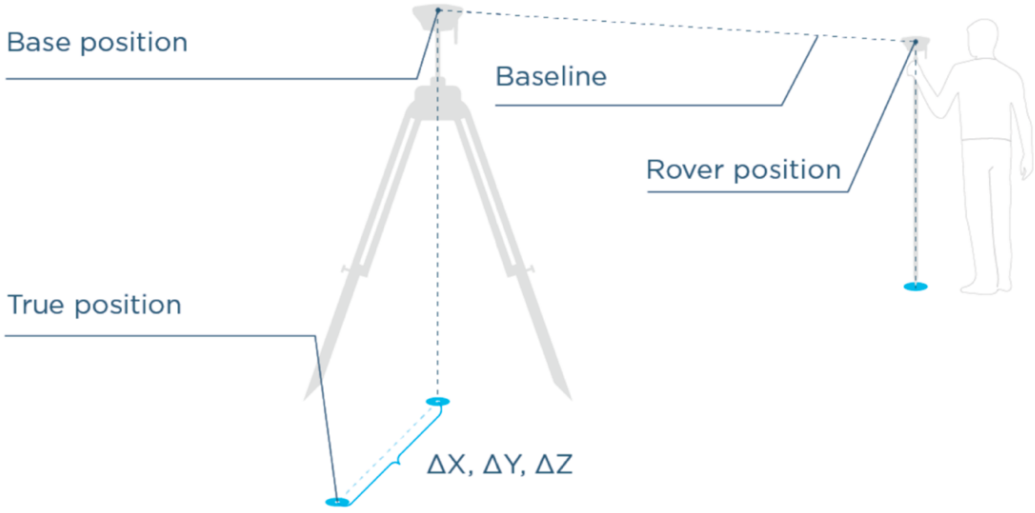

Figure 2.10 Configuration of PPK system

(https://docs.emlid.com/reachrs/common/tutorials/placing-the-base/)

2.3. Dataset Creation for Classification

2.3.1. Sentinel-2 satellite imagery

To detect mangrove changes and recovering areas of the selected abandoned sites, this study utilized two different dates of cloud-free Sentinel-2 images, which are January 21, 2020 and December 26, 2015. For creating necessary datasets for ANN classification, the sets of multispectral bands of Sentinel-2 satellite imagery were collected from the Copernicus Open Access Hub[39] by using semi-automatic classification plugin (SCP) in QGIS.

Two major products of Sentinel-2 imagery, which are Level-1 C and Level-2 A are currently disseminated to users by the European Space Agency. Level-1 C provides orthorectified Top-Of-Atmosphere (TOA) reflectance while Level-2 C, which was extended globally in December 2018 offers orthorectified Bottom-Of-Atmosphere (BOA) reflectance[40]. The spatial resolutions of multispectral bands acquired by Sentinel-2 are 10m, 20m, and 60m respectively. Detailed information is described in Table 2.2 [40]. This study applied only 10 bands other than band 1, band 9 and band 10, which are poor spatial resolution with 60m and not related with the aim of mangrove classification.

Table 2.2 Specification of Sentinel-2 bands

Bands	Spectral region	Central wavelength(nm)	Resolution
Band 1	Coastal aerosol	443	60
Band 2	Blue	490	10
Band 3	Green	560	10
Band 4	Red	665	10
Band 5	Vegetation Red Edge	705	20
Band 6	Vegetation Red Edge	740	20
Band 7	Vegetation Red Edge	783	20
Band 8	Near Infrared	842	10
Band 8A	Near Infrared narrow	865	20
Band 9	Water vapor	945	60
Band 10	Short wave infrared/ Cirrus	1380	60
Band 11	Short wave infrared (SWIR1)	1910	20
Band 12	Short wave infrared (SWIR2)	2190	20

2.3.2. Satellite image preprocessing

Since satellites acquired remotely sensed images of earth objects from space, there are radiometric and atmospheric disturbances between the satellite sensor and earth surface[41]. As a consequence, this process may undermine image quality, which is why image preprocessing is necessary to overcome this problem after obtaining desired satellite images. Atmospheric correction is a process by which

the scattering and absorption effect of gases and aerosols in the atmosphere are eliminated to improve reflectance values of satellite images[42].

As aforementioned in section 2.3.1, only Level-1 C products in 2015 were required for atmospheric correction because Sentinel-2 images acquired in 2020 are Level-2 A products. The multispectral bands of the 2015 dataset were therefore atmospherically corrected through the SCP tool in QGIS. Sentinel-2 bands with different resolutions were resampled to 10 m resolution through nearest neighbor algorithm for both 2015 and 2020[43].

2.3.3. Spectral indices of NDVI, NDWI, and CMRI

Apart from multispectral bands of satellite images, spectral indices are one of the effective features that can offer information about land-uses and land covers. Among various spectral indices, normalized difference vegetation index (NDVI), normalized difference water index (NDWI), and combined mangrove recognition Index (CMRI) were used as input features for training a neural network model in this study.

NDVI is a global vegetation index, which provides pivotal information for vegetation analysis, and land-use and land cover mapping. To provide precise data to the neural network model, NDVI was derived from band 8 (NIR) and band 4 (RED) of Sentinel-2 image by using Equation 1[44]. NDVI values range from -1 to 1 and dense vegetation cover usually produces higher values while non-vegetative areas such as water, paddy fields, shrimp ponds and the like show low NDVI values.

$$\mathrm{NDVI} = \frac{\mathrm{NIR}-\mathrm{RED}}{\mathrm{NIR}+\mathrm{RED}} \qquad (1)$$

NDWI is a widely used index, which can enhance water information in remote sensing images and assist in discriminating between water and other land covers, such as vegetation and soil[45][46]. NDWI was calculated by using band 3 (Green) and band 8 (NIR) of satellite-2 image in Equation 2 [45]. Like NDVI, the

value of NDWI also ranges from -1 to 1 but water bodies have larger values while vegetation cover produces smaller values.

$$\text{NDWI} = \frac{\text{NIR} - \text{Green}}{\text{NIR} + \text{Green}} \qquad (2)$$

With the aim of distinguishing mangrove and other vegetation, CMRI was developed based on NDVI and NDWI [47]. For study areas where mangrove and non-mangrove vegetation are mixed, CMRI produced higher accuracy than using NDVI and NDWI separately. CMRI can be derived by subtracting NDWI from NDVI values as shown in Equation 3.

$$\text{CMRI} = \text{NDVI} - \text{NDWI} \qquad (3)$$

2.3.4. Topographic information

This study applied topographic information to two sections; (1) ANN classification and (2) discussion about environmental preference of recovered mangrove species. Integration of additional features, such as topographic information, into natural resource assessment of remote sensing approach can improve accuracy of classification[48]. Accurate elevation data is critically important to compare environmental preference of recovered mangrove species. It is however difficult to collect topographic data over the whole study area during the field trip due to the inaccessibility of mangrove area. Due to a lack of regional detailed elevation data, three global digital elevation models (DEM) were therefore explored to cover the study area.

a) Shuttle Radar Topography Mission (SRTM)

During the SRTM mission in February 2000, SRTM 1 Arc Second DEM was created from C-band radar data acquired by cooperation of National Aeronautics and Space Administration (NASA) and the National Geospatial-Intelligence Agency (NGA)[49]. SRTM1 DEM provides users elevation values with 30 m resolution referring to the WGS84 ellipsoid as horizontal datum and geoid as vertical datum and can be downloaded on USGS earthexplorer website freely [50].

b) Advanced Land Observing Satellite (ALOS)

ALOS World 3D – 30m (AW3D30) is provided free of charge by the Japan Aerospace Exploration Agency (JAXA) with 30 m resolution of digital surface model (DSM) generated by the PRISM panchromatic optical sensor on the Advanced Land Observing Satellite "DAICHI" (ALOS) launched from January 2006 to April, 2011 [51][52].

c) Multi-Error-Removed-Improved-Terrain (MERIT)

MERIT DEM was developed with the aims of reduction in vertical errors of SRTM3 (90m resolution) and ALOS World 3D – 30m (AW3D30). MERIT DEM offers true digital terrain model (DTM) with 90m spatial resolution in geoid datum for global area between 90N-60S by providing significant accuracy improvement in swamp forest. MERIT DEM was downloaded free of charge on the website of MERIT DEM: Multi-Error-Removed-Improved-Terrain [53].

Since different DEMs have different pros and cons depending on the targeted area, these global DEMs were evaluated by using the PPK ground truth data in order to achieve the most appropriate one for the mangrove area. SRTM, ALOS and MERIT DEMs were geographically corrected by converting to WGS 1984 UTM zone in ArcGIS. Their elevation data with the same locations of 45 ground truth points (See Appendix 3) were then extracted to create a dataset (Figure 2.11). Root Mean Square Error (RMSE) (Equation 4) was applied to achieve the most suitable DEM, which can provide accurate elevation values for the mangrove area [54].

$$\mathrm{RMSE_z} = \sqrt{\frac{1}{\mathrm{N}} \sum_{\mathrm{i=1}}^{\mathrm{N}} \left(\mathrm{Z_{dem}} - \mathrm{Z_{ppk}}\right)^2} \quad (4)$$

In (4, N represents number of elevation points, $\mathrm{Z_{dem}}$ is elevation values of DEM, and $\mathrm{Z_{ppk}}$ is elevation values of PPK ground data.

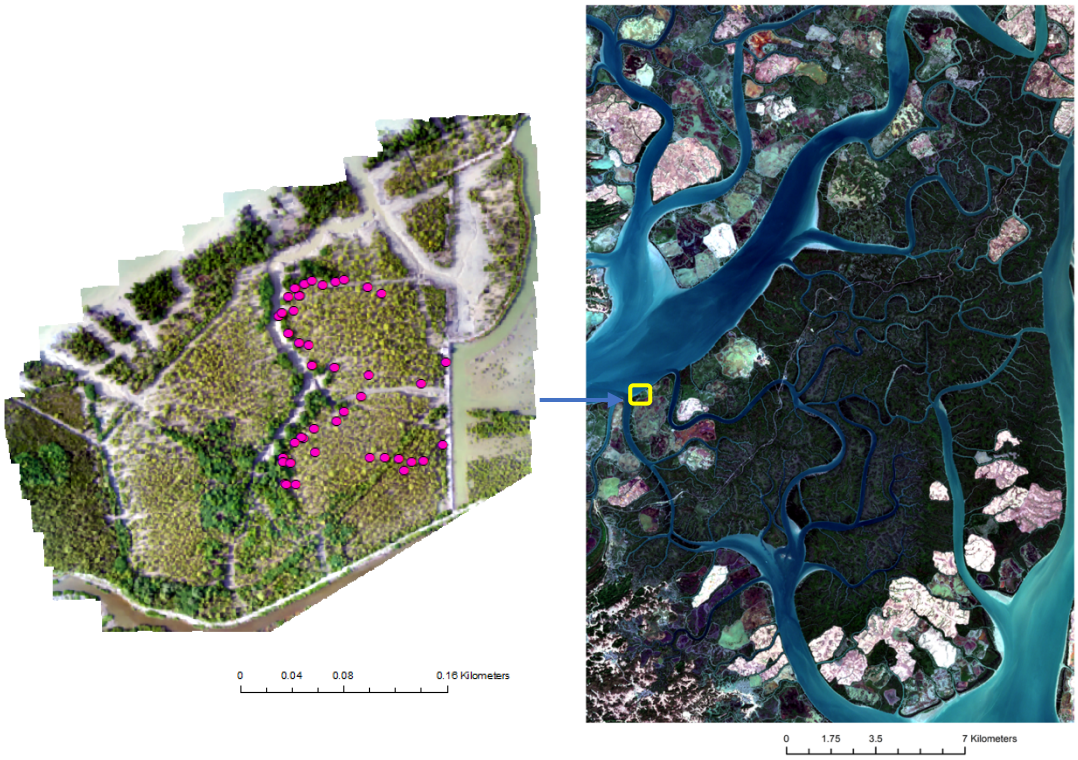

Figure 2.11 Locations of PPK ground truth points in the study area for DEM evaluation

2.3.5. Canopy height information

Canopy height information derived from multiple remote sensors such as LiDAR, SAR and unmanned aerial vehicle (UAV) has widely been used as one of the important features in tree species classification. Previous studies reveal that classification accuracy can be improved significantly for discriminating different mangrove species by incorporating canopy height features[55][56]. However, there is still need to explore the effectiveness of canopy height model (CHM) in mangrove distribution where other vegetation types are mixed other than individual tree species classification.

Since DEM consists of two forms that are digital surface model (DSM) as reflection of earth objects such as trees and building and digital terrain model (DTM) as true elevation values with no disturbance of earth objects[57]. To create CHM of the study area, SRTM 30m resolution DEM was adopted as digital surface model (DSM) [58] and MERIT DEM as digital terrain model (DTM). CHM

could be obtained by subtracting MERIT DTM from SRTM DSM and then applied as an input feature in ANN classification (Figure 2.12).

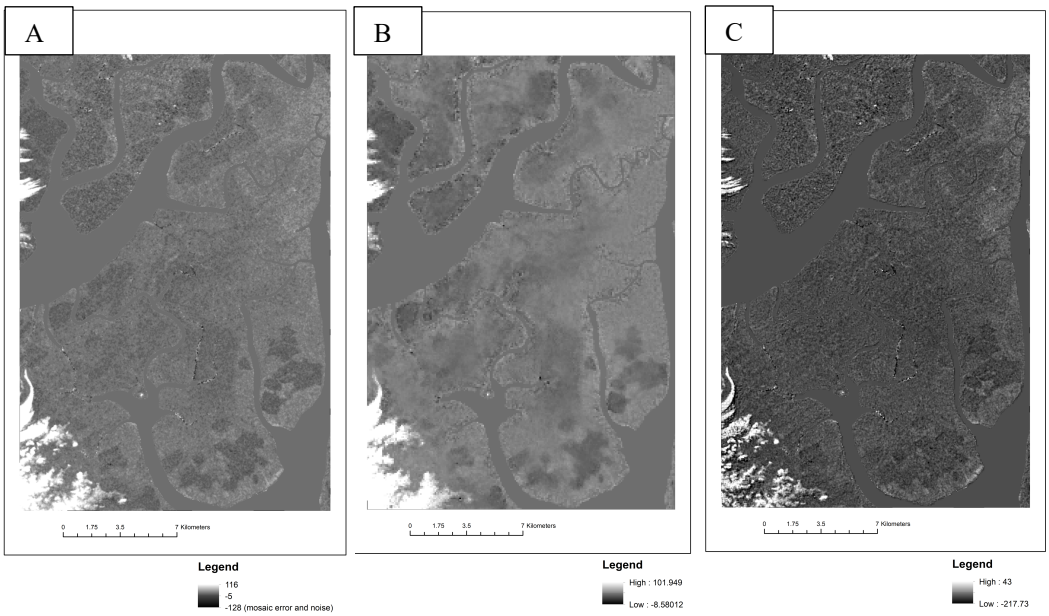

Figure 2.12 A. SRTM DSM, B. MERIT DTM and C. CHM

2.3.6. Creation of ground truth image

Preparing accurate ground truth data is necessary in supervised classification and also a major challenge for training and evaluating a neural network model. In order to obtain a reliable ground truth image, location points collected in the field (Appendix 1) were imported to ArcGIS. Using high resolution google earth imagery and different combinations of Sentinel-2 satellite bands, polygons were drawn manually by referring to same land cover of the ground truth points. With the aims of accurate mangrove recovery analysis, two major classes were then assigned as mangrove and non-mangrove, rather than multi classification which may lead to massive time consuming for ground truth image and sometimes allow to interfere with undesired classes. Assigned polygons were converted into a raster image with the 10m resolution because of pixel based classification. A ground truth image, which has assigned values of 0 and 255 for every pixel was obtained. The workflow of creating the ground truth image in this study was described in Appendix 4.

In remote sensing, image enhancement is primarily intended to assist visual interpretation of users by modifying image quality and supports ability to acquire more precise information for processing[41]. Among various approaches of image enhancement, this study conducted composite generation for Sentinel-2 satellite images in ArcGIS. By selecting and combining desired bands simply, the graphical appearance of the image was changed depending on the bands in use. This study created three combinations of bands in which firstly band 4; red, band 3; green and band 2; blue, which are visible wavelengths were selected. They are basically known as true color images in remote sensing (Figure 2.13(a)). Second combination using band 8; near infrared (NIR), green and red bands was analyzed with the aims of more distinct vegetation cover (Figure 2.13(b)). Lastly, a combination of band 12 (SWIR), band 8 (NIR) and band 3 (green) was critically effective for visual analysis of submerged mangrove, which cannot be seen in the first two combinations (Figure 2.13(c)). False color images provided to overcome such issues in manually creating an accurate ground truth image for mangrove classification.

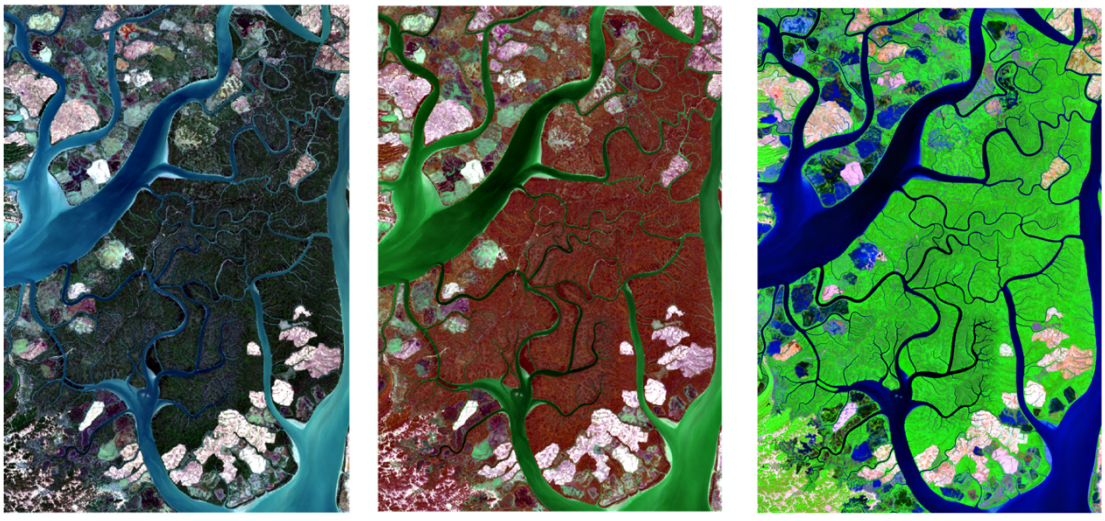

(a) (b) (c)

Figure 2.13 Combination of Sentinel-2 bands (a) band 4 (Red), band 3 (Green) and band 2 (Blue), (b) band 8 (NIR), band 3 (Green) and band 4 (Red), and (c) band 12 (SWIR), band 8 (NIR) and band 3 (Green)

2.3.7. Dataset preparation

After image preprocessing of satellite images, a multi-spectral Sentinel-2 image with selected 10 bands, NDVI, NDWI, MERIT DEM, CHM and corresponding ground truth images were obtained for input features (Figure 2.14). Although image preprocessing of all images was mentioned collectively first, reason for applying specific images will be described in each experiment since this study conducted different experiments as preliminary. Being a supervised pixel-based classification, all pixels of 53939393 of which each raster images have the same width and height of 1914 × 2814 pixel with 10m resolution were counted as the dataset.

(a) (b)

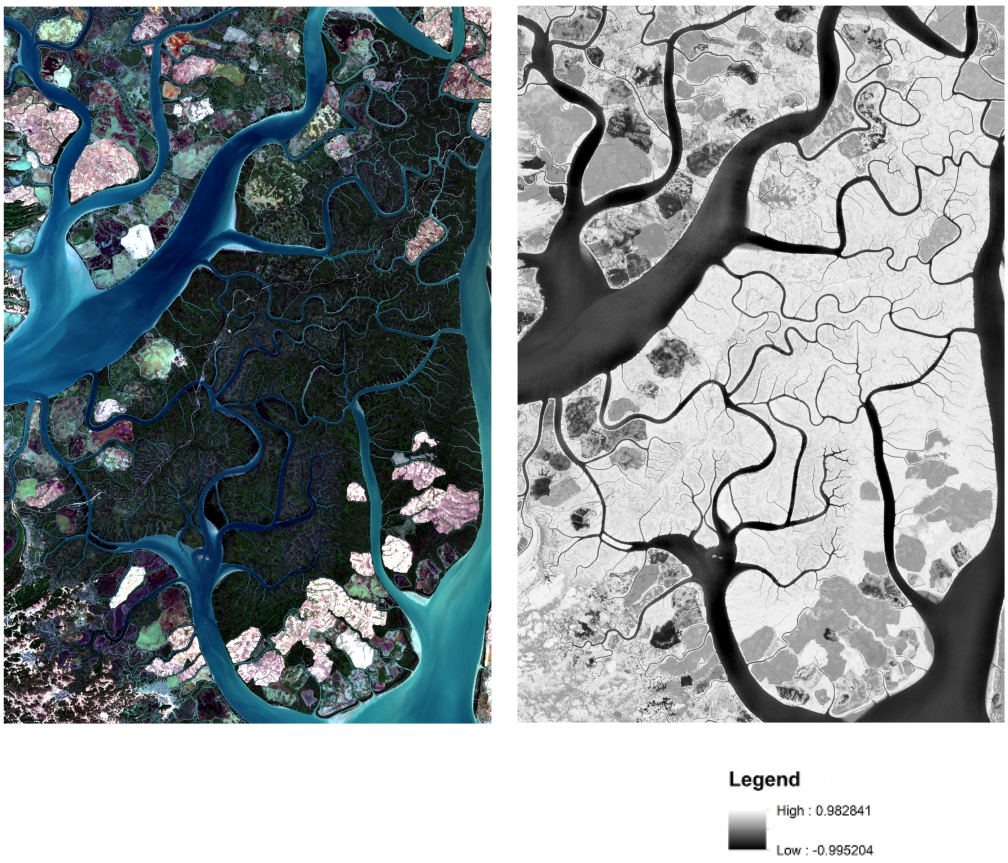

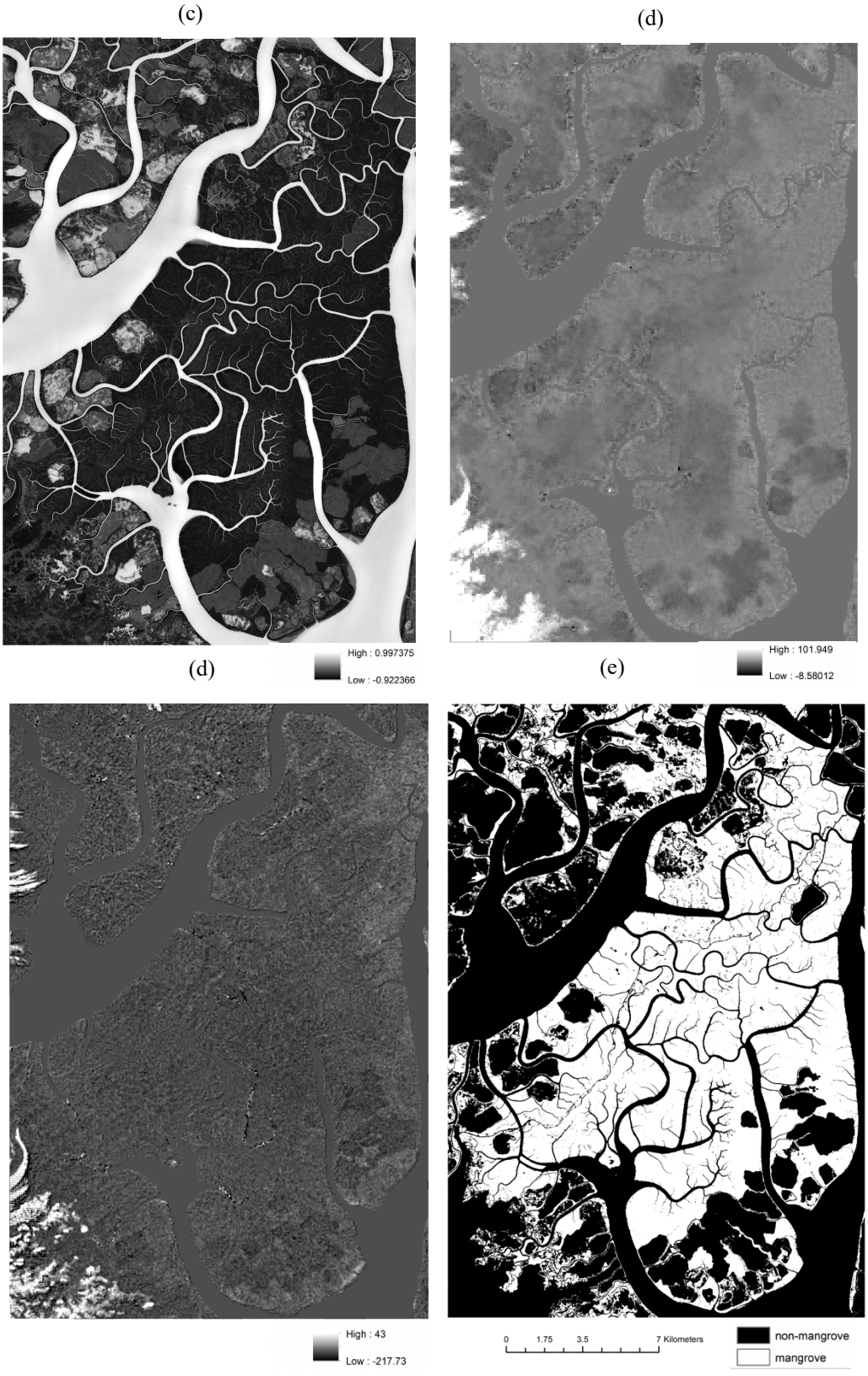

Figure 2.14 (a)Multispectral Sentinel-2 image, (b) NDVI image, (c) NDWI image, (d) MERIT DEM image, (e) CHM image and (f) ground truth image

2.4. Artificial Neural Network (ANN)

Considering the structure of the biological neural network of human nervous system, an ANN model primarily consists of multi-layer perceptron (MLP), which has an input layer, hidden layer and output layer, and interconnected operating nodes similar to brain nerve cells in each layer[59]. The nodes in the input layer transfer feature values (x_i), weight information (w_i) and bias (b) from a dataset to the hidden layer. In the hidden layer, data obtained from input layer are analyzed through an activation function in each node and convey the generated data (y_i) to the output layer as Equation 5 (Figure 2.15).

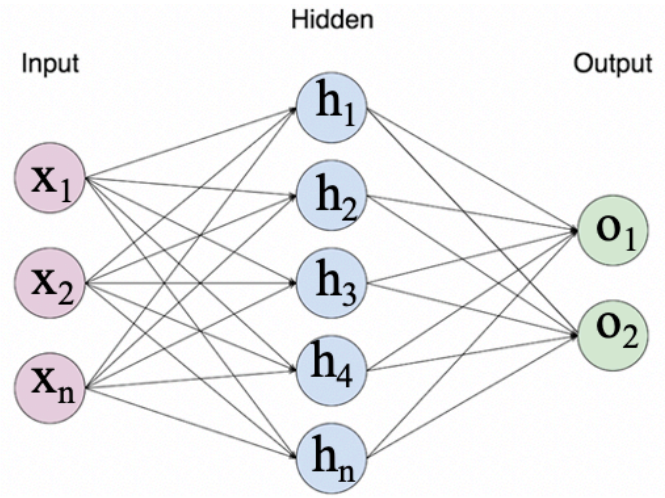

Figure 2.15 Basic architecture of an ANN model

2.4.1. Creation of a basic ANN model

Referring to the basic model architecture, an ANN model was first created by using only one hidden layer with 12 neurons as a basic model in this study (Figure 2.16). We then explored input parameter and hyperparameter tunings in which different experiments were conducted to obtain the most suitable combination of input features for mangrove classification and an optimum design of an ANN model by tuning number of hidden layers and neurons.

In case of analyzing data within a neural network, activation function in each hidden neuron is essential to determine the output of a neural network by processing input and weight information[60]. This study employed rectified linear unit (ReLU), which is actually a non-linear function using backpropagation and most popular because of less computational expensive than other activation functions[61–63]. According to ReLU equation ((6), the function produces linear values if the input data is larger than 0 but 0 for negative values. Softmax function [64][65], normalizes output value ranging values from 0 to 1 and yields the probability of the input value as a particular class by dividing the summation (Equation 7). Due to such normalized output, the function was usually applied for the output layer in the neural network and so did this study.

$$y_i = \sum(w_i x_i) + b \quad (5)$$

$$f(y_i) = \begin{cases} y_i \text{ if } y_i > 0 \\ 0 \text{ otherwise} \end{cases} \quad (6)$$

$$f(y_i) = \frac{\exp(y_i)}{\sum_i \exp(y_i)} \quad (7)$$

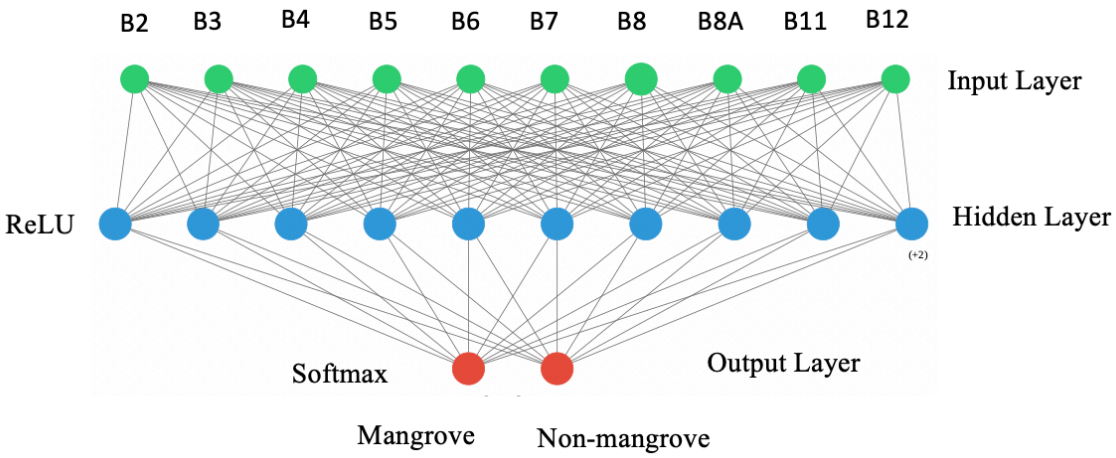

Figure 2.16 Basic ANN model used in this study

2.5. Artificial Neural Network Classification for Mangrove Distribution

This section mainly focused on ANN classification in which two different experiments for input feature selection using a basic ANN model and hyper-parameter tuning for the ANN model were explored. A new dataset was then classified in order to propose a robust ANN model. After classifications of two different datasets in 2015 and 2020, natural recovery mangroves were assessed using change detection method. A comprehensive workflow is structured as Figure 2.17 and detailed explanations for each part were described in each subsection.

After preparing necessary image dataset, preprocessing and classification were conducted on python (3.7 version) environment in Linux by using primarily rasterio, which is effective for reading and exporting raster data with geoinformation, NumPy for handling satellite data as numerical values instead of graphical interface and TensorFlow for classifying dataset by building neural network model in machine learning approach. (See Appendix 5.)

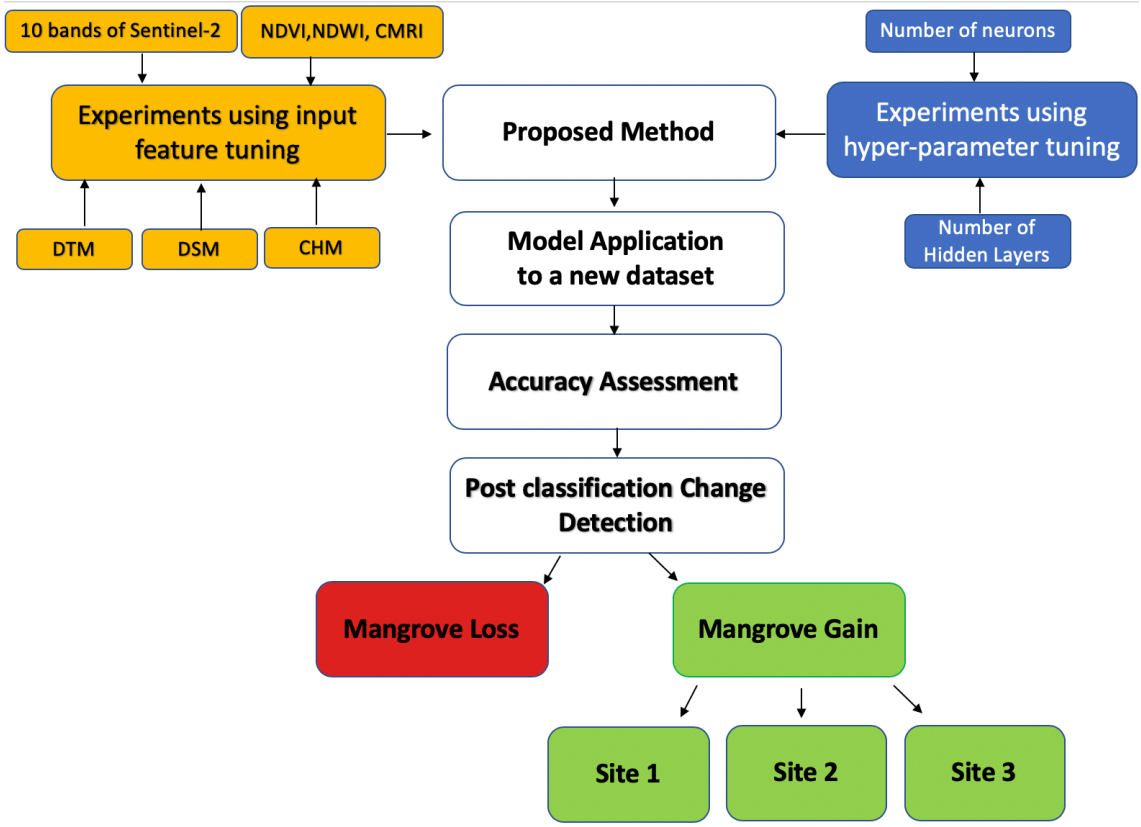

Figure 2.17 Workflow of natural recovery assessment in this study

2.5.1. Experimental analysis for input feature selection

With the objectives of selecting the most appropriate input feature combination for mangrove distribution, the study first conducted different experimental classifications by using the basic ANN model in this section. The raster images of input features and ground truth image were converted into numerical datasets and were created 15 experimental datasets through different combinations. The datasets were then reshaped into three-dimensional form as the ANN model basically expected.

The dataset was divided into three parts; (1) training data (60%), testing data (20%) and validating data (20%) by using preprocessing modules of scikit-learn data processing library. The training dataset was applied to teach an ANN model by referring to labelled data of ground truth image while the validating dataset was used to watch out the behavior of the model in every epoch of training session simultaneously. By using cross validation method, we can verify whether the model is overfitting or not in which even if the accuracy of the training data will increase, that of the validating data will be stable or decrease during training time.

The model was trained by using the training dataset with 30 epochs equally for all experiments and the trained model was applied to the testing dataset to evaluate its performance through overall accuracy and kappa index. After conducting classification using the trained model, the output dataset was exporteded as a raster format containing geographical information. The output raster images were visually analyzed by using true color Sentinel-2 images and high-resolution Google Earth imagery in ArcGIS environment. All datasets were analyzed through the same approach to select a combination of input features, which can produce not only a highest accuracy but also a high qualified output map for mangrove classification.

2.5.2. Experimental analysis using hyper-parameter tuning

Since an ANN model is composed of neurons in the multi-layer that are of great importance to the capacity of data analysis, the behavior of the ANN model and the resultant accuracy are subjected to change depending on the number of hidden layers and neuron insides. Based on a specific case, some studies have proposed various methods to meet the question, “How can the number of hidden layers and neurons be decided in an ANN model?”. [66–68]. Because of different complexity in different problems to solve, the present study decided the number of hidden layers and neurons by means of experimental results based on trial and error. The basic model was added one hidden layer in each training time and a suitable number was decided for mangrove classification. After selecting the suitable number of hidden layers, numbers of neurons in the hidden layers were tuned by decreasing and increasing double. Except for numbers of hidden layers and neurons, the model was trained with the same setting in which adaptive moment estimation (Adam) optimizer with learning rate 0.001 and the number of epochs 30 were applied.

2.5.3. Accuracy assessment

Accuracy assessment is one of the major phases in image classification to evaluate the performance of model and most widely used measures for assessing accuracy of satellite image classification are overall accuracy and kappa coefficient[69]. First of all, a confusion or error matrix, which represents ground truth pixel in a column and classified pixel in row for each class was created as shown in Table 2.3 .

Table 2.3 A confusion matrix for accuracy assessment of ANN classification

Confusion matrix		Ground truth pixel		
		Non-mangrove	Mangrove	Total
Classified pixel	Non-mangrove	N_{NT}	N_{MT}	N_{NR}
	Mangrove	N_{NF}	N_{MF}	N_{MR}
	Total	N_{NC}	N_{MC}	N

Overall accuracy can be calculated by dividing the sum of truly classified pixels of each class by total number of pixels in diagonal elements of the confusion matrix (Equation 8).

$$\text{Overall accuracy} = \frac{N_{NT}+N_{MT}}{N} \times 100 \ (\%) \qquad (8)$$

Kappa coefficient has been one of the popular measures to assess classification accuracy in remote sensing since 1983[70]. Unlike the overall accuracy, kappa coefficient takes not only true positive pixel and false negative pixel but also non diagonal elements in a confusion matrix into account by Equation 9 [71]. Kappa coefficient value ranges from 0 to 1 (the closer to 1, the higher accuracy of classification). Knowing the kappa coefficient can therefore evaluate the performance of a classification method in remote sensing.

$$\hat{K} = \frac{N\sum_{i=1}^{r} Xii - \sum_{i=1}^{r}(X_{i+}\, X_{+i})}{N^2 - \sum_{i=1}^{r}(X_{i+}\, X_{+i})} \qquad (9)$$

In the above equation, r is number of rows and columns in the error matrix, N is total number of observations (N in the error matrix), Xii is observation in row

i and column i ($N_{NT} + N_{MT}$), X_{i+}= marginal total of row i (N_{NR} N_{NC} in the error matrix), and X_{+i} = marginal total of column i (N_{MR} N_{MC} in the error matrix).

2.5.4. Post classification change detection

Knowing accurate information about mangrove changes is crucial to mangrove conservation not only to figure out what happened in the past but also to implement future restoration programs and formulate necessary regulations for sound regional management system[72]. Among various change detection methods, this study conducted post classification change detection which excels by providing promising results based on classification accuracy[73]. The two classified images in 2015 and 2020 were differentiated in the post-classification change detection analysis. Extensive changed areas were then highlighted to know main drivers of mangrove dynamics and findings were clarified by using Sentinel-2 satellite images in ArcGIS (10.6 version) and high resolution google earth imagery.

2.5.5. Assessment of natural recovery of mangrove

Since natural recovery is one of the opportunities for mangrove conservation as mentioned in the introduction section, this study focused on natural recovering mangrove at different abandoned shrimp ponds in terms of spatially and species diversity. To identify naturally recovering areas for different abandoned shrimp ponds, three selected sites were extracted from the change detection image. Naturally recovering areas were quantified based on a pixel by pixel calculation and then three selected recovering mangrove areas were compared.

This study delineated species information at the three recovered sites by using Important Value Index (IVI) formula (Equation 10)[74], which is used to measure how dominant a species is in a forested area. The values of right-hand sided parameters, Relative Density (RD1) (Equation 11), Relative Frequency (RF) (Equation 12) and Relative Dominance (RD2) (Equation 13) are often expressed as percent. IVI, the sum of these three measures, therefore ranges from 0 to 300. A species, which has higher IVI value is more dominant than other species in a site.

$$\mathrm{IVI} = \mathrm{RD1} + \mathrm{RF} + \mathrm{RD2} \qquad (10)$$

$$RD1 = \frac{\text{No of individuals of a species}}{\text{Total No. of individuals of all species}} \times 100 \qquad (11)$$

$$\mathrm{RF} = \frac{\text{No of plots containing a species}}{\text{Total of frequency of all species}} \times 100 \qquad (12)$$

$$\mathrm{RD2} = \frac{\text{Basal Area(BA) of a species}}{\text{Total basal area of all species}} \times 100 \qquad (13)$$

$$\mathrm{BA} = \frac{\pi \times (\mathrm{DBH}/_2)^2}{144} \qquad (14)$$

Moreover, the study explored mangrove species diversity of three different recovered sites by using Shannon-Weiner index (H) in Equation 15 in which $\mathrm{H_{max}}$ is maximum diversity possible or richness (Equation 16), E is evenness of species (Equation 17), $\mathrm{p_i}$ is proportion of individual of particular species i divided by total number of species found and $\mathrm{N_s}$ represents the number of species [75]. Since a larger Shannon index value represents higher species diversity of an area, we can compare species diversity of different recovered sites in this study.

$$\mathrm{H} = -\sum_{\mathrm{i}=1}^{\mathrm{S}} \mathrm{p_i} \ln \mathrm{p_i} \qquad (15)$$

$$\mathrm{H_{max}} = \ln \mathrm{N_s} \qquad (16)$$

$$\mathrm{E} = \frac{\mathrm{H}}{\mathrm{H_{max}}} \qquad (17)$$

Chapter 3 RESULTS

3.1. Selection of DEM for Study Area

According to RMSE analysis using PPK ground truth elevation, MERIT DEM produced a smallest RMSE value of 0.5914 m for the study while the values of SRTM and ALOS DEMs were 0.844 m and 2.140 m, respectively (Figure 3.1). The association of elevation derived from these three different DEMs and PPK ground truth values was shown in Figure 3.2. Therefore, this study selected MERIT DEM as one of the input features in artificial neural network classification and elevation parameters for recovering mangrove species.

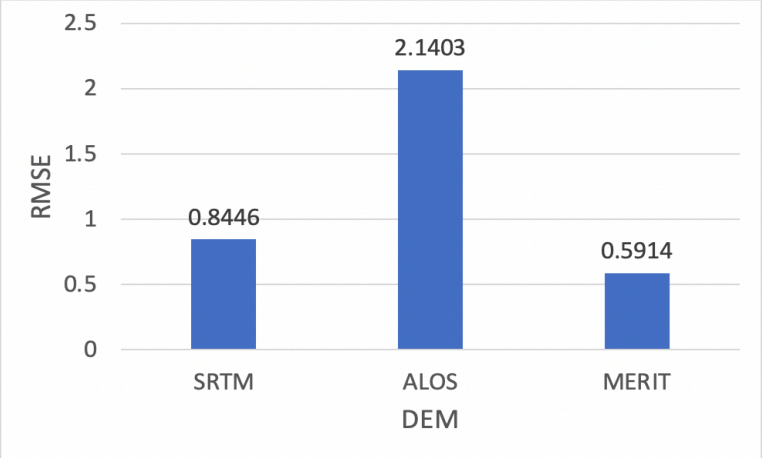

Figure 3.1 Root mean square error of three DEMs for mangrove area

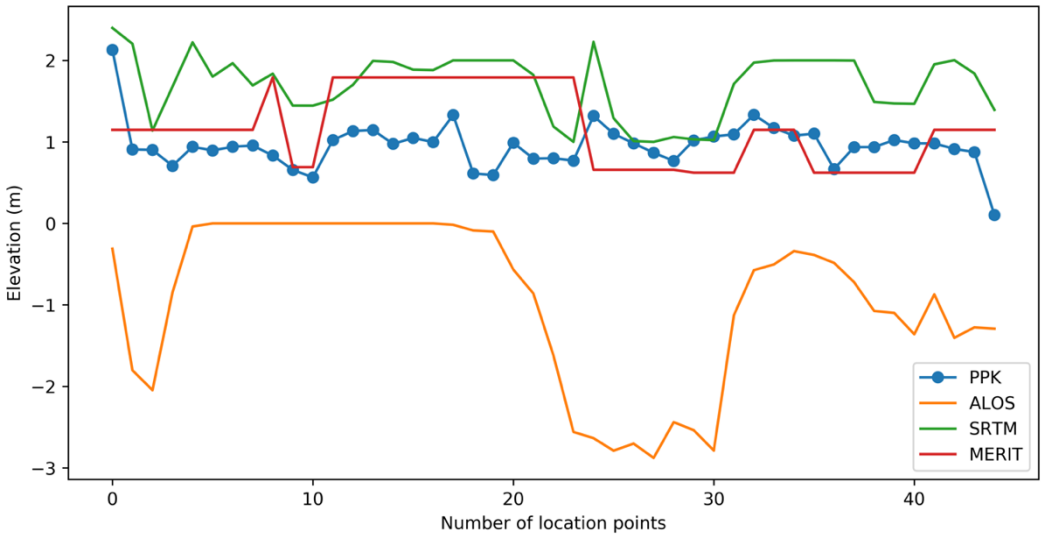

Figure 3.2 Comparison of DEM values with PPK ground truth data

3.2. Experimental Results for Input Features Selection

Of total 15 experiments after conducting different classifications by adjusting input features, the experiment 6, which contains 10 bands of Sentinel-2 image, NDVI, NDWI, MERIT DEM and CHM yielded not only highest accuracy but also smooth pixel structure of the output image for mangrove distribution. Detailed explanations for some experiments were expressed in forthcoming sections but the rest are excluded because minor changes of input features were tested to confirm the experiments that yielded high accuracy. However, the summary of resultant overall accuracy and kappa index of all experiments was described in Table 3.1.

3.2.1. Experiment with satellite band information

Since different bands have various spectral ranges of wavelength, their interpretations for earth objects are diverse depending on reflectance of the objects (Figure 3.3). Being a dry season of image acquisition date, January, 2020, the reflectance of paddy fields is more distinct than other land cover except the wavelength range between 740 nm and 865 nm. Within this range, also vegetation cover which are both mangrove and non-mangrove, become dominant but all land covers can be separately seen from 1610 nm to 2190 nm wavelength acquired by band 11 and band 12.

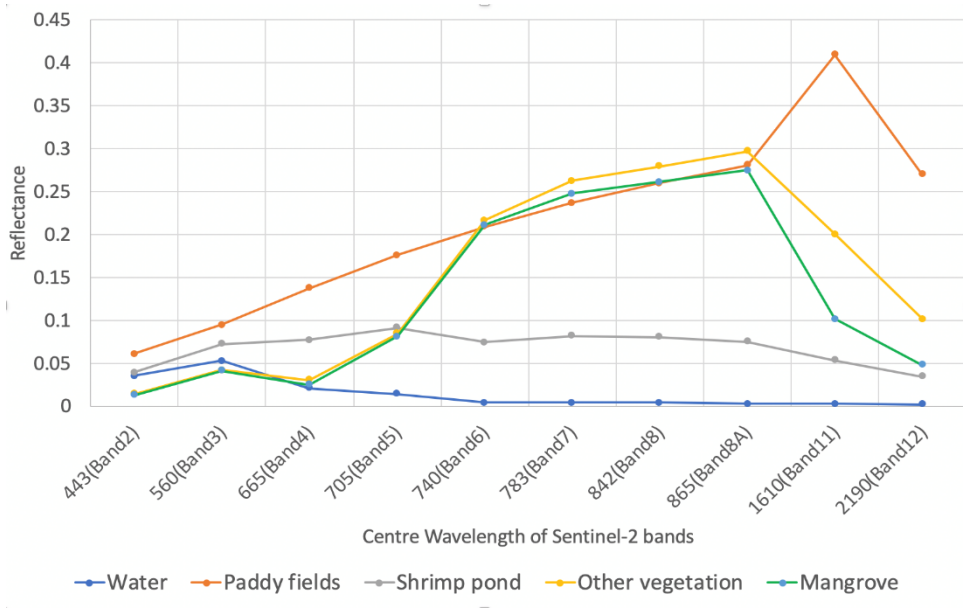

Figure 3.3 Spectral reflectance of 10 bands of Sentinel-2 image on different land covers

Therefore, 10 bands of Sentinel-2 satellite image were applied for input features as a first experiment in neural network classification. After training the model with 30 epochs and evaluation using test dataset, the experiment1 produced unsatisfactory accuracy of 56.39%. The dataset with only satellite bands was not enough to classify mangrove distribution using ANN model. The experiment 1 was neglected to produce output image of classification result because of poor accuracy.

3.2.2. Experiments adding spectral indices

According to the result of experiment 1, more informative input features were required in classification and hence two spectral indices of NDVI and NDWI were added in experiment 2. After processing as the same procedures, the relatively higher accuracy of 93.43% than the experiment 1 was achieved. Since the study area has not only mangrove but also water, shrimp ponds, paddy fields, and other vegetation, detailed analysis was considered to meet such a multi- land covered region. Despite a satisfactory accuracy in experiment 2, the output image showed that this combination of input features was still not capable of distinguishing mangrove and other vegetation area (Figure 3.4).

In order to differentiate between mangrove and other vegetation, a new developed index, CMRI was applied to the experiment 3. However, there was no effectively changes at where other vegetation mixing areas although classification accuracy was improved to 94.02% (Figure 3.5).

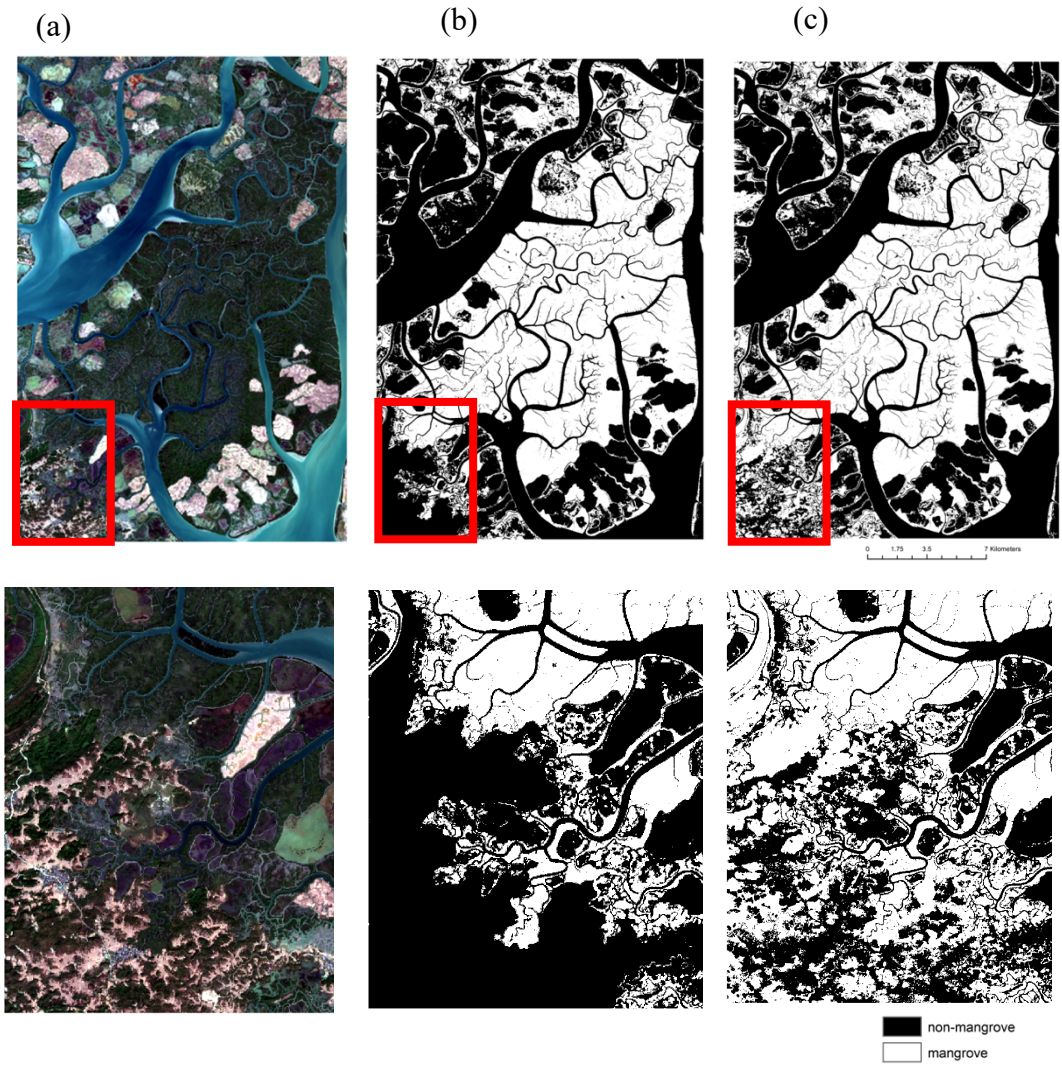

Figure 3.4 (a) Sentinel-2 True color image, (b) ground truth image and (c) output image of experiment 2

3.2.3. Experiments using topographic information

In experiment 4, instead of CMRI, topographic information was considered as another parameter because most of the other vegetations in the study area is thriving on the upper land area. MERIT DEM was therefore applied to experiment 4 with the objectives of removing misclassified pixel in other vegetation areas of experiments 2 and 3. After performing experiment 4, the other forested area misclassified as mangrove vegetation in the previous experiments could be converted into non-mangrove in the output image appreciably (Figure 3.6). Still, there were

noisy pixels in mixed vegetation areas of the output image, which can affect classification accuracy due to the 90 m spatial resolution of MERIT DEM. Since adding DEM data not only improved accuracy but also cleared misclassified pixels of previous experiments, the study tested experiment 5 using 10 bands and MERIT DEM only. However; the resultant accuracy declined to 71.05% seriously in the experiment 5.

3.2.4. Experiments adding canopy height information

The study explored the performance of CHM in this experiment 6 to classify mangrove distribution by adding to the experiment 4. A few studies have shown that accuracy of individual mangrove species classification can be improved by adding CHM extracted from LiDAR data. The present study tried to delineate the classification of mangrove distribution by applying CHM derived from SRTM DSM and MERIT DTM. After conducting different combinations of DTM, DSM and CHM in experiments (6-9), the resultant accuracy was significantly improved to 95.85% in the experiment 6, which integrated both DTM and CHM with Sentinel-2 bands, NDVI, and NDWI. Furthermore, the experiment 6 could wipe off the noisy pixel in the output image of the experiment 4 and produced a smooth map of mangrove distribution (Figure 3.7).

Figure 3.5 Classified image and misclassified area of the experiment 3

Figure 3.6 The classified image of the experiment 4

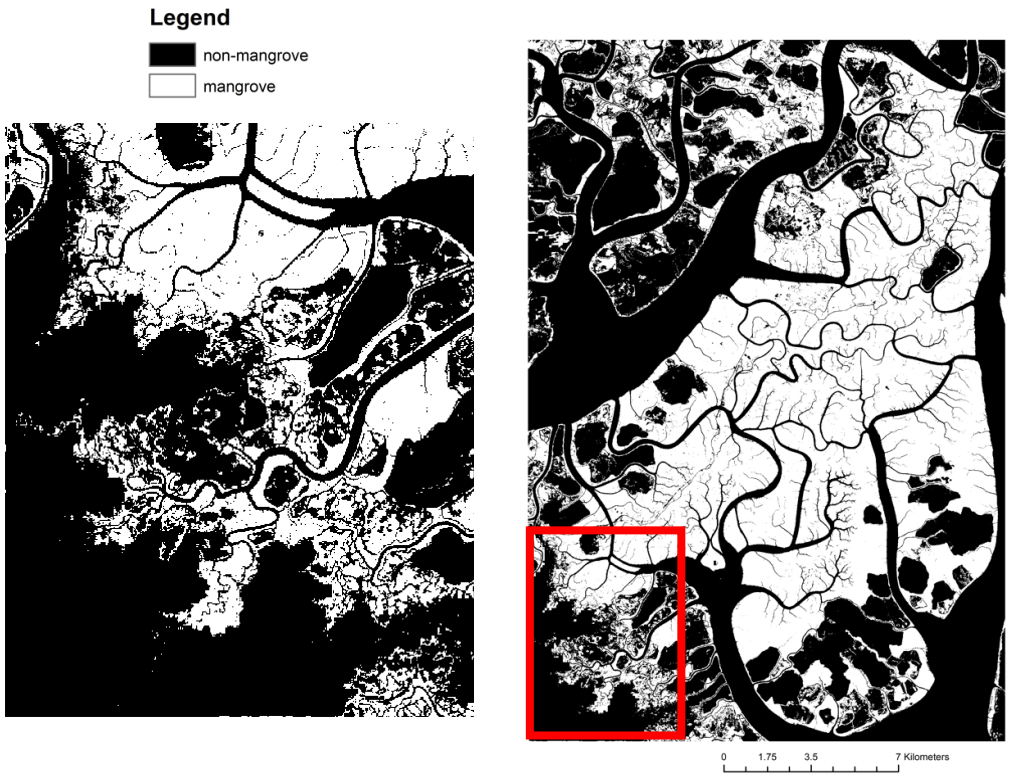

Figure 3.7 The classified image of the experiment 6

Table 3.1 Experimental results of input feature test

Experiment	Combination of input features	Overall accuracy
1	10 bands (B2, B3, B4, B5, B6, B7, B8, B8A, B11, B12) of Sentinel-2 image	56.39%
2	10 bands, NDVI, NDWI	93.43%
3	10 bands, NDVI, NDWI, CMRI	94.02%
4	10 bands, NDVI, NDWI, MERIT	95.49%
5	10 bands, MERIT	71.05%
6	10 bands, NDVI, NDWI, MERIT, CHM	95.85%
7	10 bands, NDVI, NDWI, MERIT, SRTM	95.79%
8	10 bands, NDVI, NDWI, SRTM, CHM	93.71%
9	10 bands, NDVI, NDWI, MERIT, SRTM, CHM	95.73%
10	10 bands, NDVI, NDWI, CHM	95.33%
11	10 bands, MERIT, CHM	72.00%
12	10 bands, NDVI, NDWI, CMRI, MERIT	95.70%
13	10 bands, NDVI, NDWI, CMRI, MERIT, CHM	95.81%
14	NDVI, NDWI, MERIT, CHM	95.76%
15	4 selected bands (B2, B3, B4, B8), NDVI, NDWI, MERIT, CHM	95.65%

3.3. Classification through Hyper-parameter Tuning

This section explored hyper-parameter tuning with the number of hidden layers and neurons by using the same dataset of the experiment 6 in the input parameter tuning section, which yielded the highest accuracy among 15 experiments.

3.3.1. Number of hidden layers

Firstly, one hidden layer with 10 neurons was added to the basic model used in the input parameter tuning. The model was not only trained and evaluated the accuracy but also visually checked the behavior of the model by using the validating dataset. Using two hidden layers (12:10) improved the model accuracy from 95.85% to 95.89% and loss was reduced slightly. Then, each one hidden layer was added to the model and the training process was operated as the same approach. After conducting hidden layer tuning, 95.89% of the model with two hidden layers (12:10) was the highest accuracy while the accuracy of three hidden layers (12:10:8) and four hidden layers (12:10:10:8) were stable at 95.76% (Figure 3.9).

To judge the behavior of the models, accuracy and loss of training were compared to that of validating prediction. As shown in Figure 3.8 A, the accuracy and loss of the training prediction were not only less diverged but also similar direction with the validation along the learning time of the model with 2 hidden layers. In contrast, other models with 3 and 4 hidden layers showed larger gaps between training and validating measures and moreover, encountered overfitting issue in which validating losses increased significantly although training loss decreased at the end of the epoch (Figure 3.8 B and C). The model with 2 hidden layers, therefore was selected according to the evaluation of classification accuracy and model behavior during learning time.

A

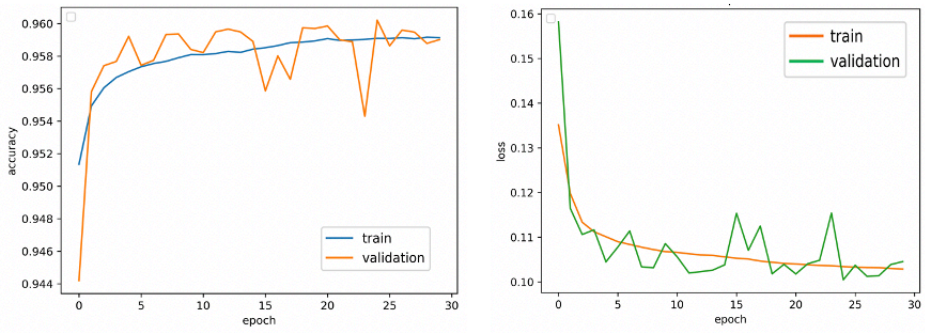

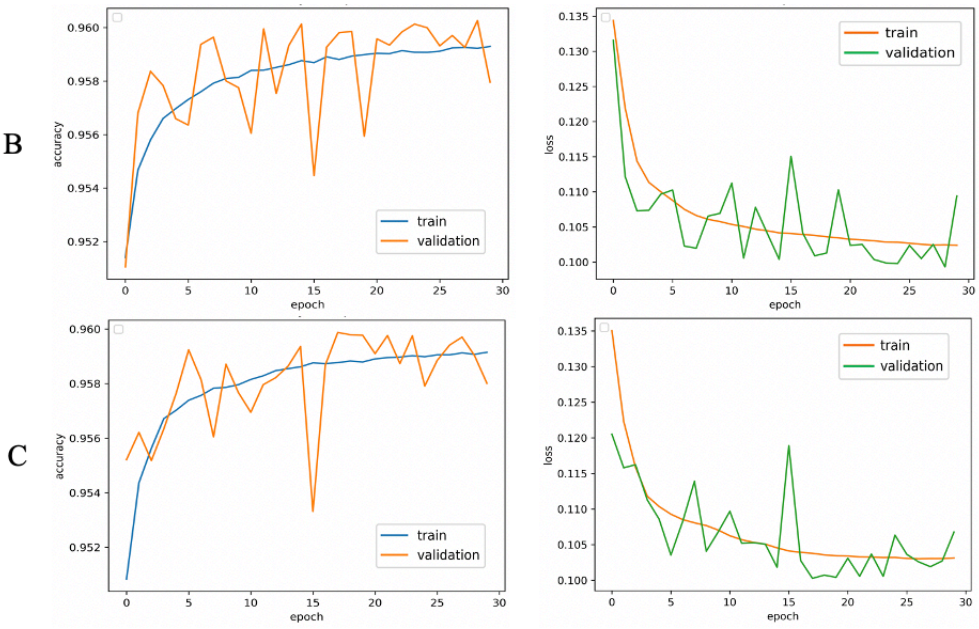

Figure 3.8 Loss and accuracy trends of A. two hidden layers, B. three hidden layers and C. four hidden layers during training phase

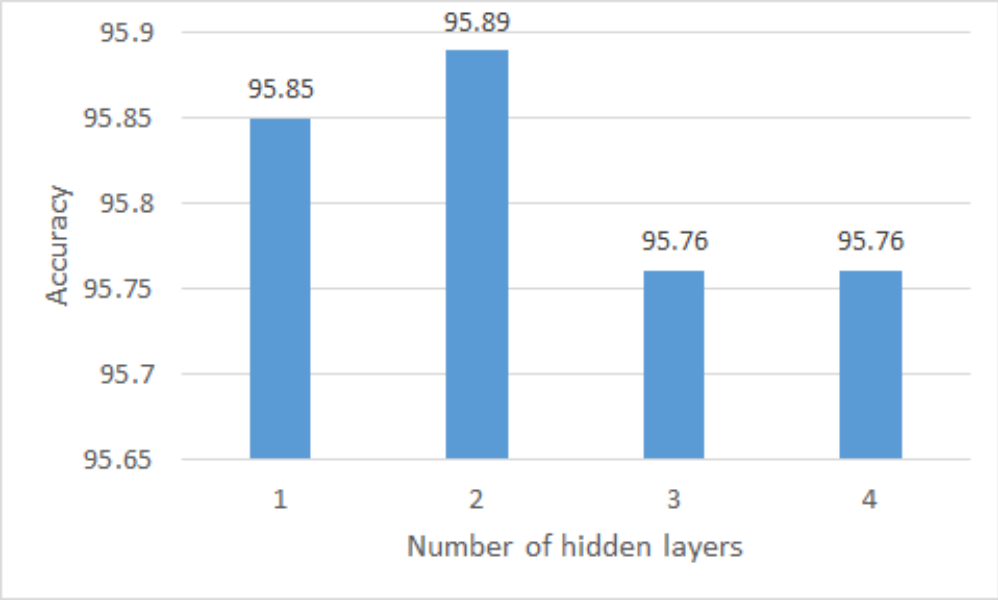

Figure 3.9 Evaluation results of ANN models with different hidden layers

3.3.2. Number of neurons

The neurons in the hidden layers play a key role as processing units, which analyze input data and produce output, which is why the number of neurons influence on the performance of an ANN model. In this section, the number of neurons in the two hidden layers was adjusted by reducing and adding double in each layer. Comparing accuracy and loss of training prediction to that of validating, overfitting problem happened to the model with numbers of neurons;(48:40), (136:80) and (272:160) (Figure 3.10). Although there was no significant change in accuracy and loss, the model using (544:320) neuron set obtained the highest accuracy of 95.98% (Figure 3.11). Finally, the model with neurons (544:320) was selected to be applied in this study because of the highest accuracy, minimum error, and the smallest difference between training and validating predictions. After conducting input feature experiments and hyperparameter tuning, the ANN model with two hidden layers, which have 544 and 320 neurons respectively, was selected as the proposed model for the input dataset of the experiment 6 (Figure 3.12).

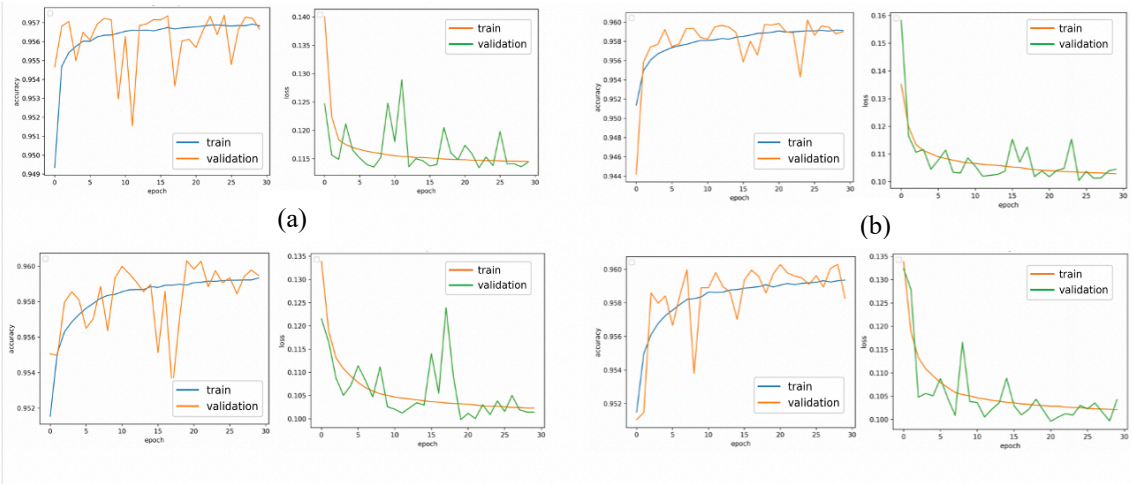

(a) (b)

(c) (d)

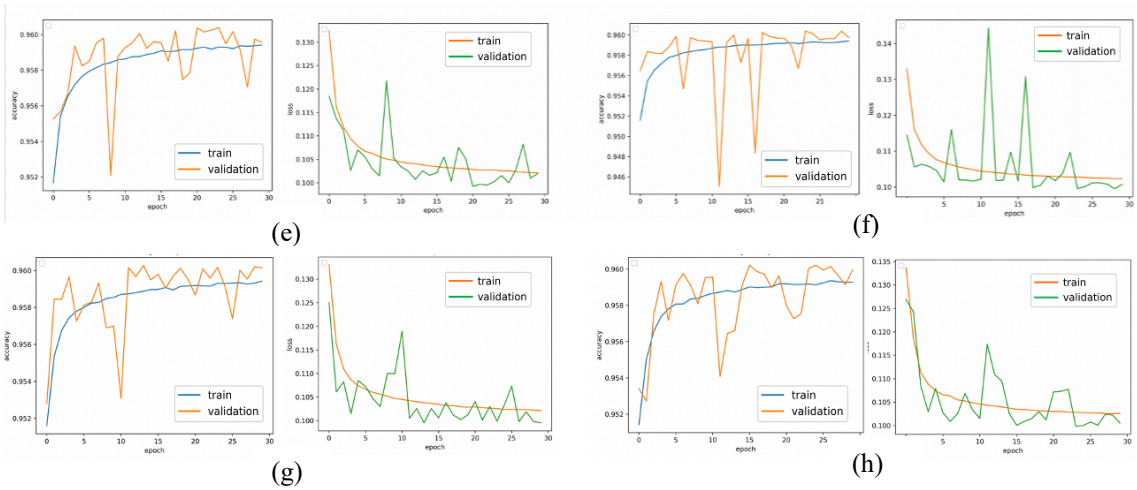

Figure 3.10 Accuracy and loss trends of two hidden layers with (a) (6:3) neurons, (b) (12:10) neurons, (c) (24:20) neurons, (d) (48:40) neurons, (e) (136:80) neurons, (f) (272:160) neurons, (g) (544:320) neurons and (h) (1088:640) neurons

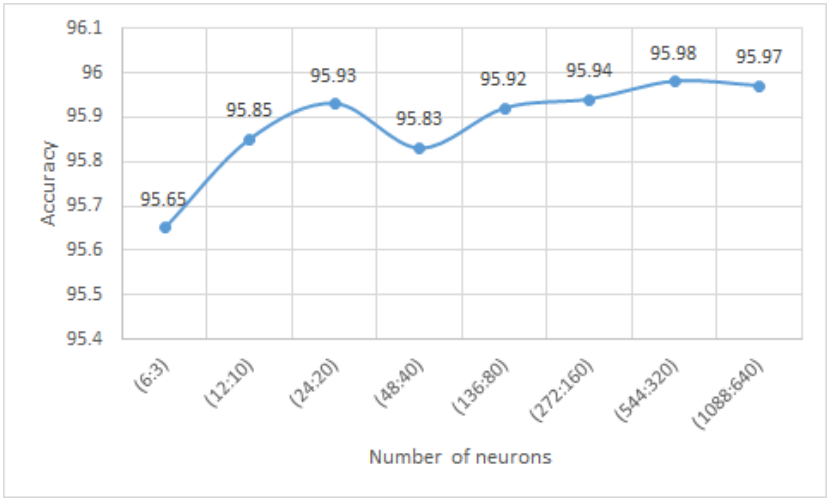

Figure 3.11 Model accuracy depending on numbers of neuron in hidden layers

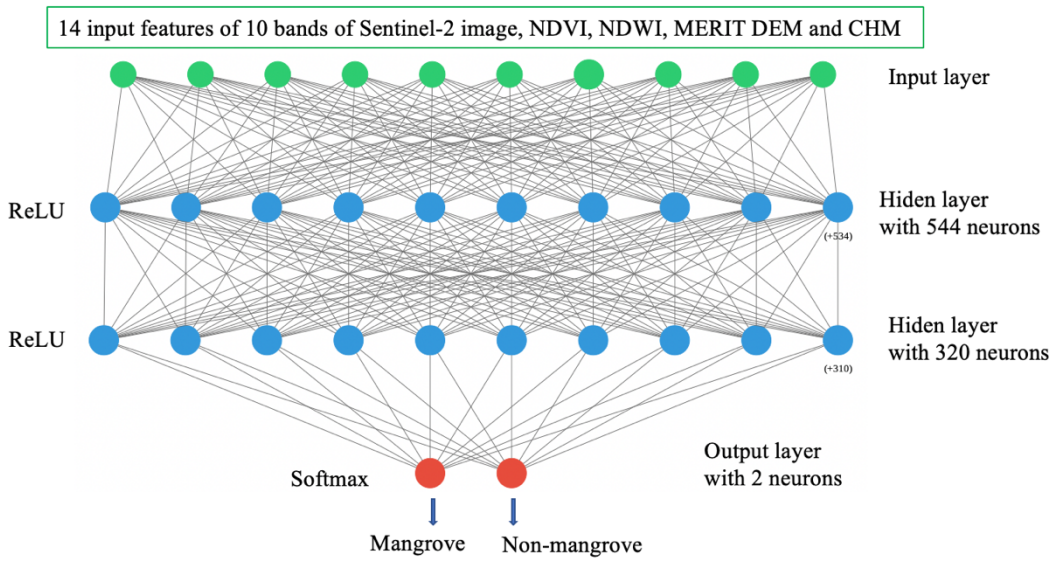

Figure 3.12 Proposed ANN model and input dataset for classification of mangrove distribution

3.4. Classification Results of New Dataset

As one of the advantages of neural network classification, once the model is achieved with the desired accuracy, any new dataset can be predicted without retraining the model. In this study, after classifying the dataset of 2020 through input parameter and hyper-parameter tuning, the ANN model having two hidden layers (544:320) was applied to a new dataset of the same input features in 2015. By checking the classified image of the new dataset via Sentinel image, despite high accuracy of 94.20%, most of the misclassified pixels were found in paddy fields, which reflects green cover even with high NDVI values almost the same as mangrove (Figure 3.15). Because, in 2015, the dataset is the only available satellite imagery for the study area and the selected three shrimp ponds were also abandoned in the same year, there were no other options to avoid this dataset.

The cause of misclassification is that the model encountered a new problem of green paddy fields that was not learned during the training session. That is reasonable because every artificial intelligent model cannot outperform over information trained. The model, therefore, was not able to identify green paddy fields as non-mangrove but predicted as mangrove falsely.

3.4.1. Transfer learning

Transfer learning is an emerging technique of machine learning field whereby theoretically, the model trained for a given problem was applied to a different but related problem. Although human beings are capable of figuring out new issues based on experience, artificial intelligence models cannot correctly solve problems that they have never encountered. It is even impossible to train the model in order to meet all real-world problems. Moreover, retraining a model whenever we confront a new problem in future predictions is a very time-consuming practice. To overcome such problems, transfer learning has become a practical and effective method in neural network classification.

Unlike traditional machine learning classifiers, the neural network model can retain knowledge learned from training lessons and transfer the knowledge to solve a different but related problem (Figure 3.13). In the model architecture composing of multi perceptron layers, by muting some layers and retraining some with new knowledge, the performance of the model can be improved effectively compared to the original one.

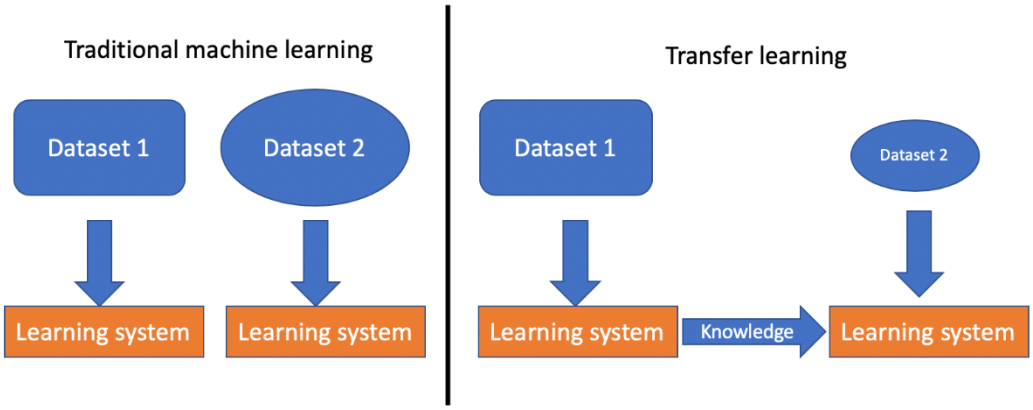

Figure 3.13 Difference between traditional machine learning and transfer learning

In case of the problem in this research, the original model trained with the dataset in 2020 predicted green paddy fields as mangrove falsely in the new da-

taset. Among all layers in the original model, which have stored weight and feature information from the training process, the study fixed some of these layers with knowledge stored. Some layers were then retrained by using a few amounts of the new dataset, which have information of green paddy fields only (Figure 3.14).

All models including the original model were applied to predict a new dataset, which is used in the transfer learning process, and the whole dataset in 2015. During transfer learning, 80 % of the new dataset with corresponding ground truth image was utilized as training data and 20% as testing data randomly. After conducting this process, the whole new dataset in 2015 was also predicted by all models. For evaluation of 2015 classification, 1000 reference points, which have geographical locations and ground truth information were generated randomly to represent the whole study area since creating ground truth images for all new projects is a time-consuming approach. The predicted points were then extracted from the classified images of 2015 by using the reference points and assessed the performance of the models to the new dataset.

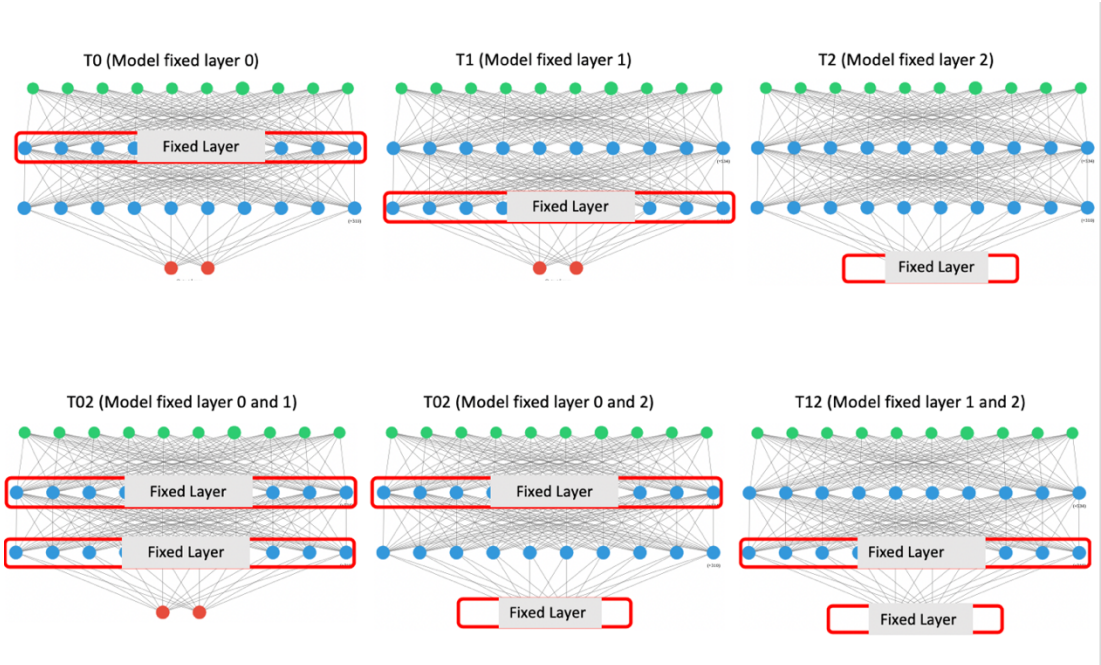

Figure 3.14 Models with different fixed layers in transfer learning

The resultant accuracy of the models for the dataset in 2015 was described in Table 3.2 and the output images are shown in Figure 3.16. The original model encountered the misclassification issues in the paddy fields despite high accuracy for the whole dataset. T12 model, which fixed the second hidden layer (layer 1) and output layer (layer 2), could be trained within the shortest training time of 32s per epoch. The model not only yielded high accuracy of 95.77% in predicting the transfer learning dataset but also outperformed other models with the highest accuracy of 97.2% in the whole dataset. Finally, the problem this study encountered could be figured out by using the T12 model.

Table 3.2 Transfer learning results of different models

Models	Transfer learning dataset		Whole dataset
	Accuracy	Training time per epoch	
original_model	72.59	-	94.5
T0 (Model fixed layer 0)	96.09	42s	93.8
T1 (Model fixed layer 1)	95.77	33s	95.10
T2 (Model fixed layer 2)	96.07	40s	93.00
T01 (Model fixed layer 0 and 1)	95.57	38s	94.00
T02 (Model fixed layer 0 and 2)	96.04	38s	96.20
T12 (Model fixed layer 1 and 2)	95.83	32s	97.20

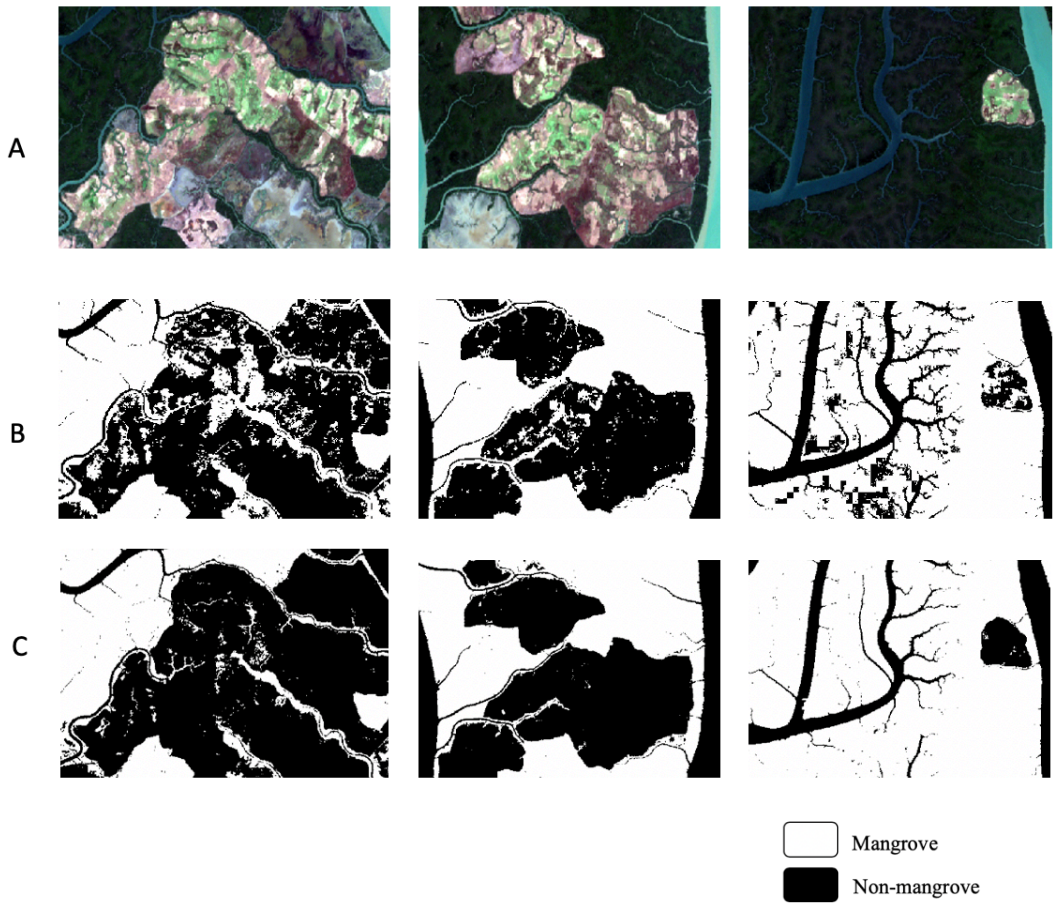

Figure 3.15 A. Sentinel-2 true color image, B. classified image of original model and C. classified image of T12 model after transfer learning in green paddy field areas

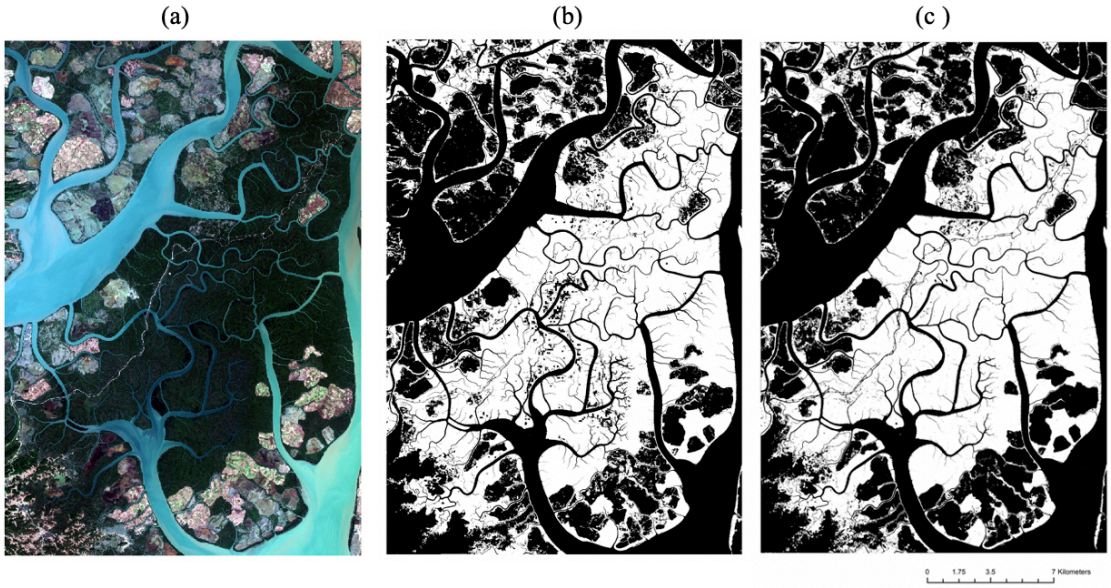

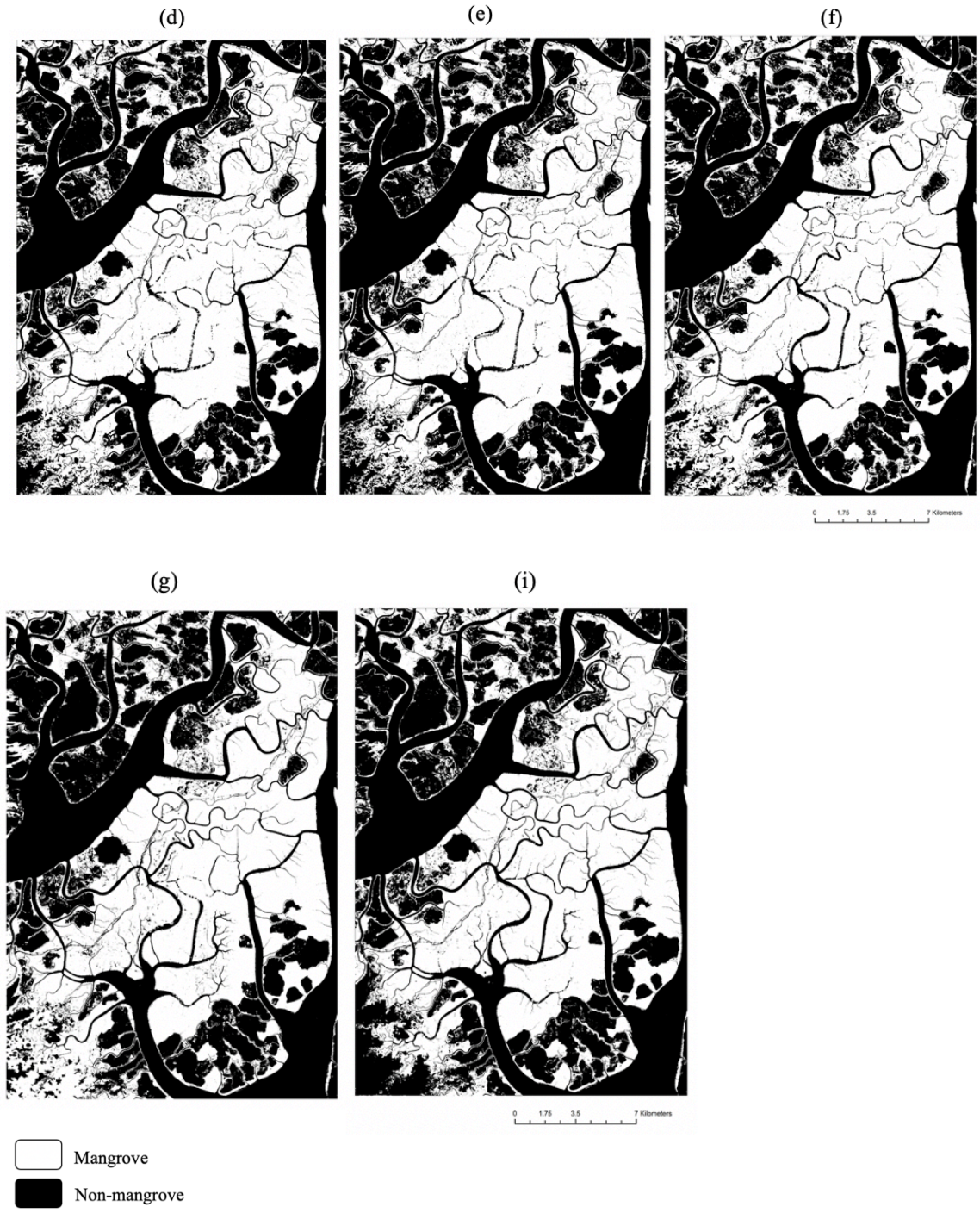

Figure 3.16 (a) Sentinel-2 true color image and classified image of the whole study area by (b) original model, (c) T0 model, (d) T1 model, (e) T2 model, (f) T01 model, (g) T02 model, and (h) T12 model

3.5. Change Detection Results

3.5.1. Spatial changes of WMF between 2015 and 2020

To provide updated information about mangrove distribution of WRMF, this study examined spatial changes of mangrove between 2015 and 2020 through post classification change detection method. Mangrove distributed area declined from 254.30 km to 249.83 km slightly whereas non-mangrove increased from 284.30 km to 288.77 km between 2015 and 2020 (Figure 3.17 (b)). By differentiating between classified images in 2015 and 2020, changed areas were found and validated with Sentinel-2 true color images (10m resolution) and very high resolution (1m) Google Earth imagery. In order to focus on major causes of mangrove loss and gain, only extensive changed areas were paid attention rather than small changed dots because of the salt and pepper effect in the original classified images (Figure 3.17 (a)).

(a)

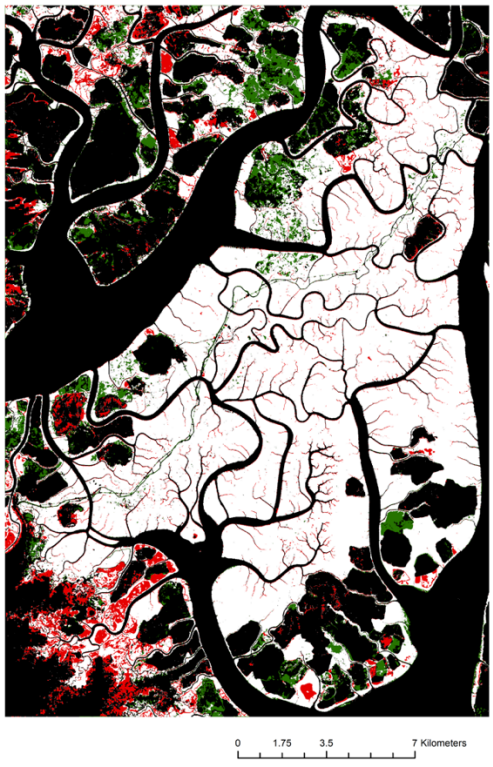

(b)

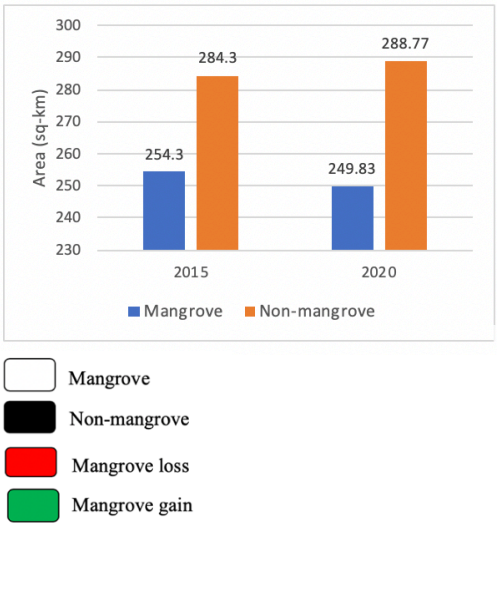

Figure 3.17 (a) Change detection result and (b) changes in mangrove and non-mangrove area between 2015 and 2020

3.5.2. Mangrove loss and gain

Between 2015 and 2020, mangrove losses were also detected in the study area and the main reasons are the expansion of shrimp ponds (Figure 3.18). There were two kinds of expansions as follows;

a) new built shrimp ponds and paddy fields, and
b) extension from existing ponds and paddy fields.

Through detailed visual analysis in ArcGIS and Google Earth Pro software, mangrove loss areas were more discovered near the local villages than within the reserved forest.

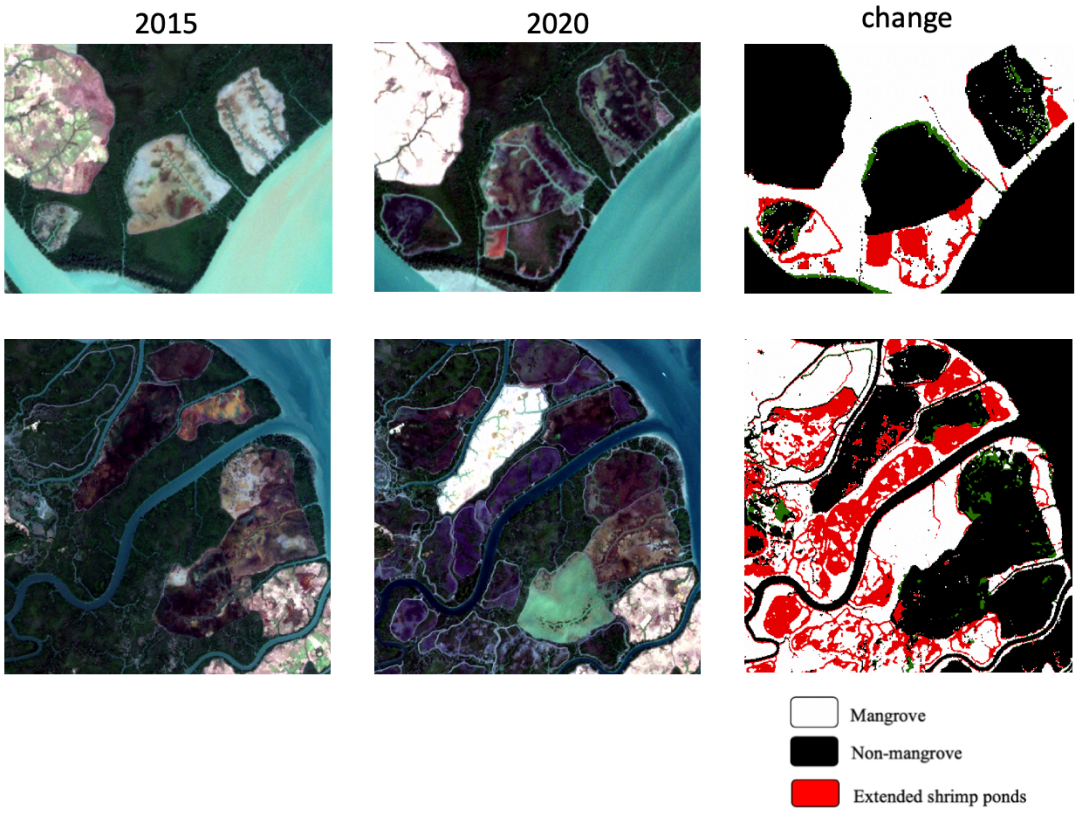

Figure 3.18 Expansion of shrimp ponds in WMF between 2015 and 2020

Turning to mangrove gain, there were two ways to recover mangrove in the study area as follows (Figure 3.19);

a) artificial plantations and
b) natural recovery mangrove.

To compensate for mangrove deforestation, artificial mangrove plantations have been established by FD yearly since 2007. Naturally recovered mangroves were found at active abandoned shrimp ponds, abandoned sites, and tidal flats. Since specific spatial information of all plantations could not be acquired on the field, it is difficult to distinguish natural recovered mangrove and plantations in the whole study area by using Sentinel-2 imagery. However, locations of artificial mangrove plantations could be recognized by using high resolution google earth imagery and GPS points collected during the field trip.

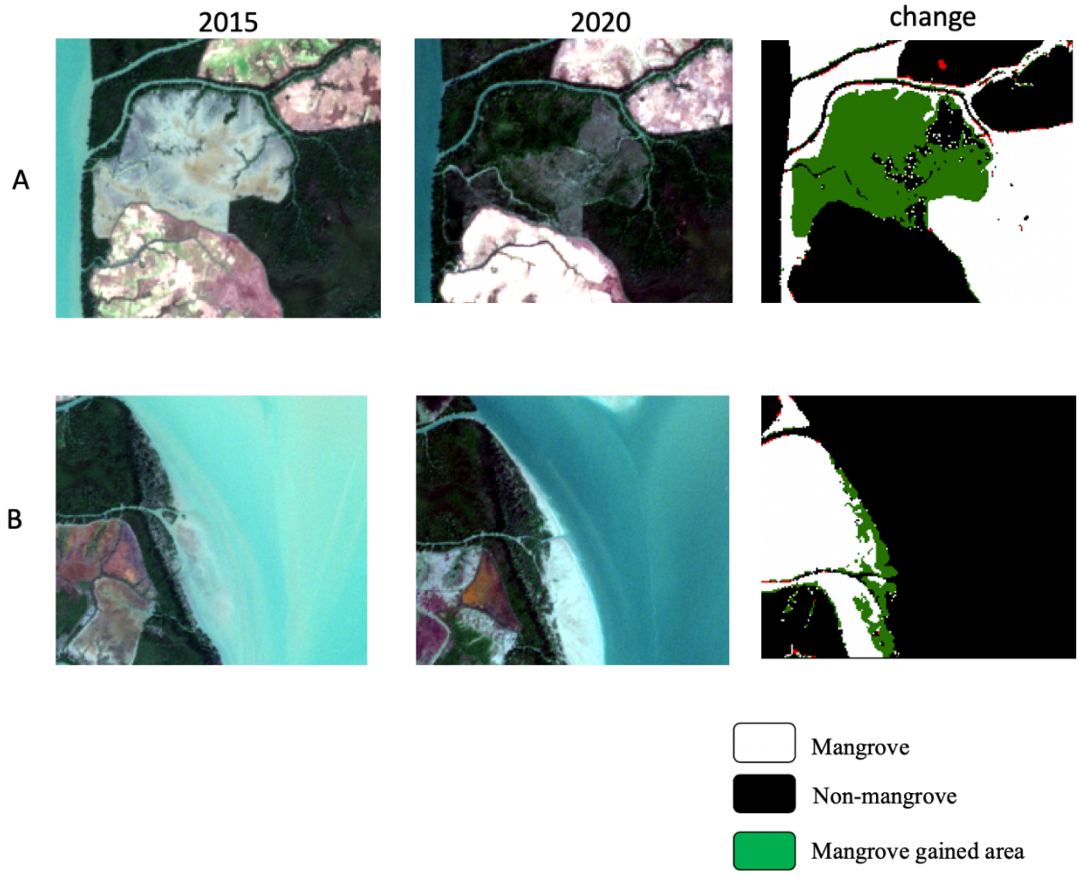

Figure 3.19 Mangrove gained area at A. artificial plantation site and B. tidal flat

3.6. Natural Recovery Process of Mangrove at Different Abandoned Sites

3.6.1. Spatial analysis for recovering mangrove

According to the interview with the local people, three abandoned shrimp ponds (Figure 2.5), which meet the aforementioned criteria (in section 2.2.3) were chosen for natural recovery analysis. These three sites were abandoned since 2015 because seasonal flooding and high tidal wave breached embankment of the ponds, which were not constructed systematically during the rainy season. To delineate natural recovering mangrove in the study area, the selected abandoned shrimp ponds were extracted from the result of change detection (Figure 3.20). The recovering mangrove area was then evaluated and compared to the extents of abandoned sites in ArcGIS. During the abandoned period from 2015 to 2020, mangrove species recovered 49.02% of the extent site 1 as well as 55.93% of the site 2 and 50.00% of the site 3 respectively (Table 3.3).

Table 3.3 Naturally Recovering percentage of mangrove at different abandoned shrimp ponds

Abandoned sites	Site_area (sq-km)	Recovering mangrove (sq-km)	Recovering precentage
Site 1	1.02	0.5	49.02
Site 2	0.59	0.33	55.93
Site 3	0.14	0.07	50.00

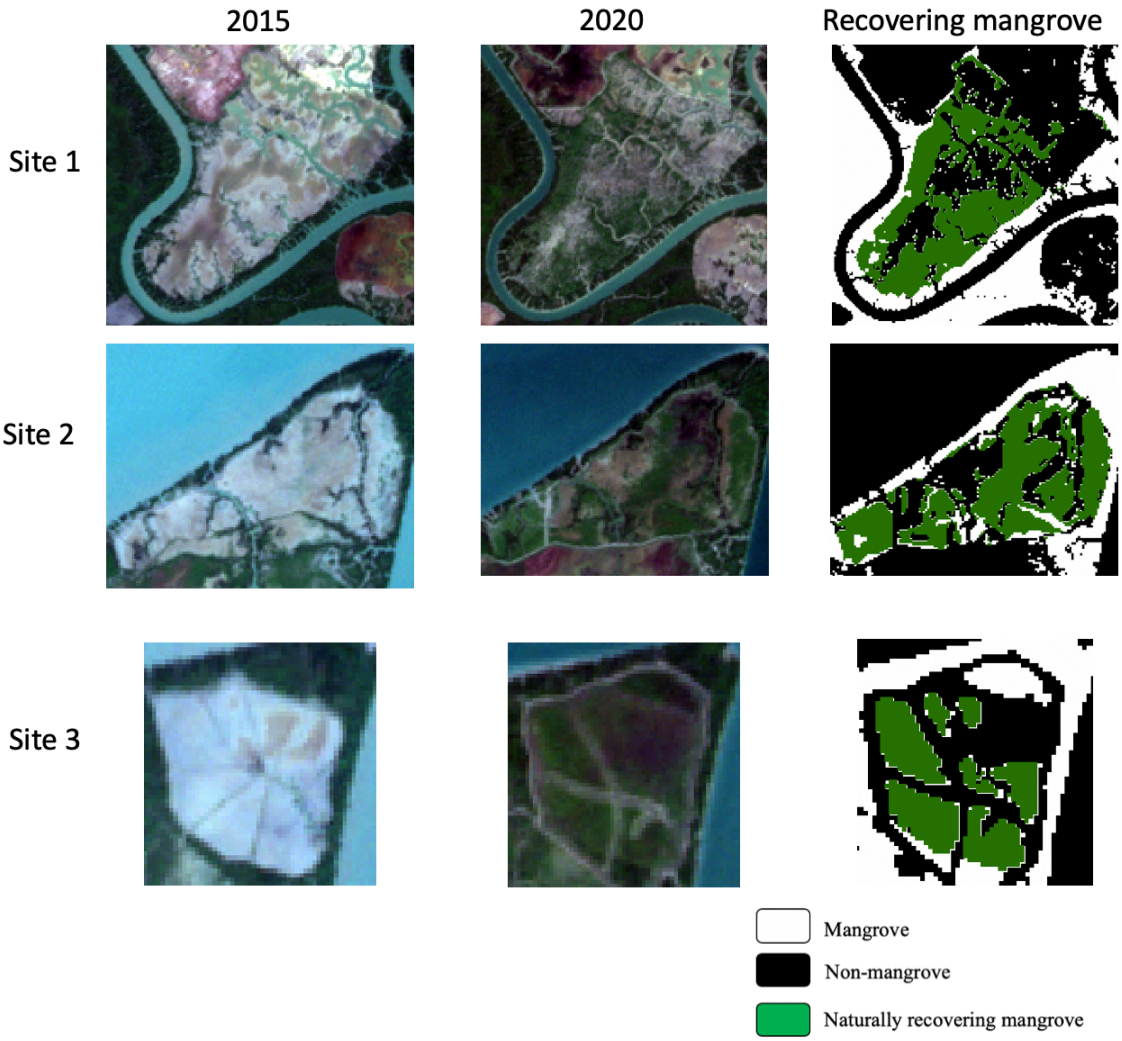

Figure 3.20 Naturally recovering mangrove at different abandoned sites between 2015 and 2020

3.6.2. Species composition and diversity

For all 50 sample plots of the three recovering sites, 12 different mangrove species could be identified through field inventory. Of these mangrove species recorded at three recovered sites, 11 mangrove species were found at site 1 while 8 and 3 species at site 2 and 3 respectively. Through IVI analysis, *Avicennia officinalis* (Figure 3.21 (a)) was the most dominant species with highest IVI values at site 1(Table 3.4). On the other hand, *Avicennia marina* (Figure 3.21(b)) which possesses higher IVI values than other species predominated at site 2 and 3 (Table 3.5 and Table 3.6).

Shannon indices expressed in Figure 3.22 inform that three recovering sites have different diversity of mangrove species. Shannon diversity index (H), evenness (E) and richness (Hmax) for site 1 were 1.19, 0.5 and 2.4 whereas 0.76, 0.37 and 2.08 for site 2 and 0.3, 0.28 and 1.1 for site 3, respectively.

Table 3.4 IVI values of recovered mangrove species at site 1

Species	**Relative Frequency**	**Relative density**	**Relative dominance**	**IVI**
Avicennia officinalis	28.5714	69.4444	39.1836	137.1995
Sonneratia apetala	22.8571	10.4167	31.3693	64.6431
Sonneratia alba	17.1429	7.2917	10.9234	35.3580
Avicennia alba	11.4286	3.8194	11.9427	27.1907
Avicennia marina	7.1429	2.4306	3.7594	13.3328
Bruguiria gyumnoriza	4.2857	1.3889	1.0044	6.6791
Rizophora apiculata	2.8571	0.6944	1.1826	4.7342
Ceriops decendra	1.4286	1.0417	0.1496	2.6198
Aegiceras corniculatum	1.4286	1.3889	0.2095	3.0269
Heritiera Fomes	1.4286	1.3889	0.1932	3.0107
Xylocarpus granatum	1.4286	0.6944	0.0822	2.2052

Table 3.5 IVI values of recovered mangrove species at site 2

Species	**Relative Frequency**	**Relative density**	**Relative dominance**	**IVI**
Avicennia marina	38.4615	82.3961	89.5546	210.4122
Rizophora apiculata	21.1538	4.1565	4.7681	30.0785
Aegialistis rotundifolia	9.6154	4.6455	0.7159	14.9768
Ceriops decendra	7.6923	4.1565	0.7423	12.5911
Bruguiria gyumnoriza	7.6923	1.2225	0.3248	9.2396
Avicennia officinalis	9.6154	2.4450	2.0858	14.1461
Sonneratia apetala	1.9231	0.4890	0.6542	3.0663
Avicennia alba	3.8462	0.4890	1.1543	5.4895

Table 3.6 IVI values of recovered mangrove species at site 3

Species	**Relative Frequency**	**Relative density**	**Relative dominance**	**IVI**
Avicennia marina	52.6316	92.7835	94.5877	240.0028
Avicennia officinalis	31.5789	5.1546	4.6917	41.4253
Aegialistis rotundifolia	15.7895	2.0619	0.7205	18.5719

(a) (b)

Figure 3.21 (a) Avicennia officinalis, dominant species of site 1 and (b) Avicennia marina dominant species of site 2 and 3

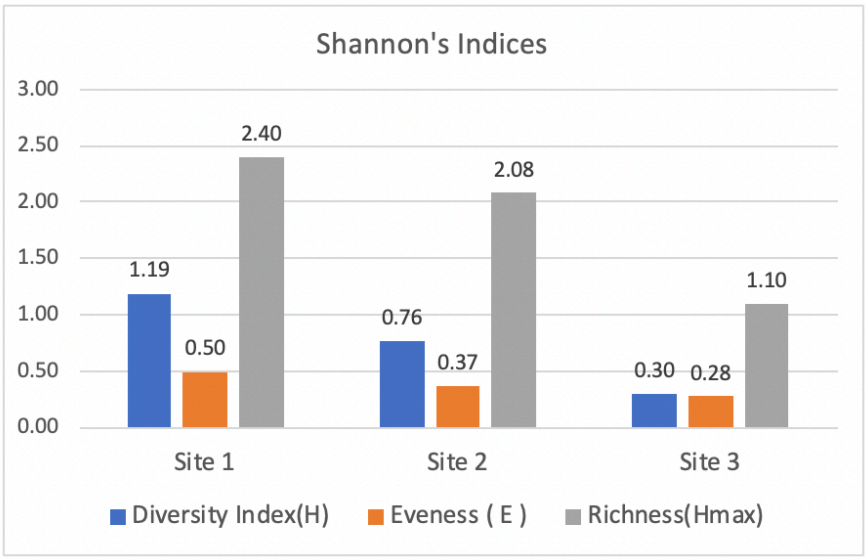

Figure 3.22 Shannon's indices of three different recovering sites

Chapter 4 DISCUSSION

4.1. Artificial Neural Network Classification for Mangrove Distribution

Remote sensing classification for mangrove fields is not straightforward since mangrove species are thriving at intertidal portions where other vegetations are usually mixing[76]. This nature of mangrove, therefore creates many challenges for the classification of mangrove distribution to produce high accuracy. To overcome such complex issues in mangrove classification, it is critical to choose not only the most appropriate method but also combination of effective input features in remote sensing analysis.

4.1.1. Experiments of input features

In the experiments of input features, although using selected 10 bands of Sentinel-2 image showed poor accuracy, it was significantly improved by adding spectral indices; NDVI and NDWI, derived from specific bands of Sentinel-2 image in the experiment 2. For mangrove classification, such spectral indices were widely applied and the resultant accuracy was relatively higher than using band information alone. Since the area of other vegetations is small compared to the mangrove portion in this study, the experiment 2, which used 10 bands and spectral indices yielded such a higher accuracy despite misclassification in other vegetation areas. If a targeted study area had large amounts of other vegetation, the resultant accuracy of the experiment 2 would decrease due to insufficient input features for such an area.

In order to achieve a robust model that fits any mangrove area, the study paid attention to distinguishing mangrove and other vegetation. To differentiate these two different types of vegetations, applying a new developed spectral index, CMRI produced higher accuracy in the experiment 3; however, there were still misclassified pixels in the output map.

4.1.2. Combination of topographic and canopy height information in mangrove classification

The corporation with the topographic feature in remote sensing classification generated an assured outcome for mangrove mapping in other studies [77,78]. The

study also achieved higher accuracy and wiped off misclassified pixels of the previous experiments by integrating topographic information derived from MERIT DEM.

Applying canopy height model (CHM) obtained from differentiation of DTM and DSM can improve the resultant accuracy of tree species classification. Some studies have employed CHM obtained from multispectral and hyperspectral images, and LiDAR data for mangrove species classification[79,80]. Jingjing Cao et al showed that CHM derived from hyper spectral sensor mounted on Unmanned Aerial Vehicle (UAV) is useful for mangrove species discrimination[55]. However, due to limited accessibility of LiDAR data and high investment for hyperspectral sensors, such canopy height information was rarely deployed in remote sensing classification[81].

The present study made the first attempt of exploring canopy height information of CHM obtained from SRTM DSM and MERIT DEM, which are freely and globally accessible. This effort found that mangrove distribution can be more accurately identified with a promising accuracy by integrating both DTM and CHM in remote sensing classification. Of the different combinations of input features after conducting various experiments, the combination of 10 bands of Sentinel-2, NDVI, NDWI, MERIT DEM and CHM is proposed as the most appropriate one in remote sensing classification for mangrove distribution.

4.1.3. Hyper parameter tuning and transfer learning in neural network

Turning to the performance of the ANN model, since there is no universal method for selecting the number of hidden layers and neurons to obtain an optimal model design [82,83], a systematic experimental analysis is a reliable and suitable path for a specific problem[84]. In this study, the basic ANN model was applied to preliminary analyses, and hidden layers and neurons were then adjusted by checking behavior of each model via cross validation. After conducting hyper-parameter tuning, the final selected model, which has two hidden layers (544:322) outperformed other models with the highest accuracy of 95.98% whereas the basic model produced 95.85% with the same dataset. The result of the analyses showed

that the setting of method deployed is one of the pivotal factors in remote sensing classification as has the selection of efficient input features. Despite no sharp improvement in the resultant accuracy, the behavior of the model was considered through cross validation to avoid overfitting problems for future predictions.

Developing advanced technologies in computer science, remote sensing community has improved many classification methods by applying state of the art approach in order to be cost and time effective computation. Transfer learning is one of the magnificent approaches in neural network, which is effective for future predictions by using a relatively small training dataset with less computational costs[85–87]. Guo has introduced and applied transfer learning to identifying buildings in rural environment in his master thesis[88]. In this study, transfer learning was employed by delineating different layer freezing to overcome the problem encountered in applying the model trained to a new dataset. As one of the advantages of transfer learning, the original model was retrained with a very small dataset by which the resultant accuracy for the whole study area was significantly improved from 94.50% to 97.20%. This study therefore proposed a promising method, which consists of the most appropriate input feature combination and a robust ANN model. The proposed model can also be applied to any mangrove area in any season.

4.2. Mangrove Forest Changes in WMF

Under threats of human disturbances, mangrove forests in the world were being declined with different rates year by year. For management of vulnerable mangrove ecosystems, acquiring updated information about existing mangrove distribution is critical before performing any restoration efforts. According to the field interview, Wunbaik mangrove reserved forest had been constituted since 1931; however, due to lack of field staff, there was no intensive management before. In the late 1990s, encroachments of shrimp ponds and paddy fields on the reserved forest were initiated by clearing natural mangrove and logging hydrological flow. In 2005, WMF was supervised under township level management and then mangrove rehabilitation programs were being implemented through artificial plantation, natural mangrove conservation, and extension programs as an annual plan.

FAO [6]and Aye Saw [28] have studied mangrove forest changes in the Wunbaik reserved forest area and described the main drivers of mangrove loss from 1990 to 2011 and 2014, respectively. Despite a large remaining mangrove and a high diversity of fauna and flora in WMF, there was a prominent information gap for mangrove distribution after 2014.

One of the interesting findings in the change detection result is that mangrove loss could be more discovered near the local villages due to the expansion of shrimp farming than within the reserved forest (Figure 4.1). According to information provided by Forest Department, Myanmar, two public protected forests adjacent to WRMF could be demarcated in 2006 and 2018 with the objectives of protecting the existing mangrove area. Although many mangrove gain areas were found in the reserved forest, some shrimp ponds were still expanding between 2015 and 2020. Mangrove forests in Myanmar declined with an annual net reduction rate of 3.60% - 3.87% between 1996 and 2016 and the main drivers were mentioned as agricultural fields, aquaculture, oil palm and rubber expansion[89,90]. Likewise, in this study, net mangrove area of WMF slightly decreased compared to non-mangrove portion during 2015 and 2020. The main reason of mangrove loss was mainly found as the expansion of shrimp ponds by local communities nearby whereas mangrove forests were gained by means of artificial plantations and natural recovery process of mangrove. This study not only fulfilled the updated mangrove distribution of WMF but also identified expansion of shrimp ponds as the current pressures for the remnant mangrove in the study area.

4.3. Natural Recovery of Mangrove

Since artificial plantations established by FD were the only one mangrove restoration project as in the WMF, other mangrove gained areas were assumed to appear by natural recovery process. Although recovering mangrove were also found at active shrimp ponds in WMF, those mangrove areas would be cleared if the owners wanted to repair or convert to paddy fields for their livelihoods. The study, therefore, highlighted natural recovery process at abandoned areas and the result showed that mangrove can naturally recover about 50% of the abandoned sites during a short period of abandonment from 2015 to 2020.

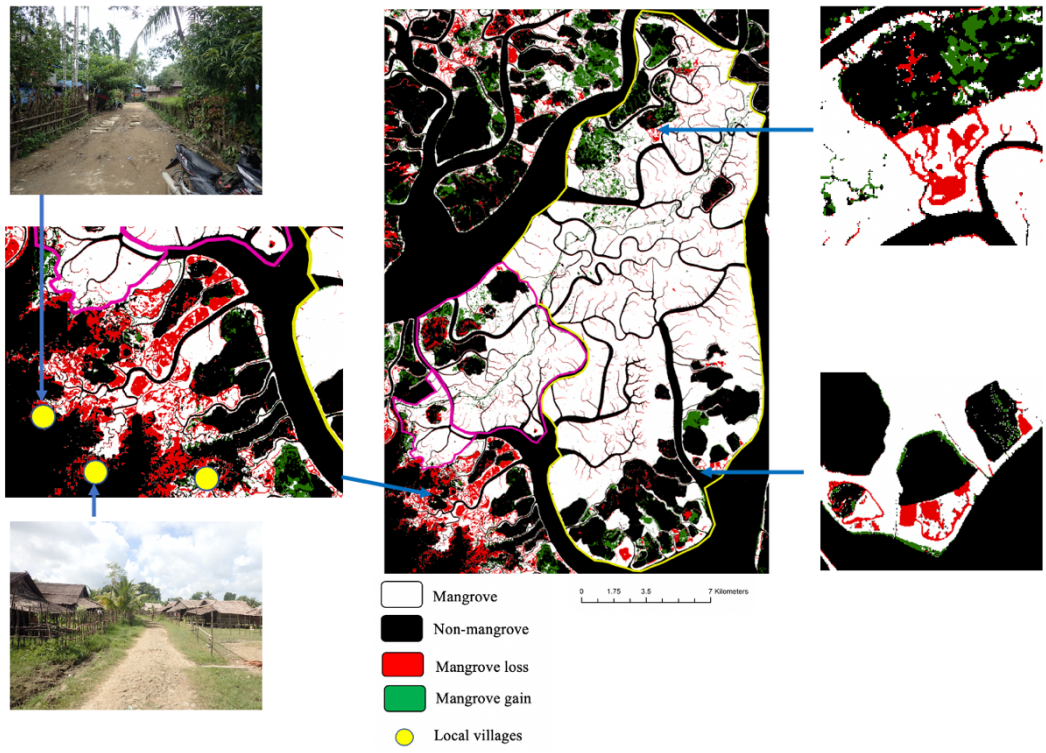

Figure 4.1 Shrimp pond expansion by local villages near the WRMF between 2015 and 2020

Regarding species analysis, Toe Aung[91] had described that 6 types of natural recovered mangrove species were found in tree form at agricultural fields in Ayeyawaddy region, which is one of the largest remaining mangrove in Myanmar whereas only one mangrove species at aquaculture affected sites. In the present study, of the total 12 different species found at the three abandoned shrimp ponds, 11 mangrove species were identified at site 1 while 8 and 3 species at site 2 and 3, respectively. Some studies presented in the literature review section have revealed that there are different species between planted and natural mangrove, and shrimp ponds and paddy fields. The findings of this research showed that natural mangrove species are diversely recovered at different disused shrimp ponds during a short period of abandonment.

4.4. Environmental Preference of Recovered Mangrove Species

Without considering the environmental preference of mangrove species, it would be difficult to achieve successful mangrove plantations if there were needed to plant artificially at where mangrove species have no chance for natural recovery. Different mangrove species have different salinity preferences that would be indicator species with respect to salinity [35]. The recovering mangrove species were observed with their preference of salinity and elevation range in this study. A.officinalis and A.marina could be found at both low and high salinity range while Aegialistis rotundifolia is only at high salinity range (Figure 4.2). This finding is consistent with the results of experimental analyses in other studies [92,93] in which different mangrove species were tested with different salinity levels. Their experimental results also reveal that due to having salt-secreting glands in the leaves of A.marina, this species is more salt tolerant than other species. Moreover, San Win et al[94] found Avicennia species at both low and high salinity ranges (0.5-28.9 PSU) of the Ayeyarwaddy mangrove region, Myanmar. As A.officinalis and A.marina were recorded at 31 and 35 out of the total 50 sample plots in this study (Table 4.1), these species have a high adaptivity to any environmental conditions at abandoned sites.

In case of elevation range, Bruguiria gyumnoriza and Ceriops decendra were occurred at only high range within the sample plots (Figure 4.3). There is however no significant difference of elevation among recovered species in the study area because the mangrove area is a flattened surface of the inland region.

It is not straightforward to approve the determinant of the distribution of mangrove species because there are many physical factors such as tidal inundation, source of seed productive trees, and seed sizes, which should be considered for seed dispersal. This study therefore showed the occurrence of salinity and elevation ranges in which each species was recorded at recovering sites during field survey. The information about environmental preferences of recovered species related with the abandoned sites should be well noted for practitioners in implementing restoration projects. By referring to this information, suitable mangrove species can be selected depending on the salinity and elevation of the restoration sites.

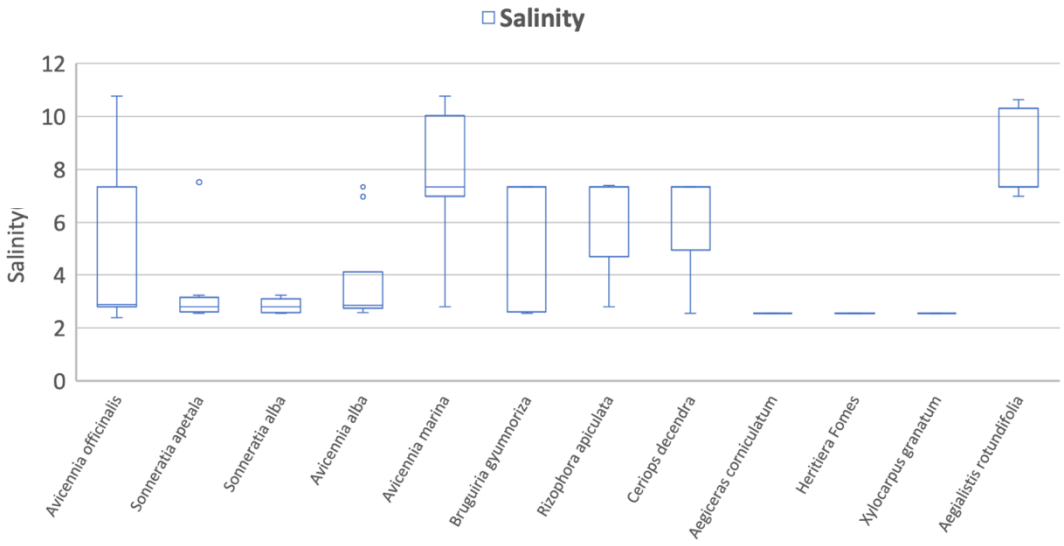

Figure 4.2 Salinity range of different recovered mangrove species

Table 4.1 Number of sample plots at which each species was recorded at the three recovering sites

No	Species name	Number of sample plots each species occurred
1	*Avicennia officinalis*	31
2	*Sonneratia apetala*	17
3	*Sonneratia alba*	12
4	*Avicennia alba*	10
5	*Avicennia marina*	35
6	*Bruguiria gyumnoriza*	7
7	*Rizophora apiculata*	13
8	*Ceriops decendra*	5
9	*Aegiceras corniculatum*	1
10	*Heritiera Fomes*	1
11	*Xylocarpus granatum*	1
12	*Aegialistis rotundifolia*	8

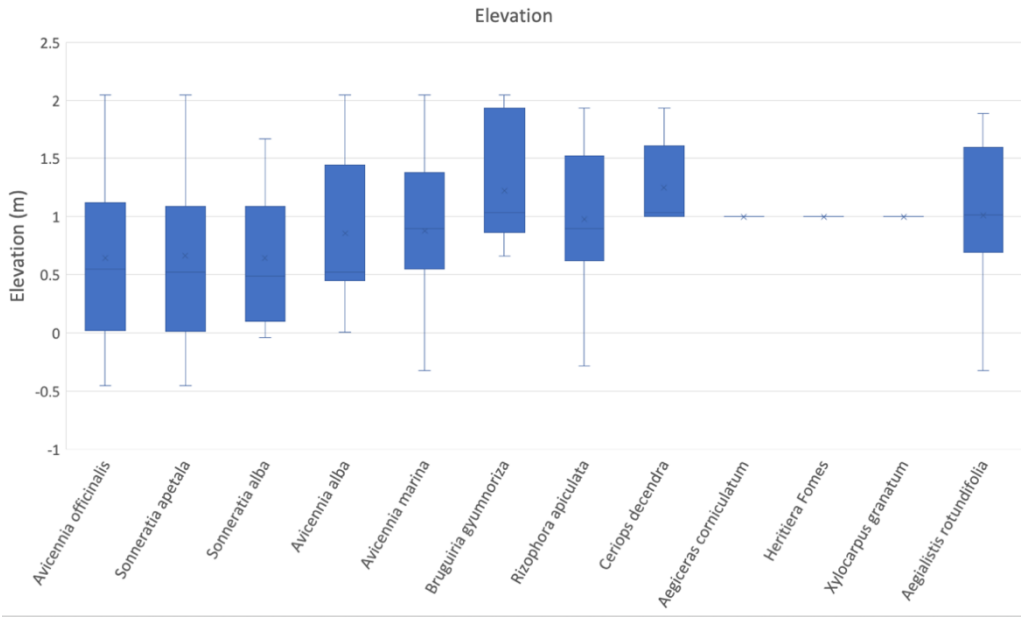

Figure 4.3 Elevation range of different recovered mangrove species

Chapter 5 CONCLUSION AND RECOMMENDATIONS

5.1. Conclusions

To my knowledge, this research is the first study of artificial neural network classification using Sentinel-2 image for mangrove distribution. In artificial neural network classification, this study presented the selection of effective input features and a suitable number of hidden layers and neurons for the ANN model. After conducting several experiments for input features selection by the basic ANN model, the combination of 10 bands of Sentinel-2 image, NDVI, NDWI, MERIT DEM, and CHM outperformed other groups of features with the highest accuracy of 95.85 %. The result of the basic model has increased by tuning hyper-parameters of hidden layer and neuron up to overall accuracy of 95.98% and kappa coefficient of 0.92. Applying transfer learning improved on the performance of the ANN model for the new dataset by producing a higher overall accuracy of 97.20% and kappa coefficient of 0.94. Consequently, the proposed method achieved a promising result in mangrove classification and the model created in this study can be deployed to any region of mangrove around the world.

Furthermore, the information about mangrove change in the WMF could be provided through post-classification change detection. By integrating field data, the study found that natural recovering mangrove areas were observed around 50% of each abandoned site during a short abandonment period with different species diversity. Of a total 12 recovering mangrove species relating to their environmental preferences, *Avicennia officinalis* and *Avicennia marina* were found as dominant species within different ranges of salinity and elevation of all recovering sites.

5.2. Recommendations

Depending on input features and methods used, a resultant accuracy varies in remote sensing classification. Artificial neural network cooperating with Sentinel-2 images in this study can perform mangrove classifications with promising results. However, remote sensing classification always creates challenges and opportunities for improvement by considering potential features and methods. To the experiences of this research, the misclassification encountered in predicting the new dataset would be

once figured out without transfer learning if the following alternative approaches were applied to training sessions of future studies.

a) Using time series data of Sentinel-2 imagery, and
b) Fusing remotely sensed data captured by multi-sensors such as Landsat and Synthetic Aperture Radar (SAR)

Due to the lack of high-resolution remote sensing data for the recovering sites, this study combined field survey data to delineate mangrove species diversity. Future studies would develop mangrove species identification if Unmanned Aerial Vehicle (UAV) mounting a multi-spectral camera and PPK GPS could be applied to data collection of mangrove specifications.

Turning to regional mangrove management, despite insubstantial reduction of mangrove during the study period, human pressures are still ongoing for existing mangrove. In contrast, natural recovery of mangrove is a high potential for mangrove rehabilitation at human disturbed areas. According to this finding, protection for existing mangroves should be more accelerated while natural mangroves recruit with diverse species at abandoned sites for mangrove rehabilitation.

References

1. Mitra, A. Sensitivity of mangrove ecosystem to changing climate; *Springer*; ISBN 9788132215097, **2013**.
2. Giri, C.; Ochieng, E.; Tieszen, L.L.; Zhu, Z.; Singh, A.; Loveland, T.; Masek, J.; Duke, N. Status and distribution of mangrove forests of the world using earth observation satellite data. *Glob. Ecol. Biogeogr. 20*, 154–159, **2011**.
3. Spalding, M. World Atlas of Mangroves; *Earthscan,* **2010**.
4. Alongi, D.M. Present state and future of the world's mangrove forests. *Environ. Conserv. 29*, 331–349, **2002**.
5. FAO The world's mangroves 1980-2005. *FAO For. Pap.* **2007**.
6. Stanley, D.O.; Broadhead, J.; Aung Aung, M.; Burma. Forest Department.; Food and Agriculture Organization of the United Nations. The atlas and guidelines for mangrove management in Wunbaik Reserved Forest. *FAO-UN, Myanmar Publ.* iii, 132 p, **2011**.
7. Giri, C. Observation and monitoring of mangrove forests using remote sensing: Opportunities and challenges. *Remote Sens. 8,* **2016**.
8. Lu, D.; Weng, Q. A survey of image classification methods and techniques for improving classification performance. *Int. J. Remote Sens. 28*, 823–870, **2007**.
9. Altaei, M.S.M. Satellite Image Classification Using Artificial Neural Network. *Int. J. Res. Advent Technol. 7*, 459–462, **2019**.
10. Toshniwal, M. Satellite image classification using neural networks. *3rd Int. JConference Sci. Electron. Technol. Inf. Telecommun.* **2005**.
11. Ge, G.; Shi, Z.; Zhu, Y.; Yang, X.; Hao, Y. Land use/cover classification in an arid desert-oasis mosaic landscape of China using remote sensed imagery: Performance assessment of four machine learning algorithms. *Glob. Ecol. Conserv. 22*, e00971, **2020**.
12. Kawabata, D.; Bandibas, J. Landslide susceptibility mapping using geological data, a DEM from ASTER images and an Artificial Neural Network (ANN).

Geomorphology ,*113*, 97–109, **2009**.

13. European Space Agency ESA - About the launch Available online: https://www.esa.int/Applications/Observing_the_Earth/Copernicus/Sentinel-2/About_the_launch (accessed on Jun 30, 2020).
14. Astola, H.; Häme, T.; Sirro, L.; Molinier, M.; Kilpi, J. Comparison of Sentinel-2 and Landsat 8 imagery for forest variable prediction in boreal region. *Remote Sens. Environ. 223*, 257–273, **2019**.
15. García-Llamas, P.; Suárez-Seoane, S.; Fernández-Guisuraga, J.M.; Fernández-García, V.; Fernández-Manso, A.; Quintano, C.; Taboada, A.; Marcos, E.; Calvo, L. Evaluation and comparison of Landsat 8, Sentinel-2 and Deimos-1 remote sensing indices for assessing burn severity in Mediterranean fire-prone ecosystems. *Int. J. Appl. Earth Obs. Geoinf. 80*, 137–144, **2019**.
16. Lima, T.A.; Beuchle, R.; Langner, A.; Grecchi, R.C.; Griess, V.C.; Achard, F. Comparing Sentinel-2 MSI and Landsat 8 OLI Imagery for Monitoring Selective Logging in the Brazilian Amazon. *Remote Sens. 11*, 961, **2019**.
17. Connette, G.; Oswald, P.; Songer, M.; Leimgruber, P. Mapping distinct forest types improves overall forest identification based on multi-spectral landsat imagery for Myanmar'S Tanintharyi Region. *Remote Sens. 8,* **2016**.
18. Morgan, R.S.; El-Hady, M.A.; Rahim, I.S. Soil salinity mapping utilizing sentinel-2 and neural networks. *Indian J. Agric. Res. 52*, 524–529, **2018**.
19. J. Mohite; N. Twarakavi; S. Pappula, Evaluating the Potential of Sentinel-2 for Low Severity Mites Infestation Detection in Grapes. *IGARSS 2018 - 2018 IEEE International Geoscience and Remote Sensing Symposium, Valencia* , 4655–4658, **2018**.
20. Pereira-Pires, J.E.; Aubard, V.; Ribeiro, R.A.; Fonseca, J.M.; Silva, J.M.N.; Mora, A. Semi-automatic methodology for fire break maintenance operations detection with sentinel-2 imagery and artificial neural network. *Remote Sens. 12,* **2020**.
21. Kristollari, V.; Karathanassi, V. Artificial neural networks for cloud masking of Sentinel-2 ocean images with noise and sunglint. *Int. J. Remote Sens. 41*, 4102–

4135, **2020**.

22. Lee, Y.S.; Lee, S.; Jung, H.S. Mapping forest vertical structure in Gong-Ju, Korea using sentinel-2 satellite images and artificial neural networks. *Appl. Sci. 10,* **2020**.

23. Wang, L.; Jia, M.; Yin, D.; Tian, J. A review of remote sensing for mangrove forests: 1956–2018. *Remote Sens. Environ. 231,* **2019**.

24. Yoshino, K.; Pham, T.D.; Bui, D.T.; Friess, D.A.; Yokoya, N.; Bui, D.T.; Yoshino, K.; Friess, D.A. Remote sensing approaches for monitoring mangrove species, structure, and biomass: Opportunities and challenges. *Remote Sens. 11*, 1–24, **2019**.

25. Yu, X.; Shao, H.B.; Liu, X.H.; Zhao, D.Z. Applying neural network classification to obtain mangrove landscape characteristics for monitoring the travel environment quality on the Beihai Coast of Guangxi, P. R. China. *Clean - Soil, Air, Water* ,*38*, 289–295, **2010**.

26. Chun, B.B.; Jafri, M.Z.M.; San, L.H. Mangrove mapping in Penang Island by using artificial neural network technique. *2011 IEEE Conf. Open Syst. ICOS 2011*, 251–255, **2011**.

27. Chun, B.B.; Mat Jafri, M.Z.; San, L.H. Comparison of remote sensing approach for mangrove mapping over Penang Island. *2012 Int. Conf. Comput. Commun. Eng. ICCCE 2012*, 258–262, **2012**.

28. Saw, A.A. Deforestation and Local Livelihood Strategy: A Case of Encroachment into the Wunbaik Reserved Mangrove Forest, Myanmar. **2017**.

29. Andrieu, J.; Lombard, F.; Fall, A.; Thior, M.; Ba, B.D.; Dieme, B.E.A. Botanical field-study and remote sensing to describe mangrove resilience in the Saloum Delta (Senegal) after 30 years of degradation narrative. *For. Ecol. Manage. 461*, 117963, **2020**.

30. Ferreira, A.C.; Ganade, G.; Luiz de Attayde, J. Restoration versus natural regeneration in a neotropical mangrove: Effects on plant biomass and crab communities. *Ocean Coast. Manag. 110*, 38–45, **2015**.

31. Sidik, F.; Proisy, C.; Rahmania, R.; Viennois, G.; Andayani, A.; Lovelock, C.; Prosperi, J.; Suhardjono; Widagti, N.; Subki, B.; et al. Mangrove restoration in

abandoned ponds : natural recruitment vs . replanting. *ECSA 55 Unbounded Boundaries Shifting Baselines* . 2, **2015**.

32. Win, M. The mangrove vegetation of Wubaik Reserved Forest. *FAO-UN, Myanmar Publ.* iii, 191 p, **2011**.

33. Wang, D.; Wan, B.; Qiu, P.; Su, Y.; Guo, Q.; Wang, R.; Sun, F.; Wu, X. Evaluating the performance of Sentinel-2, Landsat 8 and Pléiades-1 in mapping mangrove extent and species. *Remote Sens. 10,* **2018**.

34. Kamal, M.; Phinn, S.; Johansen, K. *Object-based approach for multi-scale mangrove composition mapping using multi-resolution image datasets*; Vol. 7; ISBN 6173346702, 2015.

35. Barik, J.; Mukhopadhyay, A.; Ghosh, T.; Mukhopadhyay, S.K.; Chowdhury, S.M.; Hazra, S. Mangrove species distribution and water salinity: an indicator species approach to Sundarban. *J. Coast. Conserv.22*, 361–368, **2018**.

36. Kitaya, Y.; Jintana, V.; Piriyayotha, S.; Jaijing, D.; Yabuki, K.; Izutani, S.; Nishimiya, A.; Iwasaki, M. Early growth of seven mangrove species planted at different elevations in a Thai estuary. *Trees - Struct. Funct. 16*, 150–154, **2002**.

37. Emlid.com How PPK works - Reach RS/RS+ docs Available online: https://docs.emlid.com/reachrs/common/tutorials/ppk-introduction/ (accessed on Jun 29, 2020).

38. Geoid Height Calculator | Software | UNAVCO Available online: https://www.unavco.org/software/geodetic-utilities/geoid-height-calculator/geoid-height-calculator.html (accessed on Jun 29, 2020).

39. Open Access Hub Available online: https://scihub.copernicus.eu/ (accessed on Jun 27, 2020).

40. European Space Agency *SENTINEL-2 User Handbook*; 2015;

41. Eastman, J. IDRISI Guide to GIS and Image Processing Volume 1. *Clark Labs*, *1*, 87–131, **2001**.

42. Pettorelli, N. Satellite Remote Sensing and the Management of Natural Resources.

Satell. Remote Sens. Manag. Nat. Resour. **2019**.

- 43. Congedo, L. Semi-Automatic Classification Plugin Documentation;
- DOI: 10.13140/RG.2.2.29474.02242/1, 2016;

44. Teillet, P.M.; Staenz, K.; Williams, D.J. Effects of spectral, spatial, and radiometric characteristics on remote sensing vegetation indices of forested regions. *Remote Sens. Environ.* **1997**.

45. McFeeters, S.K. The use of the Normalized Difference Water Index (NDWI) in the delineation of open water features. *Int. J. Remote Sens. 17,* 1425-1432*,* **1996**.

46. Saravanan, S.; Jegankumar, R.; Selvaraj, A.; Jacinth Jennifer, J.; Parthasarathy, K.S.S. *Utility of Landsat Data for Assessing Mangrove Degradation in Muthupet Lagoon, South India*; Elsevier Inc., ISBN 9780128143513, **2018**.

47. Gupta, K.; Mukhopadhyay, A.; Giri, S.; Chanda, A.; Datta Majumdar, S.; Samanta, S.; Mitra, D.; Samal, R.N.; Pattnaik, A.K.; Hazra, S. An index for discrimination of mangroves from non-mangroves using LANDSAT 8 OLI imagery. *MethodsX*, *5*, 1129–1139, **2018**.

48. Hutchinson, C.F. Techniques for combining Landsat and ancillary data for digital classification improvement. *Photogramm. Eng. Remote Sens. 48*, 123–130, **1982**.

49. USGS EROS Archive - Digital Elevation - Shuttle Radar Topography Mission (SRTM) 1 Arc-Second Global Available online: https://www.usgs.gov/centers/eros/science/usgs-eros-archive-digital-elevation-shuttle-radar-topography-mission-srtm-1-arc?qt-science_center_objects=0#qt-science_center_objects (accessed on May 28, 2020).

50. Yap, L.; Kandé, L.H.; Nouayou, R.; Kamguia, J.; Ngouh, N.A.; Makuate, M.B. Vertical accuracy evaluation of freely available latest high-resolution (30 m) global digital elevation models over Cameroon (Central Africa) with GPS/leveling ground control points. *Int. J. Digit. Earth*, *12*, 500–524, **2019**.

51. EORC JAXA ALOS Global Digital Surface Model (DSM) " ALOS World 3D-30m " (AW3D30) Dataset product format description. 1–11, **2020**.

52. JAXA, J.A.E.A. ALOS Data Users Handbook. *Earth Obs. Res. Appl. Cent. Japan*

Aerosp. Explor. Agency, 158, **2008**.

53. Yamazaki, D.; Ikeshima, D.; Tawatari, R.; Yamaguchi, T.; O'Loughlin, F.; Neal, J.C.; Sampson, C.C.; Kanae, S.; Bates, P.D. A high-accuracy map of global terrain elevations. *Geophys. Res. Lett. 44*, 5844–5853, **2017**.

54. Weng, Q. Quantifying Uncertainty of Digital Elevation Models Derived from Topographic Maps. *Adv. Spat. Data Handl.* 403–418, **2002**.

55. Cao, J.; Leng, W.; Liu, K.; Liu, L.; He, Z.; Zhu, Y. Object-Based mangrove species classification using unmanned aerial vehicle hyperspectral images and digital surface models. *Remote Sens. 10,* **2018**.

56. Zhang, Z.; Kazakova, A.; Moskal, L.M.; Styers, D.M. Object-based tree species classification in urban ecosystems using LiDAR and hyperspectral data. *Forests*, *7*, 1–16, **2016**.

57. Alganci, U.; Besol, B.; Sertel, E. Accuracy assessment of different digital surface models. *ISPRS Int. J. Geo-Information*, *7*, 1–16, **2018**.

58. Lee, W.J.; Lee, C.W. Forest canopy height estimation using multiplatform remote sensing dataset. *J. Sensors* , *2018*, **2018**.

59. Aggarwal, C.C. *Neural Networks and Deep Learning*; ISBN 9783319944623, 2018.

60. Sootla, S. Artificial neural network for image classification. Computational neuroscience project. *Univ. Tartu*, 15, **2015**.

61. Brownlee, J. A Gentle Introduction to the Rectified Linear Unit (ReLU) Available online: https://machinelearningmastery.com/rectified-linear-activation-function-for-deep-learning-neural-networks/ (accessed on May 16, 2020).

62. Maas, A.L.; Hannun, A.Y.; Ng, A.Y. Rectifier nonlinearities improve neural network acoustic models. *ICML Work. Deep Learn. Audio, Speech Lang. Process. 28,* **2013**.

63. Francois, C. Deep Learning with Python; *Manning publication Co.*, ISBN 9780996452762, 2018.

64. Grave, E.; Joulin, A.; Cissé, M.; Grangier, D.; Jégou, H. Efficient softmax approximation for GPUs. *34th Int. Conf. Mach. Learn. ICML* , *3*, 2111–2119, **2017**.

65. Uniqtech Understand the Softmax Function in Minutes - Data Science Bootcamp - Medium Available online: https://medium.com/data-science-bootcamp/understand-the-softmax-function-in-minutes-f3a59641e86d (accessed on Jun 15, 2020).

66. Wright, J.L.; Manic, M. Neural network architecture selection analysis with application to cryptography location. *Proc. Int. Jt. Conf. Neural Networks* **2010**.

67. Shibata, K.; Ikeda, Y. Effect of number of hidden neurons on learning in large-scale layered neural networks. *ICCAS-SICE 2009 - ICROS-SICE Int. Jt. Conf. 2009, Proc.* 5008–5013, **2009**.

68. Doukim, C.A.; Dargham, J.A.; Chekima, A. Finding the number of hidden neurons for an MLP neural network using coarse to fine search technique. *10th Int. Conf. Inf. Sci. Signal Process. their Appl. ISSPA* , 606–609, **2010**.

69. Rwanga, S.S.; Ndambuki, J.M. Accuracy Assessment of Land Use/Land Cover Classification Using Remote Sensing and GIS. *Int. J. Geosci. 08*, 611–622, **2017**.

70. Congalton, R.G. Assessing Landsat Classification Accuracy Using Discrete Multivariate Analysis Statistical Techniques. *Photogramm. Eng. Remote SENSING; Vol. 49; No. 12; December 1983; pp. 1671-1678. 27*, 83–92, **1983**.

71. Cohen, J. A Coefficient of Aggrement for Normal Scales. *Curr. Contents, 20,* 37-46, **1960**.

72. Gandhi, S.; Jones, T.G. Identifying mangrove deforestation hotspots in South Asia, Southeast Asia and Asia-Pacific. *Remote Sens. 11,* **2019**.

73. Afify, H.A. Evaluation of change detection techniques for monitoring land-cover changes: A case study in new Burg El-Arab area. *Alexandria Eng. J. 50*, 187–195, **2011**.

74. Cintrón, G.; Schaeffer-Novelli, Y. Methods for studying mangrove structure. In The Mangrove Ecosystem: Research Methods, *UNESCO, Paris; 8;*ISBN 9231021818, 1984.

75. C. E. SHANNON A Mathematical Theory of Communication. *Bell Syst. Tech. J. 27*, 379–423, **1948**.

76. Green, E.P.; Clark, C.D.; Mumby, P.J.; Edwards, A.J.; Ellis, A.C. Remote sensing techniques for mangrove mapping. *Int. J. Remote Sens. 19*, 935–956, **1998**.

77. Alsaaideh, B.; Al-Hanbali, A.; Tateishi, R.; Nguyen Thanh, H. The integration of spectral analyses of Landsat ETM+ with the DEM data for mapping mangrove forests. *Int. Geosci. Remote Sens. Symp.* 1914–1917, **2011**.

78. Alsaaideh, B.; Al-Hanbali, A.; Tateishi, R.; Kobayashi, T.; Hoan, N.T. Mangrove Forests Mapping in the Southern Part of Japan Using Landsat ETM+ with DEM. *J. Geogr. Inf. Syst. 05*, 369–377, **2013**.

79. Chadwick, J. Integrated LiDAR and IKONOS multispectral imagery for mapping mangrove distribution and physical properties. *Int. J. Remote Sens. 32*, 6765–6781, **2011**.

80. Liu, X.; Bo, Y. Object-based crop species classification based on the combination of airborne hyperspectral images and LiDAR data. *Remote Sens. 7*, 922–950, **2015**.

81. Liu, M.; Cao, C.; Dang, Y.; Ni, X. Mapping forest canopy height in mountainous areas using ZiYuan-3 stereo images and Landsat data. *Forests*, *10,* **2019**.

82. Stathakis, D. How many hidden layers and nodes? *Int. J. Remote Sens. 30*, 2133–2147, **2009**.

83. Mas, J.F.; Flores, J.J. The application of artificial neural networks to the analysis of remotely sensed data. *Int. J. Remote Sens. 29*, 617–663, **2008**.

84. Brownlee, J. How to Configure the Number of Layers and Nodes in a Neural Network Available online: https://machinelearningmastery.com/how-to-configure-the-number-of-layers-and-nodes-in-a-neural-network/ (accessed on Jul 1, 2020).

85. Han, D.; Liu, Q.; Fan, W. A new image classification method using CNN transfer learning and web data augmentation. *Expert Syst. Appl. 95*, 43–56, **2018**.

86. Fchollet Transfer learning & fine-tuning Available online:

https://keras.io/guides/transfer_learning/ (accessed on Jun 19, 2020).

87. Arrigoni, A. Transfer Learning in Tensorflow (VGG19 on CIFAR-10): Part 1 Available online: https://towardsdatascience.com/transfer-learning-in-tensorflow-9e4f7eae3bb4 (accessed on Jun 19, 2020).

88. Guo, Z. Identification of Buildings in Rural Environment based on Convolutional Neural Networks, *Master Thesis, The University of Tokyo*, 2017.

89. De Alban, J.D.T.; Jamaludin, J.; Wong, D. de W.; Than, M.M.; Webb, E.L. Improved estimates of mangrove cover and change reveal catastrophic deforestation in Myanmar. *Environ. Res. Lett.15,* **2019**.

90. Gaw, L.Y.F.; Linkie, M.; Friess, D.A. Mangrove forest dynamics in Tanintharyi, Myanmar from 1989–2014, and the role of future economic and political developments. *Singap. J. Trop. Geogr. 39*, 224–243, **2018**.

91. Aung, T.T. Resilience of the Mangrove Ecosystem and Its Restoration Perspectives in the Mega Delta of Myanmar, *Doctral Desertation, Graduate School of Environment and Information Sciences, Yokoham National University,* **2012**.

92. Clough, B.F. Growth and salt balance of the mangroves Avicennia marina (Forsk.) Vierh. and Rhizophora stylosa Griff. in relation to salinity. *Aust. J. Plant Physiol. 11*, 419–430, **1984**.

93. Khan, M.A.; Aziz, I. Salinity tolerance in some mangrove species from Pakistan. *Wetl. Ecol. Manag. 9*, 219–223, **2001**.

94. Win, S.; Towprayoon, S.; Chidthaisong, A. Adaptation of mangrove trees to different salinity areas in the Ayeyarwaddy Delta Coastal Zone, Myanmar. *Estuar. Coast. Shelf Sci. 228,* **2019**.

Appendices

Appendix 1 GPS points to create a ground truth image for artificial neural network classification

Id	Label	Latitude	Longitude
1	Water	19.2653	93.8874
2	Water	19.2987	93.9218
3	Water	19.3228	93.9362
4	Water	19.3494	93.9588
5	Water	19.3826	93.9716
6	Water	19.3869	94.0018
7	Water	19.376	94.0156
8	Water	19.1879	93.9267
9	Water	19.1556	93.9372
10	Water	19.255	93.8883
11	Water	19.245	93.8861
12	Water	19.2461	93.8977
13	Water	19.247	93.9133
14	Water	19.2571	93.9237
15	Water	19.2581	93.8759
16	Water	19.2541	93.8643
17	Water	19.2468	93.8637
18	Water	19.2395	93.8627
19	Water	19.2296	93.8569
20	Water	19.2217	93.8582
21	Paddy field	19.1742	93.9622
22	Paddy field	19.163	93.9428
23	Paddy field	19.1576	93.9257
24	Paddy field	19.1561	93.9441
25	Paddy field	19.3118	94.0136
26	Paddy field	19.216	93.8662
27	Shrimp pond	19.2498	93.8667
28	Shrimp pond	19.2509	93.8765
29	Shrimp pond	19.24	93.8898
30	Shrimp pond	19.2333	93.8621
31	Shrimp pond	19.2372	93.8648
32	Shrimp pond	19.2443	93.8652
33	Shrimp pond	19.2129	93.8778
34	Shrimp pond	19.3773	93.981
35	Shrimp pond	19.3794	93.9852
36	Shrimp pond	19.3439	93.9636

37	Shrimp pond	19.3614	93.976
38	Shrimp pond	19.3508	93.972
39	Other vegetation	19.1435	93.9141
40	Other vegetation	19.1476	93.9018
41	Other vegetation	19.1413	93.8756
42	Other vegetation	19.1524	93.8677
43	Other vegetation	19.1791	93.8568
44	Other vegetation	19.1709	93.8553
45	Natural mangrove	19.168	93.9372
46	Natural mangrove	19.1495	93.9479
47	Natural mangrove	19.2117	93.8714
48	Natural mangrove	19.2184	93.892
49	Natural mangrove	19.228	93.9147
50	Natural mangrove	19.256	93.9291
51	Natural mangrove	19.253	93.9217
52	Natural mangrove	19.2601	93.8868
53	Natural mangrove	19.2615	93.8924
54	Natural mangrove	19.2519	93.8722
55	Natural mangrove	19.2798	93.9151
56	Natural mangrove	19.2857	93.9191
57	Natural mangrove	19.295	93.9266
58	Natural mangrove	19.3029	93.9383
59	Natural mangrove	19.2687	93.927
60	Natural mangrove	19.2813	93.9365
61	Natural mangrove	19.2921	93.9483
62	Natural mangrove	19.2973	93.9755
63	Natural mangrove	19.3121	93.9969
64	Natural mangrove	19.3236	94.0026
65	Natural mangrove	19.3364	94.0111
66	Natural mangrove	19.3437	94.0234
67	Natural mangrove	19.341	94.029
68	Natural mangrove	19.3675	94.016
69	Natural mangrove	19.3758	94.0067
70	Natural mangrove	19.3805	93.9997
71	Natural mangrove	19.3848	93.9824
72	Natural mangrove	19.3737	93.9777
73	Natural mangrove	19.2168	93.8849
74	Natural mangrove	19.2592	93.9249
75	Shrimp pond	19.2694	93.9177
76	Mangrove plantation	19.2537	93.8909

77	Mangrove plantation	19.2093	93.9999
78	Mangrove plantation	19.2083	94.0055
79	Mangrove plantation	19.1624	93.9481
80	Mangrove plantation	19.3662	93.9961

Appendx 2 Spatial information of sample plots at three recovered sites

Study sites	Sample plots	Latitude	Longitude
Site 1	1	19.375533330	93.987650000
	2	19.376083330	93.985983330
	3	19.374100000	93.990400000
	4	19.373333330	93.986850000
	5	19.373933330	93.990116670
	6	19.371933330	93.986800000
	7	19.370266670	93.988366670
	8	19.369883330	93.988516670
	9	19.370900000	93.986716670
	10	19.370266670	93.987066670
	11	19.367983330	93.985650000
	12	19.367850000	93.985300000
	13	19.367933330	93.984816670
	14	19.367900000	93.984233330
	15	19.367783330	93.983550000
	16	19.367566670	93.983283330
	17	19.368166670	93.983000000
	18	19.366133330	93.980633330
	19	19.366400000	93.981500000
	20	19.365866670	93.981283330
Site 2	21	19.259100000	93.883750000
	22	19.258766670	93.886166670
	23	19.258433330	93.886150000
	24	19.258083330	93.882900000
	25	19.257833330	93.882500000
	26	19.257416670	93.885866670
	27	19.256666670	93.886083330
	28	19.256250000	93.886466670
	29	19.257000000	93.882333330
	30	19.255350000	93.886316670
	31	19.254683330	93.877183330
	32	19.254100000	93.882416670
	33	19.254200000	93.882766670
	34	19.254416670	93.883066670
	35	19.253500000	93.876966670
	36	19.253700000	93.876800000
	37	19.253783330	93.876500000
	38	19.254283330	93.876750000
	39	19.254216670	93.875616670

	40	19.253916670	93.876016670
Site 3	41	19.248916670	93.860633330
	42	19.249383330	93.861100000
	43	19.249633330	93.861400000
	44	19.247566670	93.861800000
	45	19.247583330	93.862216670
	46	19.247616670	93.860816670
	47	19.247550000	93.860466670
	48	19.248683330	93.860550000
	49	19.248533330	93.861683330
	50	19.247116670	93.862000000

Appendix 3 Elevation dataset for selection of a suitable DEM

Points	Latitude	Longitude	PPK	ALOS	SRTM	MERIT
1	19.254315	93.87746	2.129	-0.310526	2.3979	1.14728
2	19.254162	93.877279	0.907	-1.80229	2.2041	1.14728
3	19.254229	93.876895	0.902	-2.0459	1.1389	1.14743
4	19.254279	93.876643	0.706	-0.846617	1.6788	1.14743
5	19.254293	93.876479	0.94	-0.037959	2.2213	1.14743
6	19.254434	93.876454	0.894	0	1.8007	1.14743
7	19.25445	93.876379	0.941	0	1.9653	1.14743
8	19.254522	93.876304	0.955	0	1.6934	1.14743
9	19.254682	93.876344	0.833	0	1.8368	1.79044
10	19.254641	93.876235	0.656	0	1.4456	0.69018
11	19.25464	93.876235	0.565	0	1.445	0.69018
12	19.254662	93.876255	1.023	0	1.5181	1.79044
13	19.25478	93.876306	1.133	0	1.7002	1.79044
14	19.25478	93.876387	1.146	0	1.994	1.79044
15	19.254787	93.876384	0.975	0	1.9807	1.79044
16	19.254837	93.876357	1.048	0	1.8863	1.79044
17	19.254836	93.876356	0.998	0	1.8808	1.79044
18	19.254869	93.876426	1.33	-0.017133	2	1.79044
19	19.254891	93.876476	0.613	-0.08682	2	1.79044
20	19.254857	93.876556	0.594	-0.100393	2	1.79044
21	19.254883	93.876654	0.989	-0.566396	2	1.79044
22	19.254891	93.876716	0.795	-0.859957	1.8219	1.79044
23	19.254844	93.876892	0.8	-1.61874	1.1886	1.79044
24	19.254797	93.87699	0.769	-2.55887	1	1.79044
25	19.253736	93.877439	1.319	-2.63507	2.2281	0.65733
26	19.253624	93.87729	1.1	-2.78851	1.291	0.65733
27	19.253614	93.877204	0.982	-2.70195	1.0099	0.65733
28	19.253555	93.877153	0.867	-2.8778	1	0.65733

29	19.253639	93.87711	0.767	-2.43841	1.0598	0.65733
30	19.25365	93.877007	1.018	-2.53738	1.0311	0.62204
31	19.253648	93.876899	1.067	-2.78673	1.0215	0.62204
32	19.253684	93.876498	1.092	-1.12903	1.7109	0.62204
33	19.253787	93.87641	1.333	-0.574308	1.9728	1.14743
34	19.253793	93.87639	1.171	-0.503712	1.9987	1.14743
35	19.253758	93.876345	1.077	-0.340524	2	1.14743
36	19.253654	93.876261	1.101	-0.387036	2	0.62204
37	19.253622	93.876257	0.667	-0.484776	2	0.62204
38	19.253611	93.876311	0.936	-0.721512	1.9979	0.62204
39	19.25347	93.876271	0.937	-1.07459	1.4901	0.62204
40	19.253464	93.876277	1.023	-1.09878	1.4716	0.62204
41	19.253463	93.87635	0.982	-1.36004	1.4675	0.62204
42	19.253853	93.876492	0.981	-0.871128	1.9519	1.14743
43	19.253903	93.876653	0.913	-1.40389	2.0026	1.14743
44	19.25397	93.876711	0.875	-1.27548	1.8393	1.14743
45	19.254079	93.876835	0.104	-1.29155	1.3926	1.14743

Appendix 4 Workflow of creating a ground truth image in ArcGIS

1. Importing GPS points collected in the field (Appendix 1) into ArcGIS using Google Earth Imagery as a base map

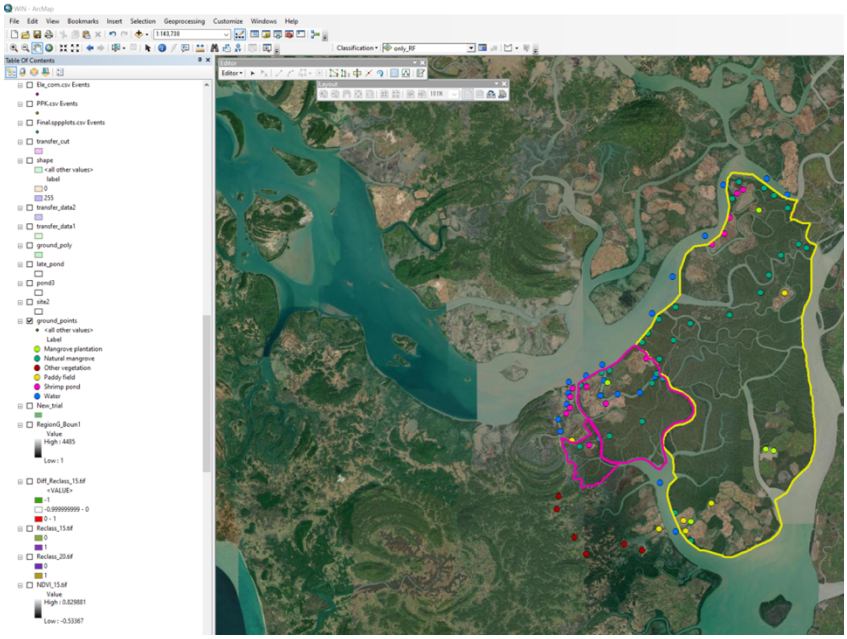

2. Creating true and false color maps using Sentinel-2 bands (section 2.3.6) to provide updated information and assist visualization

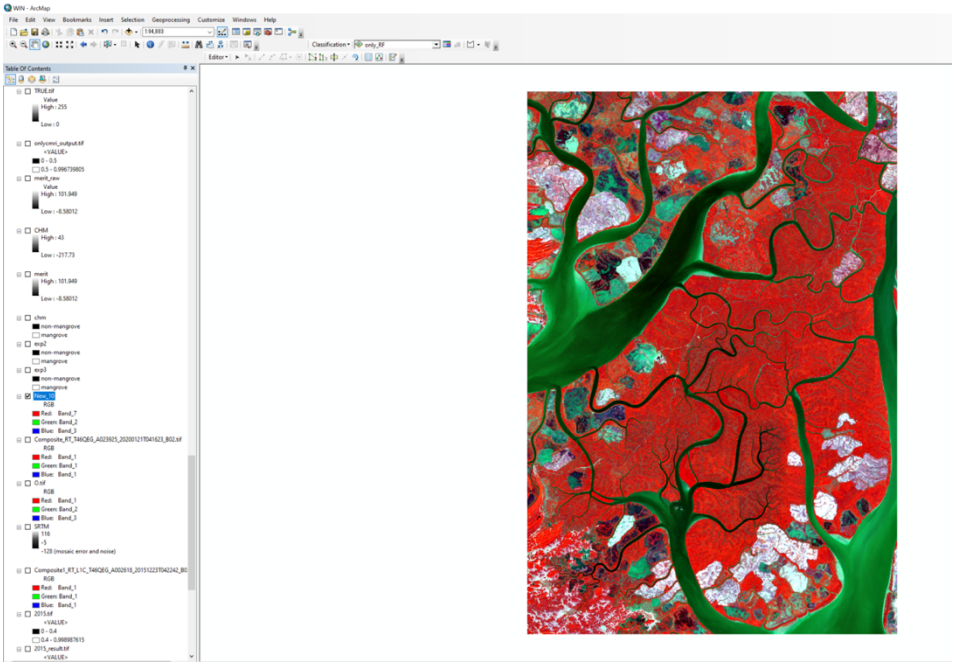

3. Drawing mangrove and non-mangrove polygons manually using polygon creation tools in ArcGIS

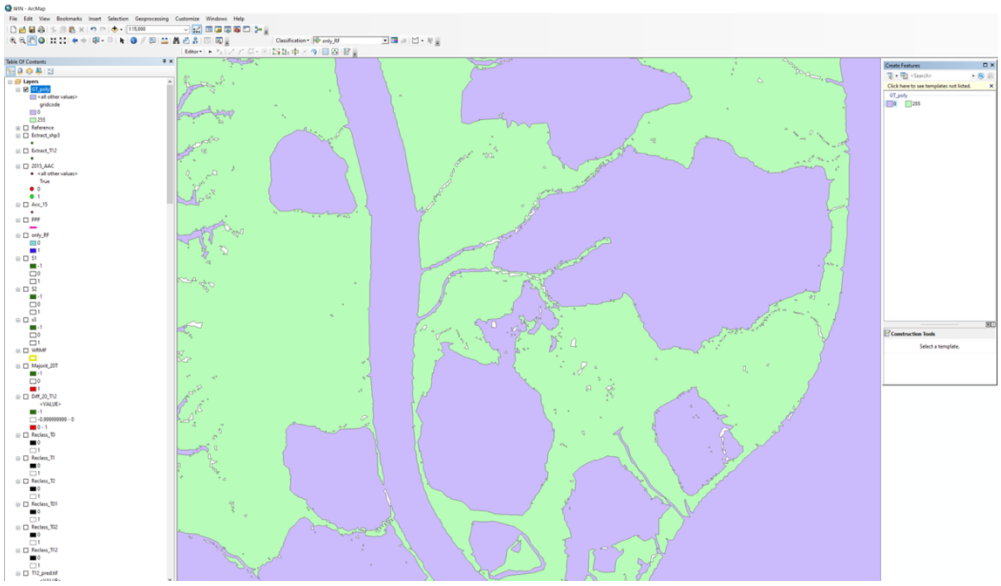

4. Referring to Sentinel-2 color maps in drawing polygons

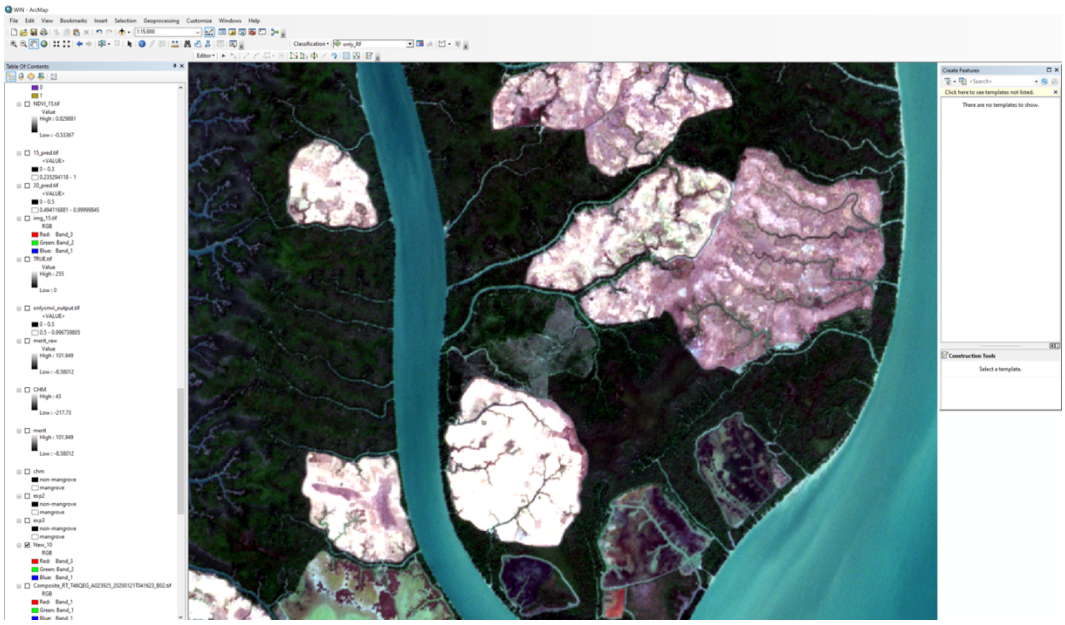

5. Converting polygons to raster after drawing polygons by assigning 0 for non-mangrove and 255 for mangrove

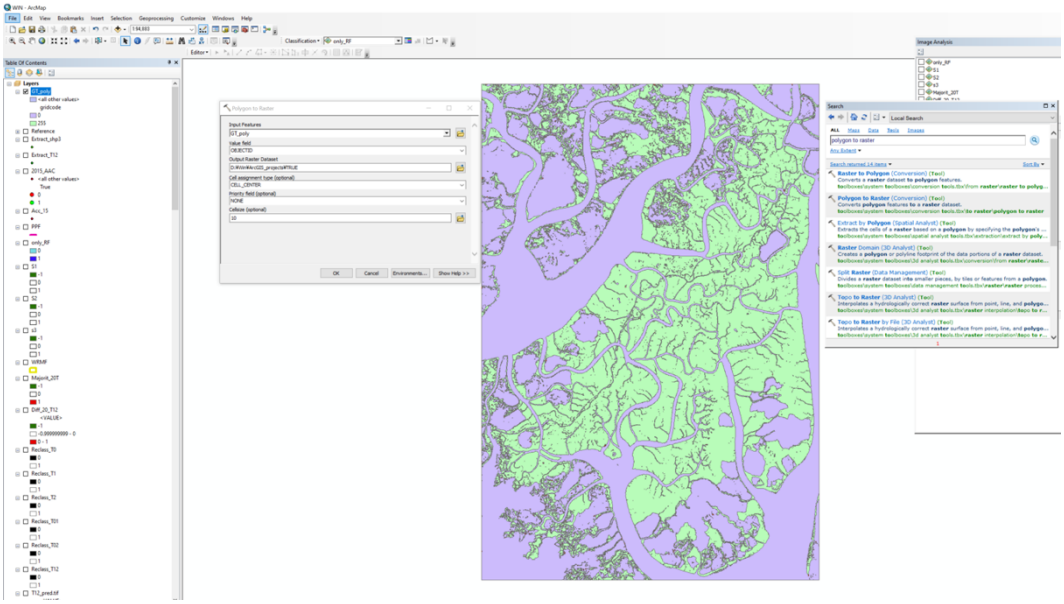

6. Saving a ground truth image labeled as 0 and 255

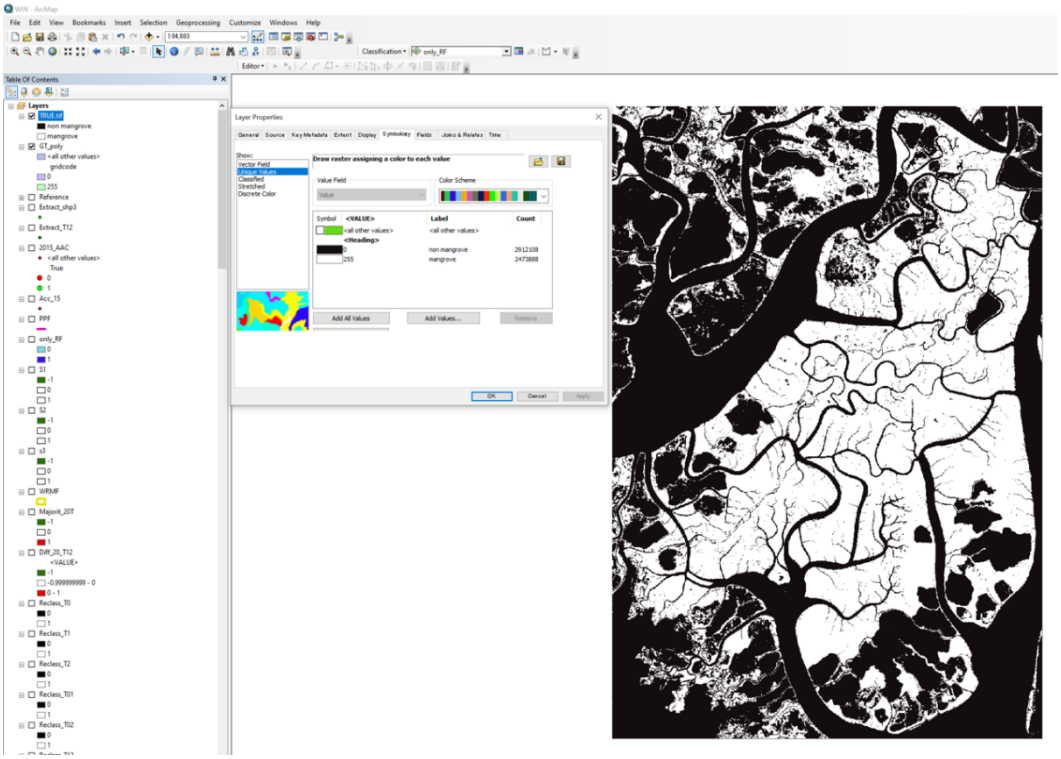

Appendix 5 Workflow of neural network classification for mangrove distribution

Importing necessary libraries for analysis

```
import os
import rasterio
import matplotlib.pyplot as plt
import numpy as np
import tensorflow as tf
from tensorflow import keras
from sklearn.metrics import accuracy_score, confusion_matrix
from sklearn.metrics import classification_report
from sklearn.metrics import cohen_kappa_score
```

Importing images for a dataset in 2020, 2015 and transfer learning

```
img20 = rasterio.open('10bands.tif')
ndvi20 = rasterio.open('NDVI_2020.tif')
ndwi20 = rasterio.open('NDWI_2020.tif')
label20 = rasterio.open('TRUE.tif')
dem = rasterio.open('merit.tif')
dsm = rasterio.open('SRTM.tif')

img15 = rasterio.open('img_15.tif')
ndvi15 = rasterio.open('NDVI_15.tif')
ndwi15 = rasterio.open('NDWI_15.tif')
```

```
label_t=rasterio.open('transLable.tif')
img_t =rasterio.open('trans_img.tif')
ndvi_t =rasterio.open('trans_ndvi.tif')
ndwi_t=rasterio.open('trans_ndwi.tif')
dem_t=rasterio.open('trans_merit.tif')
chm_t=rasterio.open('trans_chm.tif')
```

Read raster image into numerical data and reshape

```
img20=img20.read()
label20=label20.read()
ndvi20 = ndvi20.read()
ndwi20 = ndwi20.read()

img15=img15.read()
ndvi15 = ndvi15.read()
ndwi15 = ndwi15.read()
dem = dem.read()
dsm = dsm.read()
img_t=img_t.read()
label_t=label_t.read()
ndvi_t= ndvi_t.read()
ndwi_t= ndwi_t.read()
dem_t = dem_t.read()
dsm_t = dsm_t.read()
#Reshape into 2D array
img20=np.reshape(img20,(-1,10))
label20=np.reshape(label20,(-1,1))
ndvi20 =np.reshape(ndvi20,(-1,1))
ndwi20 =np.reshape(ndwi20,(-1,1))
img15=np.reshape(img15,(-1,10))
ndvi15 =np.reshape(ndvi15,(-1,1))
ndwi15 =np.reshape(ndwi15,(-1,1))
img_t =np.reshape(img_t,(-1,10))
ndvi_t =np.reshape(ndvi_t,(-1,1))
ndwi_t =np.reshape(ndwi_t,(-1,1))
dem =np.reshape(dem,(-1,1))
dsm =np.reshape(dsm,(-1,1))
```

```
chm = dsm-dem
dem_t =np.reshape(dem_t,(-1,1))
chm_t =np.reshape(chm_t,(-1,1))
```

Concatenating different features into a dataset

```
dataset20 = np.concatenate((img20, ndvi20, ndwi20, dem, chm), axis=1)
dataset15 = np.concatenate((img15, ndvi15, ndwi15, dem, chm), axis=1)
dataset_t = np.concatenate((img_t, ndvi_t, ndwi_t, dem_t, chm_t), axis=1)
```

Dividing dataset and ground truth data into training (60%), testing(20%), and validating(20%) to train an ANN model

```
from sklearn.model_selection import train_test_split
xTrain, xTest, yTrain, yTest = train_test_split(dataset20, label20,
    test_size=0.2, random_state=42)
xTrain, xVal, yTrain, yVal = train_test_split(xTrain, yTrain, test_size=0.25,
    random_state=42)

xTrain = xTrain / 255.0
xTest = xTest / 255.0
xVal = xVal / 255.0

yTrain = yTrain / 255.0
yTest = yTest / 255.0
yVal = yVal / 255.0
xTrain = xTrain.reshape((xTrain.shape[0], 1, xTrain.shape[1]))
xTest = xTest.reshape((xTest.shape[0], 1, xTest.shape[1]))
xVal = xVal.reshape((xVal.shape[0], 1, xVal.shape[1]))
input_shape = xTrain[0].shape
```

Building and training an ANN model for classification

```
model = keras.Sequential([
    keras.layers.Dense(544, activation=tf.nn.relu, input_shape=(input_shape)),
    keras.layers.Dense(320, activation=tf.nn.relu),
    keras.layers.Dense(2, activation=tf.nn.softmax)])

model.compile(optimizer='adam', loss="sparse_categorical_crossentropy",
    metrics=["accuracy"])

model.summary()
history = model.fit(xTrain, yTrain, epochs=30, batch_size=16,
    validation_data=(xVal, yVal), verbose=2)
```

Evaluating trained model using test dataset

```
y_pred = model.predict(xTest, verbose=0)
y_class = model.predict_classes(xTest, verbose=0)

y_pred = y_pred[:,0]
y_class= y_class[:,0]
accuracy = accuracy_score(yTest, y_class)
print('Accuracy: %f' % accuracy)


matrix = confusion_matrix(yTest, y_class)
print(matrix)
print(classification_report(yTest,y_class))
kappa = cohen_kappa_score(yTest, y_class)
print('Cohens kappa: %f' % kappa)
```

Saving the trained model when accuracy is satisfied

```
model.save('o_model.h5')
model.save_weights("o_model_weight.h5")
```

Applying the trained model for whole datasets in 2020 and 2015, and exporting as raster files

```
data20 = dataset20.reshape((dataset20.shape[0], 1, dataset20.shape[1]))
data15 = dataset15.reshape((dataset15.shape[0], 1, dataset20.shape[1]))
data20 = data20/ 255.0
data15 = data15/ 255.0
n1= 'o20_output.tif'
n2 = 'o15_output.tif'
img1 = rasterio.open('10bands.tif')#To use same geoinformation for output images
def pred(data, name)
    pred= model.predict(data)
    pred= np.reshape(pred, (5385996, 2))
    pred = pred[:,1]
    pred= np.reshape(pred, (img1.height, img1.width))

    #Export prediction as tiff file
    output = rasterio.open(name, 'w',driver='Gtiff',
                               width=img1.width, height = img1.height,
                                count=1,
                                crs=img1.crs,
                                transform=img1.transform,
                                dtype= 'float32'
                               )
    output.write(pred,1)
    output.close()

pred(data20,n1)
pred(data15,n2)
```

Applying transfer learning with a new dataset since the original model produced misclassified pixels in the 2015 dataset

```
xTrain, xTest, yTrain, yTest = train_test_split(dataset_t, label_t,
    test_size=0.2, random_state=42)

xTrain = xTrain / 255.0
xTest = xTest / 255.0

yTrain = yTrain / 255.0
yTest = yTest / 255.0
xTrain = xTrain.reshape((xTrain.shape[0], 1, xTrain.shape[1]))
xTest = xTest.reshape((xTest.shape[0], 1, xTest.shape[1]))
```

Retraining some layers of the original model using transfer dataset

```
model.layers[1].trainable = False #Fixed second hidden layer
model.layers[2].trainable = False #Fixed output layer
model.compile(optimizer='adam', loss="sparse_categorical_crossentropy",
    metrics=["accuracy"])
model.summary()
history =model.fit(xTrain, yTrain, epochs=50, batch_size=16, verbose =2)
model.save('t_model.h5') #Saving transfer learning model
model.save_weights("t_model_weight.h5")
```

Loading the two models to test transfer learning dataset

```
o_model = tf.keras.models.load_model('o_model.h5')
t_model = tf.keras.models.load_model('t_model.h5')

#Predict transfer learning dataset by two models and evaluate their performance
def pred(model):
    y_pred = model.predict(xTest, verbose=0)
    y_class = model.predict_classes(xTest, verbose=0)

    y_pred = y_pred[:,0]
    y_class= y_class[:,0]
    accuracy = accuracy_score(yTest, y_class)
    print('Accuracy: %f' % accuracy)


    matrix = confusion_matrix(yTest, y_class)
    print(matrix)
    print(classification_report(yTest,y_class))

    kappa = cohen_kappa_score(yTest, y_class)
    print('Cohens kappa: %f' % kappa)

o_model_pred = pred(o_model)
t_model_pred = pred(t_model)
```

Predicting the 2015 dataset using transfer learning models and export a raster output

```
pred(model, output)
pred= t_model.predict(data15)
pred= np.reshape(pred, (5385996, 2))
pred = pred[:,1]
pred= np.reshape(pred, (img1.height, img1.width))

#Export prediction as tiff file
output = rasterio.open(tmodel_output15, 'w',driver='Gtiff',
                           width=img1.width, height = img1.height,
                            count=1,
                            crs=img1.crs,
                            transform=img1.transform,
                            dtype= 'float32'
                           )
output.write(pred,1)
output.close()
```